

# **Improvements and Optimisation of Water Electrolysis for Hydrogen Production**

Kai Zeng

M. Eng.

Centre for Energy



**THE UNIVERSITY OF  
WESTERN AUSTRALIA**

This thesis is presented for the degree of

Doctor of Philosophy

in

Chemical Engineering

of

The University of Western Australia

June 2012

## **Declaration**

To the best of my knowledge and belief this thesis contains no material previously published by any other person except where due acknowledgment has been made. This thesis contains no material which has been accepted for the award of any other degree or diploma in any university.

Signature: .....

Date:.....

**To My Beloved Family**

## Acknowledgements

I would like to express my deepest gratitude to my supervisor, Professor Dongke Zhang FTSE, for giving me the opportunity to carry out my PhD with him. He has guided and inspired me with his patience, experience, knowledge and invaluable advice on both academic matter and life philosophy. Without his supervision, continuous support and encouragement, this thesis would not have come to its completion.

I would like to gratefully acknowledge The University of Western Australia for offering me the SIRF scholarship and Centre for Energy at The University of Western Australia for offering me a PhD stipend. I acknowledge Australia Research Council and BHP Billiton Iron Ore Pty Ltd for their financial and other support for this research.

Sincere thanks go to the staff of the Centre for Microscopy Characterisation and Analysis at The University of Western Australia, Professor Martin Saunders, Associate Professor Alexandra Suvorova, Dr Janet Muhling and Ms Lyn Kirilak for their training and help with the SEM and EDS facility and data interpretation.

I would like to acknowledge colleagues at the Centre for Energy: Dr Meining Song, Ms Yii Leng Chan, Mr Zhezi Zhang, Ms Yu Ma, and all other colleagues for the administrative or technical assistance, discussion, their friendship, encouragement their help and support in many ways.

I thank all the friends I have met in Perth for your sincere friendship and the time we had spent together, which made my life enjoyable and happy.

Special thanks to Ms Shaojun Lin, Dr Peisheng Huang, Dr Mingliang Wang, Dr Xiaoxue Xu, Dr Alex Elliot for their sincere friendship and kind help. I also wish to thank my friends, peers and teachers back in China who have guided, helped, encouraged me and supported me during my study in Australia.

Last but certainly not the least, a special thank you goes to Ms Wei Hua for her support, patience and understanding. To my Mum, Dad, Sister and other family members in China, I would also like to say thank you all for your support.

## **Abstract**

Hydrogen as an important energy carrier has wide applications and great potentials. With ever increasing energy costs and concerns with climate change associated with carbon dioxide emissions from the use of fossil fuels, hydrogen has in recent years become very popular as it is perceived as a clean fuel that emits almost no pollutants other than water and can be produced using any primary energy sources, with renewable energy being most attractive. More importantly, hydrogen works with fuel cells and together, they may serve as one of the solutions to sustainable energy supply and use in the long run.

Alkaline water electrolysis for producing hydrogen has been known for centuries and has the advantage of producing ultra-pure hydrogen which is perfect for fuel cells. However its applications are often limited to small scales and unique situations where access to large scale hydrogen production plants is not possible or uneconomical. The widespread utilisation of alkaline water electrolysis is faced with a number of technical and cost challenges due to its high energy consumption and low efficiency.

The present research aims to investigate the origins of the causes for the high energy consumption of water electrolysis. Efforts are also made to understand and alleviate the high energy consumption by applying electrode modifications and managing the behaviour of electrolytic bubbles.

Through reviewing the literature, a number of scientific and technical gaps between the current state of knowledge about alkaline water electrolysis and the industrial practice were identified. There has not been any effort for

quantifying the energy barriers or resistances of the water electrolysis process. Many research efforts mainly focus on finding or evaluating new electrode materials, and the effect of electrode modification and electrode composition on electrode reactions has not been fully understood and studied. Last but not the least, the behaviour and the effect of electrolytic bubbles on the electrolysis cell voltage have not been systematically investigated.

In order to understand and improve the water electrolysis process, four specific objectives were also set for this thesis work, namely, (1) a study aiming at identifying and quantifying the energy barriers in the water electrolysis process, (2) a study on the effect of electrode preparation methods on electrode performances, (3) an investigation into the effect of electrode modification on the kinetics of electrode reactions and (4) a study of the behaviour of electrolytic bubbles together with their effect on the cell voltage. To help the interpretation of the effect of electrode preparation and electrode modification, the electrode surface profiles were characterised using a scanning electron microscope equipped with an energy-dispersive X-ray spectroscopy (SEM-EDX). The kinetic studies were carried out using a standard three-electrode reactor employing the steady state polarisation technique and electrochemical impedance spectrum technique and the study on the bubble behaviour was conducted in a custom made cell that enabled the observation of bubbles. These analytical and experimental techniques enabled the unveiling of some new and exciting findings as follows.

For the first time, the resistances of an electrolysis process were generalised and defined using an analogy of electrical circuit. These resistances were

categorised, ranked and where possible, quantified, according to their nature and quantified using the existing data from the literature. This would serve as a guide for improving the water electrolysis and other electrochemical reactions.

The electrode surface profile images proved that the alkaline leaching is a good way to produce a porous structure of the electrodes, and it was revealed that overpotential of the hydrogen evolution reaction was reduced. The apparent activity was characterised using the Tafel equation of the hydrogen evolution reaction on Ni electrode, written as  $\eta = 0.14 + 0.108 \cdot \text{Log} j$ . These findings are consistent with the literature values and validated against the experimental data.

The effect of surface area was investigated by comparing the electrode kinetics of electrodes with different modifications. The roughness factor was employed to quantify the effect of electrode modifications. The intrinsic activity of a nickel electrode was expressed as  $\eta = 0.02 + 0.191 \cdot \text{Log} j$ . This validated the experimental techniques and can further serve as a guide for preparing electrode materials.

A model of the electrolytic gas bubbles behaviour in the alkaline water electrolysis was established using a fundamental force analysis methodology. The experimental data of the critical diameter for bubble departure were in good agreement with the predictions from the model. It was found that the properties of the electrolyte and electrode potential had a great influence on the detachment of electrolytic bubbles. The convection caused by electrolyte movements or circulation forced the bubbles to depart

prematurely. These findings can be used to manage or minimise the resistance caused by the electrolytic bubbles.

Finally, these findings are discussed and evaluated against the objectives set in the literature review. To alleviate the resistance of the electrode reaction, alkaline leaching and electrode modifications are suggested to be used for preparing electrodes with large surface area. The use of the roughness factor is recommended to be used for benchmarking and selecting electrode materials. Recommendations are also made for the future work in two main areas. Firstly, a further study to investigate the role of the electrode composition on the electrode reactions will be useful to guide the preparation of electrode materials. Secondly and more importantly, the effect of convection on the behaviour of electrolytic bubbles is worth investigating for managing the resistance caused by the electrolytic bubbles.

# Table of Contents

Acknowledgements .....	iii
Abstract .....	ix
Table of Contents .....	ix
List of Figures .....	xiv
List of Tables.....	xx
Chapter 1    Introduction .....	1
1.1    Hydrogen, Its Production and Use .....	1
1.2    Overall Aims and Structure of the Thesis .....	6
Chapter 2    Literature Review .....	9
2.1    The Fundamentals of Alkaline Water Electrolysis.....	9
2.1.1    Chemistry of Alkaline Water Electrolysis .....	9
2.1.2    Electrical Circuit Analogy of Water Electrolysis Cells .....	11
2.1.3    Thermodynamic Consideration .....	14
2.1.4    Cell Efficiencies .....	17
2.1.5    Electrode Kinetics .....	21
2.1.6    Electrochemical Reaction Resistances .....	33
2.1.7    Bubble Phenomena.....	38
2.2    Historical Development of Water Electrolysis.....	41
2.3    Research Development and Trend .....	48

---

2.3.1	Electrode Material Searching .....	48
2.3.2	Electrolyte and Additives .....	53
2.3.3	Bubble Management .....	54
2.4	Summary .....	56
Chapter 3	Methodology, Approaches and Techniques .....	58
3.1	Introduction .....	58
3.2	Experimental Designs and Materials .....	60
3.2.1	Three-electrode Cell Reactor Experiments .....	60
3.2.2	Rectangular Tube Cell Reactor Experiments .....	66
3.2.3	Materials .....	70
3.3	Analytical Methods and Instrumentation .....	71
3.3.1	Scanning Electron Microscopy (SEM) .....	72
3.3.2	Electron Dispersive X-Ray Spectroscopy (EDS) .....	72
3.3.3	Potentiostatic Technique .....	72
3.3.4	Electrochemical Impedance Spectroscopy (EIS) .....	73
3.4	Data Analysis .....	73
3.4.1	Polarisation Curve .....	74
3.4.2	Tafel Curve .....	74
3.4.3	Nyquist Plot and Bode Plot .....	76
3.5	Summary .....	76
Chapter 4	Kinetics of Electrode Reactions on Ni Base Electrodes .....	77

4.1	Introduction .....	77
4.2	Electrode Surface Characterisation .....	77
4.3	Kinetics of Hydrogen Evolution Reaction .....	79
4.4	Electrochemical Impedance Spectroscopy .....	82
4.4.1	Electrode Kinetics on Ni Electrode.....	82
4.4.2	Electrode Kinetics on Ni-Fe-Zn Electrode.....	84
4.5	Effect of Electrode-Deposition.....	86
4.6	Summary .....	88
Chapter 5 Evaluating the Effect of Surface Modifications on Ni Based Electrodes for Water Electrolysis..... 89		
5.1	Introduction .....	89
5.2	Hydrogen Evolution Reaction on Ni electrodes.....	89
5.3	Relative Roughness Factor .....	92
5.4	Intrinsic Activity of Ni Electrode .....	99
5.5	Hydrogen Evolution on Ni-Co Electrodes .....	100
5.6	Intrinsic Activity of Ni-Co Electrodes .....	102
5.7	Summary .....	107
Chapter 6 Evaluating the Behaviour of Electrolytic Gas Bubbles and Their Effect on the Cell Voltage in Alkaline Water Electrolysis..... 108		
6.1	Introduction .....	108
6.2	Theoretical Analysis.....	109
6.2.1	Force Analysis.....	109

6.2.2	Buoyancy .....	111
6.2.3	Expansion Force.....	112
6.2.4	Interfacial Tension Force .....	112
6.2.5	Drag and Lift Forces .....	114
6.3	Bubble Departure Diameter Predictions.....	114
6.4	Dependence of Critical Diameter for Bubble Departure on Cell Voltage .....	118
6.5	Dependence of Critical Diameter for Bubble Departure on Electrolyte Concentration.....	122
6.6	Bubble Behaviour at High Cell Voltages .....	124
6.7	The Effect of Electrolyte Circulation .....	126
6.8	Comparison of Model Predictions with Experimental Observations	128
6.9	Summary .....	130
Chapter 7	Evaluation and Practical Implications.....	132
7.1	The Electrode Kinetics on Ni and Ni-Co .....	133
7.2	Electrode Modifications and Their Effect .....	136
7.3	Electrolytic Bubble Behaviour and Their Effect .....	138
7.4	Practical Implications .....	141
7.4.1	Feasibility Analysis .....	144
7.4.2	Cost Analysis .....	145
7.5	Summary .....	146

---

Chapter 8	Conclusions and Recommendations .....	148
8.1	Conclusions .....	148
8.1.1	The Electrode Kinetics on Ni and Ni-Fe-Zn .....	148
8.1.2	Electrode Modifications and Their Effect.....	149
8.1.3	Electrolytic Bubble Behaviour and Their Effect.....	150
8.2	Practical Implications .....	151
8.3	Recommendations for Future Work .....	152
References	.....	155
Publications	.....	168

## List of Figures

Figure 1-1 A schematic illustration of a conceptual distributed energy system with water electrolysis playing an important role in hydrogen production as a fuel gas and energy storage mechanism .....	4
Figure 2-1 A schematic illustration of a basic water electrolysis system ....	10
Figure 2-2 An electrical circuit analogy of resistance in the water electrolysis system .....	11
Figure 2-3 Cell potential for hydrogen production by water electrolysis as a function of temperature .....	17
Figure 2-4 A schematic illustrations of electrical double layer and the potential distribution near an electrode surface .....	23
Figure 2-5 Effect of potential change on Gibbs energy energies: (a) the overall relationship between energy change and state of reaction and (b) Magnified picture of shaded area of (a) .....	25
Figure 2-6 Typical Tafel plots for both hydrogen and oxygen evolution ....	32
Figure 2-7 An illustration of the contributions of anode and cathode polarisation to the cell voltage of an alkaline water electrolysis cell.....	32
Figure 2-8 Compositions of the typical cell voltage of an alkaline water electrolysis cell.....	33
Figure 2-9 A qualitative comparison of the energy losses caused by reaction resistances, ohmic resistance, ionic resistance and bubble resistance .....	37
Figure 2-10 An illustration of the contact angle at the three phase boundary of the gas bubble, electrode and the electrolyte .....	39

Figure 3-1 Research methodology map of the thesis structure .....	59
Figure 3-2 An illustration of the three-electrode reactor. (a) the lid, (b) the main body (font view) (c) the main body (side view ).....	62
Figure 3-3 The three-electrode electrochemical cell with the lid .....	62
Figure 3-4 A schematic illustration of the three-electrode reaction experimental setup .....	66
Figure 3-5 An image of the experimental setup with three-electrode reactor, water bath and Autolab potentiostat.....	66
Figure 3-6 An illustration of (a) rectangular tube cell and (b) the electrode holder.....	67
Figure 3-7 An image of (a) rectangular tube cell and the electrode holder (b) the electrode holder .....	68
Figure 3-8 A schematic illustration of rectangular tube cell experiments ...	70
Figure 3-9 A image of the rectangular tube cell experiments .....	70
Figure 4-1 SEM images of Ni base electrode .....	78
Figure 4-2 SEM images of Ni-Fe-Zn (a) before and (b) after alkaline leaching .....	78
Figure 4-3 EDS of Ni-Fe-Zn (a) before and (b) after alkaline leaching .....	79
Figure 4-4 The Tafel curves of hydrogen evolution reaction on both Ni and Ni-Fe-Zn electrodes .....	80
Figure 4-5 An analogous circuit for describing the resistances of hydrogen evolution reaction on Ni electrodes.....	83

Figure 4-6 The Nyquist plots for hydrogen evolution reaction on the Ni electrode polished with a sandpaper with 5 $\mu$ m grand size. The experiments were carried out at -1.3V, -1.4V and -1.5 V against Silver/Silver Chloride electrode (SCE), respectively. The dot points are experimental impedances and the continuous lines are the curves-fitted impedances. ....	83
Figure 4-7 The equivalent circuit employed for EIS data fitting for the Ni-Fe-Zn Electrode.....	84
Figure 4-8 The Nyquist plots for hydrogen evolution reaction on the Ni-Fe-Zn electrode at different potentials against SCE and corresponding fitting. The dot points are experimental impedances and the continuous lines are the curves-fitted impedances.....	85
Figure 4-9 The Bode modulus (a) and Bode phase (b) plots of EIS data and corresponding fitting. Scatters are experimental data; lines are EIS fitting using a non-linear regression procedure .....	86
Figure 4-10 Linear relationship between overpotential and $\text{Log}(R_{ct}^{-1})$ of the hydrogen evolution reaction on Ni and Ni-Fe-Zn electrodes in 0.5M KOH at 298K.....	87
Figure 5-1 Tafel curves of hydrogen evolution reaction illustrating the apparent activity of the Ni electrodes polished with different sandpapers ..	91
Figure 5-2 SEM images of Ni electrodes at the magnification of 5000 times [(a) base Ni electrode, (b) Ni electrode polished with the P4000 sandpaper, (c) Ni electrode polished with the P2000 sandpaper and (d) Ni electrode polished with the P400 sandpaper] .....	92

Figure 5-3 An analogous circuit for describing the resistances of hydrogen evolution reaction on Ni electrodes.....	94
Figure 5-4 The Nyquist plots for hydrogen evolution reaction on the Ni electrode polished with the sandpapers at the three selected potentials -1.3V, -1.4V and -1.5 V against SCE, respectively. (a)Ni electrode (b) Ni electrode polished with P4000 sandpaper, (c) Ni electrode polished with P2000 sandpaper (d) Ni electrode polished with P400 sandpaper. The dot points are experimental impedances and the continuous lines are the curves-fitted impedances.....	95
Figure 5-5 The Bode plots for hydrogen evolution reaction on the Ni electrode polished with the sandpapers at the three selected potentials -1.3V, -1.4V and -1.5 V against SCE, respectively. (a)Ni electrode; (b) Ni electrode polished with P4000 sandpaper; (c) Ni electrode polished with P2000 sandpaper; (d) Ni electrode polished with P400 sandpaper. The dot points are experimental impedances and the continuous lines are the curves-fitted impedances.....	97
Figure 5-6 Tafel curves of hydrogen evolution reaction illustrating the intrinsic activity of the mechanical polished Ni electrodes .....	99
Figure 5-7 Tafel curves of hydrogen evolution reaction illustrating the apparent activity of the Ni-Co electrodes.....	101
Figure 5-8 The Bode plots for hydrogen evolution reaction on the Ni electrode and Ni-Co electrodes at the three selected potentials -1.3V, -1.4V and -1.5 V against SCE, respectively. (a)Ni electrode; (b) Ni-Co(1) electrode; (c) Ni-Co(2) electrode; (d) Ni-Co(3) electrode. The dot points are	

experimental impedances and the continuous lines are the curves-fitted impedances.....	102
Figure 5-9 Tafel curves of hydrogen evolution reaction illustrating the intrinsic activity of the Ni and Ni-Co electrodes .....	104
Figure 5-10 SEM images of Ni-Co electrodes at the magnification of 5000 times [(a) Ni polished with P4000 sandpaper; (b) Ni-Co (1); (c) Ni-Co (2); (d) Ni-Co (3)] .....	105
Figure 6-1 A schematic diagram of a gas bubble on an electrode surface (a), and the forces acting on the bubble (b) .....	110
Figure 6-2 Advancing and receding angles of a gas bubble attached to a vertical electrode surface.....	115
Figure 6-3 Typical images of hydrogen bubbles in 0.5M KOH, at $22\pm 1^\circ\text{C}$ , at different current densities: (a) $0.3\text{ mA}\cdot\text{cm}^{-2}$ (b) $0.45\text{ mA}\cdot\text{cm}^{-2}$ (c) $0.6\text{ mA}\cdot\text{cm}^{-2}$ (d) $0.75\text{ mA}\cdot\text{cm}^{-2}$ .....	119
Figure 6-4 Typical images of oxygen bubbles in 0.5M KOH, at $22\pm 1^\circ\text{C}$ at different current densities ( $\text{mA}\cdot\text{cm}^{-2}$ ): (a) 0.3 (b) 0.45 (c) 0.6 (d) 0.75 .....	120
Figure 6-5 Typical images of hydrogen bubbles at $0.6\text{mA}\cdot\text{cm}^{-2}$ at $22\pm 1^\circ\text{C}$ in KOH solutions of different concentrations (a) 0.5M (b) 1M (c) 2M (d) 4M .....	124
Figure 6-6 Typical images of hydrogen bubbles in the water electrolysis at different cell voltage in 0.5M KOH electrolyte of $22\pm 1^\circ\text{C}$ (a) 2.2V (b) 2.4V (c) 2.6V (d) 2.8V .....	125
Figure 6-7 Typical images of hydrogen bubbles in 0.5M KOH at the current density of $0.75\text{mA}\cdot\text{cm}^{-2}$ (a) without circulation; (b) with circulation; and at	

the current density of $200\text{mA}\cdot\text{cm}^{-2}$ (c) without circulation (d) with circulation The Reynolds number for both cases were 2521 .....	127
Figure 6-8 Polarisation curves at different KOH concentrations with and without electrolyte circulation.....	127
Figure 6-9 Comparison of the predicted and measured critical diameters for hydrogen and oxygen gas bubbles .....	130
Figure 7-1 The Tafel curves of hydrogen evolution reaction on both Ni and Ni-Fe-Zn electrodes .....	134
Figure 7-2 Tafel curves of hydrogen evolution reaction illustrating the intrinsic activity of the mechanical polished Ni electrodes .....	137
Figure 7-3 Comparison of the predicted and measured critical diameters for hydrogen and oxygen gas bubbles .....	139
Figure 7-4 A schematic illustration of a conceptual distributed energy system with energy storage technique playing an important role in utilisation of renewable energy .....	142
Figure 7-5 Range of power and applications for small scale wind turbines (a) and PV cells (b).....	143

## List of Tables

Table 2-1 Kinetics parameters of hydrogen production on different electrode metals .....	29
Table 2-2 Kinetic parameters of oxygen production on different metals ....	31
Table 2-3 Historical events of water electrolysis .....	41
Table 2-4 Water electrolyser developers and cell operating conditions (Kinoshita, 1992) .....	45
Table 2-5 A comparison of the two types of commercialised electrolyzers (Pletcher and Walsh, 1990) .....	48
Table 2-6 Tafel slopes of Ni alloys .....	50
Table 2-7 Oxygen overpotential of different electrode materials .....	52
Table 2-8 Hydrogen overpotential of different electrode materials .....	53
Table 3-1: Details and description of the chemical and other materials used in this thesis .....	71
Table 4-1 Tafel parameters extracted from Figure 4-4 .....	81
Table 4-2 Kinetics parameters for hydrogen evolution reaction on Ni-Fe-Zn electrode and other electrode materials reported in the literature .....	82
Table 4-3 Estimated values of the electrical components by impedance fitting at various overpotentials on the Ni base electrode .....	87
Table 4-4 Estimated values of the electrical components at various overpotentials on the Ni-Fe-Zn coated electrode .....	87

Table 5-1 Estimated values of the electrical components by impedance fitting and double layer capacitances at various overpotentials on Ni electrodes.....	98
Table 5-2 Estimated values of the electrical components by impedance fitting and double layer capacitances at various overpotentials on Ni-Co electrodes.....	103
Table 5-3 Surface compositions of the Ni-Co coatings at different deposition times as determined in the EDX analysis .....	106
Table 6-1 The critical diameters for hydrogen and oxygen bubble departure at different cell voltages in 0.5M KOH at $22\pm 1^{\circ}\text{C}$ .....	122
Table 6-2 The critical diameters for hydrogen bubble in different KOH concentrations at $22\pm 1^{\circ}\text{C}$ at current density $0.6\text{mA}\cdot\text{cm}^{-2}$ .....	124
Table 6-3 A summary of parameters for predicting the critical diameter for bubble departure.....	129
Table 7-1 A comparison of the experimental conditions and kinetic parameters of the hydrogen evolution reaction obtained in KOH .....	135
Table 7-2 A comparison between the experimental conditions and roughness factor of current study and that of by Herraiz-Cardona et al.'s study.....	137
Table 7-3 Estimated construction costs of a distributed energy system for a hypothetical remote community .....	145

## Chapter 1 Introduction

### 1.1 Hydrogen, Its Production and Use

Hydrogen is mainly used in petroleum refining (Barreto *et al*, 2003, Mueller-Langer *et al*, 2007), ammonia production (Ramachandran and Menon, 1998, Lattin and Utgikar, 2007) and, to a lesser extent, metal refining such as nickel, tungsten, molybdenum, copper, zinc, uranium and lead (Eliezer *et al*, 2000, Eliaz *et al*, 2000), amounts to more than 50 million metric tonnes worldwide in 2006 (Richards and Shenoy, 2007). The large scale nature of such hydrogen consumptions requires large scale hydrogen production to match them. As such, the hydrogen production is dominated by reforming of natural gas (Turner, 2004) and gasification of coal and petroleum coke (Rosen and Scott, 1998, Trommer *et al*, 2005), as well as gasification and reforming of heavy oil (Momirlan and Veziroglu, 2002, Sato *et al*, 2003). Although water electrolysis to produce hydrogen (and oxygen) has been known for around 200 years (Stojic *et al*, 2003, Tarasatti, 1999) and has the advantage of producing ultra-pure hydrogen, its applications are often limited to small scale and unique situations where access to large scale hydrogen production plants is not possible or economical, such as marine, rockets, space crafts, electronic industry and food industry as well as medical applications. Water electrolysis represents only 4% of the world hydrogen production (Dunn, 2002, De Souza *et al*, 2007).

With ever increasing energy costs owing to the dwindling availability of oil reserves, production and supply (Bockris *et al*, 1981) and concerns with global warming and climate change blamed on man-made carbon dioxide (CO<sub>2</sub>) emissions associated with fossil fuel use (Turner, 1999), particularly coal use (Mueller-Langer *et al*, 2007), hydrogen has in recent years become very popular for a number of reasons: (1) it is perceived as a clean fuel, emits almost nothing other than water at the point of use; (2) it can be produced using any energy sources, with renewable energy being most attractive (Steinfeld, 2002); (3) it works with fuel cells (Grigoriev *et al*, 2006, Granovskii *et al*, 2006, Kreuter and Hofmann, 1998) and together, they may serve as one of the solutions to the sustainable energy supply and use puzzle in the long run, in so-called “hydrogen economy” (Bockris, 2002, Bockris and Veziroglu, 2007).

Water electrolysis can work beautifully well at small scales and, by using renewable electricity, it can also be considered more sustainable. In a conceptual distributed energy production, conversion, storage and use system for remote communities, as illustrated in Figure 1-1, water electrolysis may play an important role in this system as it produces hydrogen using renewable energy as a fuel gas for heating applications and as an energy storage mechanism. When abundant renewable energy is available, excessive energy may be stored in the form of hydrogen by water electrolysis. The stored hydrogen can then be used in fuel cells to generate electricity or used as a fuel gas. A number of studies have been reported according to the different renewable energy sources. Isherwood *et al* (2000) presented an analytical optimisation of a remote system for a hypothetical

Alaskan village. In this hypothetical system, wind and solar energies are utilised to reduce the usage of diesel for electricity generation. The electricity generated by the renewable energy is either merged into the grid or used to produce hydrogen or zinc. With such a hybrid energy system, 50% of diesel fuel and 30% annual cost savings by wind turbines were estimated. Energy storage devices such as phosphoric acid fuel cell and zinc-air fuel cell were found to be helpful to reduce the fuel consumption further. Young *et al* (2007) considered the technical and economic feasibility of using renewable energy with hydrogen as the energy storage mechanism for remote community in the mountain area of Sengor, Bhutan. The abundant hydro power, at  $840 \text{ MWh}\cdot\text{year}^{-1}$ , can not only satisfy the need of local lighting and other household uses, but can also be exported to India. Electrolyser capable of producing hydrogen at the rate of  $20 \text{ N}\cdot\text{m}^3 \text{ h}^{-1}$  is proposed. The practical problems of extending the grid over long distance and mountainous terrain could then be solved by using such a system. Hanley and Nevin (1999) applied two economic appraisal techniques to evaluate three renewable energy options for a remote community in North West Scotland. Economic benefits, environmental implications and tourism are taken into account. The authors believe that the renewable energy development may well be beneficial for remote rural communities. Although Hanley *et al*'s work does not include hydrogen, we believe that if the renewable energy options referred to in their study are coupled with hydrogen production and use, it will provide much greater flexibility and reliability of the systems.

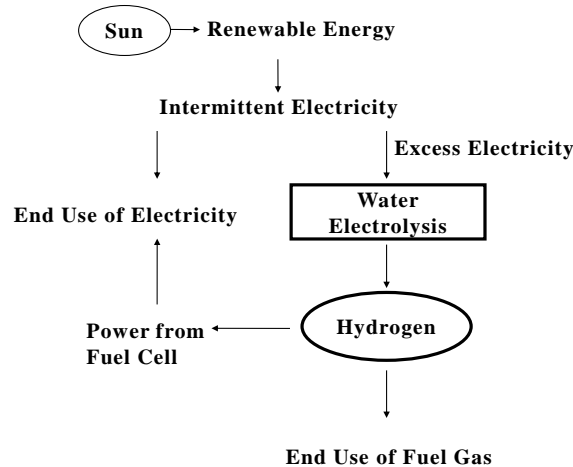


**Figure 1-1 A schematic illustration of a conceptual distributed energy system with water electrolysis playing an important role in hydrogen production as a fuel gas and energy storage mechanism**

Remote areas with abundant solar and/or wind electricity resources can take advantage of the water electrolysis to produce hydrogen to meet their energy need for households such as lighting and heating (Hollmuller *et al*, 2000), powering telecommunication stations (Varkaraki *et al*, 2003) and small-scale light manufacturing industry applications, electricity peak shaving, and in integrated systems, both grid-connected and grid-independent (Barbir, 2005). Hydrogen produced by renewable energy has a great advantage, mobility, which is essential to the energy supply in remote areas away from the main electricity grid. Agbossou *et al* (2001) studied an integrated renewable energy system for powering remote communication stations. The system is based on the production of hydrogen by water electrolysis whereby electricity is generated by a 10kW wind turbine and a 1kW photovoltaic array. When power is needed the electricity is regenerated from the stored hydrogen via a 5kW proton exchange membrane (PEM) fuel cell system. The system gives stable electrical power for communication stations. Degiorgis *et al* (2007) studied the feasibility of a hydrogen fuelled trial

village which was based on hydrogen as the primary fuel. In this work, the hydrogen is produced by water electrolysis and stored for the use in hydrogen vehicles and for thermal purposes (heating requirement of three buildings). Water electrolyzers are designed to produce  $244,440 \text{ Nm}^3 \cdot \text{year}^{-1}$  of  $\text{H}_2$ , with an energy efficiency of 61%. The light industry applications of water electrolysis may include mechanical workshops where hydrogen and oxygen gases produced from water electrolysis can replace oxygen-acetylene for metal braising, cutting and welding (Carter and Cornish, 2001, Suban *et al*, 2001).

Small scale water electrolyzers can avoid the need for a large fleet of cryogenic, liquid hydrogen tankers or a massive hydrogen pipeline system. The existing electrical power grid could be used as the backbone of the hydrogen infrastructure system, contributing to the load levelling by changing operational current density in accordance with the change in electricity demand (Oi and Sakaki, 2004). A small scale pure hydrogen and oxygen can find diverse applications including gases in laboratories and oxygen to life-support system in hospitals (Kato *et al*, 2005).

While possessing these advantages of availability, flexibility and high purity, to achieve widespread applications, hydrogen production using water electrolysis needs improvements in energy efficiency, safety, durability, operability and portability and, above all, reduction in costs of installation and operation. These open up many new opportunities for research and development leading to technological advancements in water electrolysis. This thesis aims to identify such new research and development

opportunities and then try to tackle some of the critical issues and try to answer the questions.

## **1.2 Overall Aims and Structure of the Thesis**

The present research aims to investigate the origins of the causes for the high energy consumption of water electrolysis. Efforts are also made to understand and alleviate the high energy consumption by applying electrode modifications and managing the behaviour of electrolytic bubbles.

This thesis consists of eight chapters. Each chapter has its own aims and roles which are presented in the form of a Thesis Map as shown in Figure 1-2.

Chapter 2 begins with an overview of the fundamentals of water electrolysis in the context of electrochemistry, laying a theoretical basis for scientific analysis of the published electrolysis systems and data. We then analyse various water electrolysis techniques in a broad range of applications and examine recent trends in research and innovations to identify the gaps for improvements – the needs for further research and development. Chapter 3 describes the methodology and approach, the materials and the experimental set up, analytical techniques, and data analysis employed in this thesis work.

Chapter 4 investigates the kinetics of electrode reaction and the influence of electrode preparation method on the kinetics. Chapter 5 investigates the influence of electrode preparation method and the effect of surface area on the electrode reaction. Chapter 6 evaluates the electrolytic bubble behaviours. The critical diameter for the bubble departure is predicted and compared with the experimental results.

Chapter 7 provides a critical and broad-scope evaluation of the findings from the present study. Finally, Chapter 8 summarises the conclusions from the present study and recommendations for future research and development.

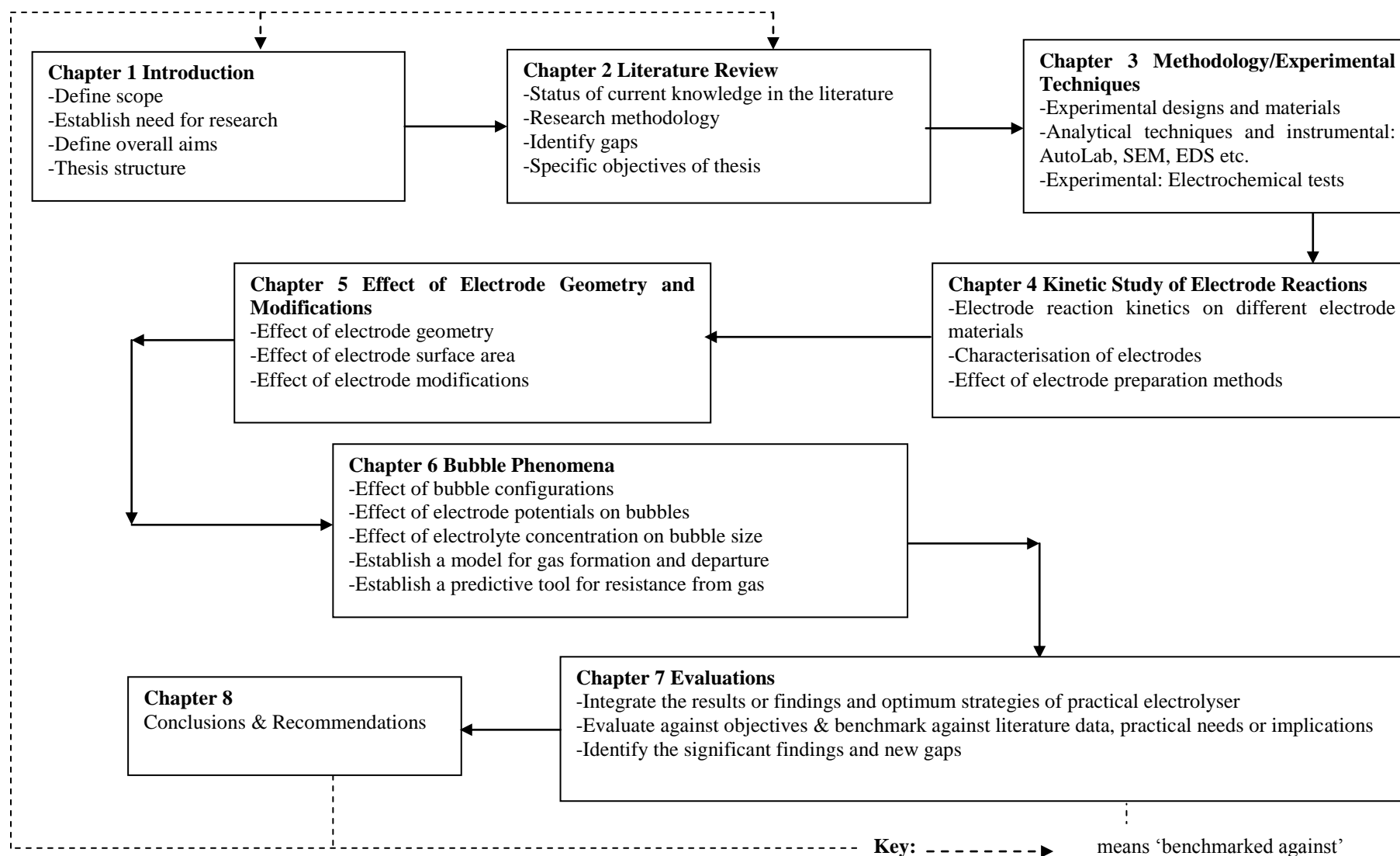


Figure 1-2 Thesis structure

## **Chapter 2      Literature Review**

The purpose of this chapter is to examine the current state of knowledge and technology of hydrogen production by water electrolysis and identifies areas where R&D effort is needed in order to perfect this technology.

Following an overview of the fundamentals of alkaline water electrolysis, an electrical circuit analogy of resistances in the electrolysis system is introduced. A thorough analysis of each of the resistances is performed by means of thermodynamics and kinetics, to provide a scientific guidance to minimising the resistance in order to achieve a greater efficiency of alkaline water electrolysis. These lay the foundation to identify the future research needs which were discussed from the aspects of electrode materials, electrolyte additives and bubble management, serving as a comprehensive guide for continuous development of the water electrolysis technology.

### **2.1 The Fundamentals of Alkaline Water Electrolysis**

#### **2.1.1 Chemistry of Alkaline Water Electrolysis**

A basic water electrolysis unit consists of an anode, a cathode, power supply, and an electrolyte, as illustrated in Figure 2-1. A direct current (DC) is applied to maintain the electricity balance and electrons flow from the negative terminal of the DC source to the cathode at which the electrons are consumed by hydrogen ions (protons) to form hydrogen. In keeping the electrical charge (and valence) in balance, hydroxide ions (anions) transfer through the electrolyte solution to anode, at which the hydroxide ions give away electrons and these electrons return to the positive terminal of the DC

source. In order to enhance the conductivity of the solution, electrolytes which generally consist of ions with high mobility are applied in the electrolyser (Oldham and Myland, 1993). Potassium hydroxide is most commonly used in water electrolysis, avoiding the huge corrosion loss caused by acid electrolytes (Leroy, 1983). Nickel is a popular electrode material due to its high activity and availability as well as low cost (Janjua and Leroy, 1985). However, the introduction of these conductive components could also bring about some side effects, which will be discussed in the following sections. During the process of water electrolysis, hydrogen ions move towards cathode, and hydroxide ions, move towards the anode. By the use of a diaphragm, gas receivers can collect hydrogen and oxygen, which form on and depart from the cathode and the anode, respectively.

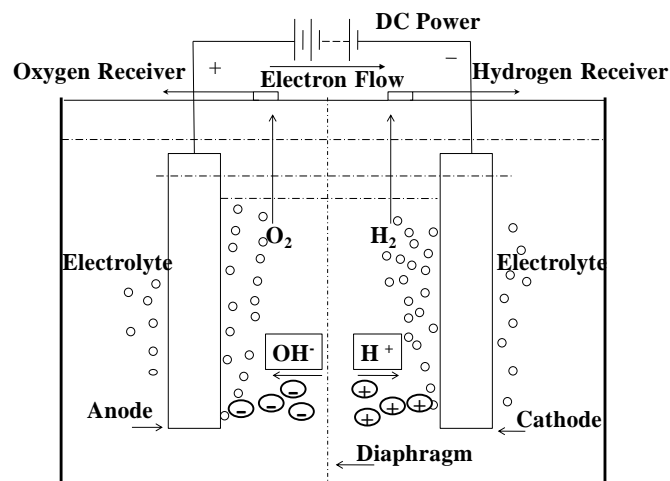


**Figure 2-1 A schematic illustration of a basic water electrolysis system**

The half reactions occurring on the cathode and anode, respectively, can be written as



The overall chemical reaction of the water electrolysis can be written as



### 2.1.2 Electrical Circuit Analogy of Water Electrolysis Cells

For this electrochemical reaction process to proceed, a number of barriers have to be overcome, requiring a sufficient electrical energy supply. These barriers include electrical resistance of the circuit, activation energies of the electrochemical reactions occurring on the surfaces of the electrodes, availability of electrode surfaces due to partial coverage by gas bubbles formed and the resistances to the ionic transfer within the electrolyte solution. It is important that these barriers are analysed in the contexts of thermodynamics and kinetics as well as transport process principles.

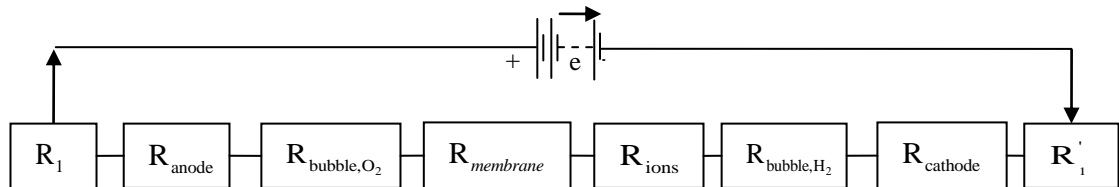


**Figure 2-2 An electrical circuit analogy of resistance in the water electrolysis system**

Figure 2-2 shows the resistances (the barriers) presented in a typical water electrolysis system. The first resistance from the left-hand-side  $R_l$  is the external electrical circuit resistance including the wiring and connections at anode.  $R_{anode}$  is originated from the overpotential of the oxygen evolution reaction on the surface of the anode.  $R_{bubble,O_2}$  is the resistance due to partial coverage of the anode by the oxygen bubbles, hindering the contact between

the anode and the electrolyte. The resistances come from electrolyte and membrane are noted as  $R_{ions}$  and  $R_{membrane}$ , respectively. Similarly,  $R_{bubble,H_2}$  roots from the blockage of the cathode by hydrogen bubbles;  $R_{cathode}$  is the resistance caused by the overpotential for oxygen evolution reaction and  $R_l'$  is the electrical resistance of the wiring and connections at cathode. Thus, the total resistance can be expressed in Equation 2-1 below.

$$R_{Total} = R_l + R_{anode} + R_{bubble,O_2} + R_{ions} + R_{membrane} + R_{bubble,H_2} + R_{cathode} + R_l' \quad 2-1$$

These resistances in electrolysis systems can be classified into three categories, the first category includes all the electrical resistances; the second includes the reaction resistances; and the third includes the transport resistances.

### Electrical Resistances

The *electrical* resistances can be calculated using the Ohm's law:  $R = U / I$  (Oldham and Myland, 1993), in which  $I$  is the current when voltage  $U$  is applied only at the circuit. Or, it can be calculated from the physics equation:  $R = L / (\kappa \cdot A)$ , in which  $L$ ,  $\kappa$  and  $A$  are the length, specific conductivity and cross-sectional area of the conductor, respectively.  $R_l$  and  $R_l'$  belong to this category and are usually considered as one integral part  $R_{cir}$ .

### Transport-related Resistances

These are the *physical* resistances experienced in the electrolysis process such as gas bubbles covering the electrode surfaces and present in the electrolyte solution, resistances to the ionic transfer in the electrolyte and

due to the membrane used for separating the  $H_2$  and  $O_2$  gases.  $R_{bubble,O_2}$ ,  $R_{membrane}$ ,  $R_{ions}$  and  $R_{bubble,H_2}$  are considered as transport resistances.

Both electrical resistances and transport resistances cause heat generation according to the Joule's law (Oldham and Myland, 1993) and transport phenomena (Bird *et al*, 2007) and thus inefficiency of the electrolysis system. The lost energy due to these resistances is also known as the ohmic loss (Belmont and Girault, 1994).

### **Electrochemical Reaction Resistances**

The *reaction resistances* are due to the overpotentials required to overcome the activation energies of the hydrogen and oxygen formation reactions on the cathode and anode surfaces, which directly cause the increase in the overall cell potential. These are the inherent energy barriers of the reactions, determining the kinetics of the electrochemical reactions whose rates can be expressed by the Arrhenius law (Bard and Faulkner, 2001).

The reaction resistances or overpotentials are inherent resistances of the electrochemical reactions depending on the surface activities of the electrodes employed.  $R_{anode}$  and  $R_{cathode}$  are reaction resistances.

Clearly, the strategies in any effort to improve the energy efficiency of water electrolysis and thus the performance of the system must involve the understanding of these resistances so as to minimise them. It is then obviously important to identify the origins of these resistances and to quantify these resistances so that we can determine which resistances are the most significant and worth researching. One of the objectives of this

chapter is quantifying these resistances and it is achieved in the following sessions.

### 2.1.3 Thermodynamic Consideration

Water is one of the thermodynamically most stable substances in the nature and it is always an uphill battle to try to pull water molecules apart to make its elements into hydrogen and oxygen molecules. No pain, no gain. If we want hydrogen (and oxygen) from water by electrolysis, we have to at least overcome an *equilibrium cell voltage*,  $E^\circ$ , which is also called “electromotive force”. With established reversibility and absence of cell current between the two different electrode reactions, the open cell potential is called the equilibrium cell voltage, it is defined as equilibrium potential difference between the respective anode and cathode (Wendt and Kreysa, 1999) and is described by Equation 2-2 below.

$$E^\circ = E_{anode}^\circ - E_{cathode}^\circ \quad 2-2$$

Equation 2-3 relates the change in the Gibbs free energy  $\Delta G$  of the electrochemical reaction to the equilibrium cell voltage as follows.

$$\Delta G = nFE^\circ \quad 2-3$$

where  $n$  is the number of moles of electrons transferred in the reaction, and  $F$  is the Faraday constant. The overall water electrolysis cell reaction,  $E^\circ$  (25°C) is 1.23V and the Gibbs free energy change of the reaction is + 237.2 kJ·mol<sup>-1</sup> (Kim *et al*, 2006), which is the minimum amount of electrical energy required to produce hydrogen. The cell voltage at this point is known as *reversible potential*. Hence the electrolysis of water to hydrogen and oxygen is thermodynamically unfavourable at room temperature and can

only occur when sufficient electrical energy is supplied. In contrast, when the electrolysis process is performed under adiabatic conditions, the total reaction enthalpy must be provided by electrical current. Under this circumstance, the *thermo-neutral* voltage is required to maintain the electrochemical reaction without heat generation or adsorption (Leroy *et al*, 1980).

Therefore, even when the equilibrium potential is met, the electrode reactions are inherently slow and then an *overpotential*  $\eta$ , above the equilibrium cell voltage is necessary in order to kick start the reaction due to the activation energy barrier, low reaction rate and the bubble formation (Bard and Faulkner, 2001, Rossmeisl *et al*, 2005). According to the resistances mentioned above, input of additional energy is also essential to drive the ionic migration process and overcome the resistance of the membrane as well as the electrical circuit. This extra energy requirement causes a *potential drop*,  $i \times R_{Cell}$  (where  $i$  is the current through the cell and  $R_{Cell}$  is the sum of electrical resistance of the cell, a function of electrolyte properties, the form of the electrodes and cell design) within the cell. The *cell potential*  $E_{Cell}$  can be written as Equation 2-4, which is always 1.8 – 2.0 V at the current density of 1000-3000 A·m<sup>-2</sup> in industry water electrolysis (Kinoshita, 1992). The total overpotential is the sum of overpotentials or barriers from the hydrogen and oxygen evolution reactions, electrolyte concentration difference and bubble formation. If one has a mild condition under which gas bubble and concentration differences can be neglected, the sum of overpotential can be calculated using Equation 2-5, where  $j$  is the current density (current divided by electrode surface area) at which

electrolysis cell operates. Both of the overpotential and the ohmic loss increase with current density and may be regarded as causes of inefficiencies in the electrolysis whereby electrical energy is degraded into heat which must be taken into account in any consideration of energy balance.

$$E_{cell} = E_{anode} - E_{cathode} + \sum \eta + i \times R_{cell} \quad 2-4$$

$$\sum \eta = |\eta_{anode}(j)| + |\eta_{cathode}(j)| \quad 2-5$$

Figure 2-3 shows the relationship between the electrolyser cell potential and operating temperature (Viswanath, 2004, Bockris *et al*, 1981). The cell potential – temperature plane is divided into three zones by the so-called equilibrium voltage line and thermo-neutral voltage line. The equilibrium voltage is the theoretical minimum potential required to dissociate water by electrolysis, below which the electrolysis of water cannot proceed. The equilibrium voltage decreases with increasing temperature. The thermo-neutral voltage is the actual minimum voltage that has to be applied to the electrolysis cell, below which the electrolysis is endothermic and above which, exothermic. The thermo-neutral voltage naturally includes the overpotentials of the electrodes, which are only weakly dependent on temperature. Thus, the thermo-neutral voltage only exhibits a slight increase with temperature. We denote thermo-neutral voltage as  $E_{\Delta H}$ . If water electrolysis takes place in the shaded area in Figure 2-3, the reaction will be endothermic.

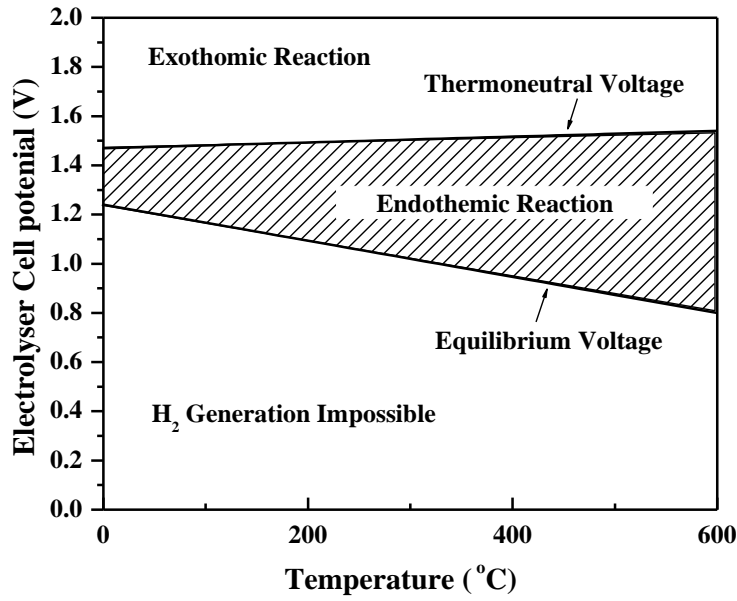


Figure 2-3 Cell potential for hydrogen production by water electrolysis as a function of temperature

#### 2.1.4 Cell Efficiencies

Energy efficiency is commonly defined as the percentage share of the energy output in the total energy input. However, there are a number of ways of expressing the efficiency of electrolysis, depending on how the electrolysis system is assessed and compared.

Generally, in the electrochemistry sense, the *voltage efficiency* of an electrolysis cell can always be calculated using Equation 2-6 (Bloom and Futmann, 1977, Bockris *et al*, 1981) below.

$$\% \text{ voltage efficiency} = \frac{(E_{\text{anode}} - E_{\text{cathode}}) \times 100}{E_{\text{cell}}} \quad 2-6$$

The physical meaning of this equation is the proportion of effective voltage to split water in the total voltage applied to the whole electrolysis cell. It is a good approximation of the efficiency of the electrolysis system.

There are two other efficiencies calculated based on the energy changes of the water electrolysis reaction, known as the *Faradic efficiency* and the *thermal efficiency*. They use the Gibbs free energy change and enthalpy change of water decomposition reaction as the energy input, respectively. Both  $\eta_{Faradic}$  and  $\eta_{Thermal}$  adopt the theoretical energy requirement plus energy losses as the energy input. As shown in the Equations 2-7 and 2-8 below.

$$\eta_{faradic} = \frac{\Delta G}{\Delta G + Losses} = \frac{E_{\Delta G}}{E_{cell}} \quad 2-7$$

$$\eta_{thermal} = \frac{\Delta H}{\Delta G + Losses} = \frac{E_{\Delta H}}{E_{cell}} \quad 2-8$$

Both equations can be simplified using cell potential and total cell voltage as shown in Equations 2-9 and 2-10 below

$$\eta_{faradic}(25^{\circ}C) = \frac{1.23(V)}{E_{cell}} \quad 2-9$$

$$\eta_{thermal}(25^{\circ}C) = \frac{1.48(V)}{E_{cell}} \quad 2-10$$

where the  $E_{cell}$  is cell voltage.  $E_{\Delta G}$  and  $E_{\Delta H}$  are the equilibrium and thermo-neutral voltages, respectively.

The physical meaning of Equation 2-7 is the percentage of the theoretical energy needed to force apart the water molecules in the real cell voltage and is a measure of the cell efficiency purely from the cell voltage point of view. On the contrast, Equation 2-8 means that an additional cell voltage, above the reversible voltage, is required to maintain the thermal balance and the percentage of the actual energy input in the real voltage defines the thermal efficiency. It is then possible that the thermal efficiency of a water

electrolysis cell may exceed 100% as the system may absorb heat from the ambient if it operates in endothermic mode (in the shaded area of Figure 2-3).

The Gibbs free energy and the enthalpy of the reaction are also a function of temperature as illustrated in Figure 2-3. Equations 2-9 and 2-10 give the efficiencies at 25°C. The values of Faradic efficiency are always less than 1 because there are always losses. While the thermal efficiency can be higher than 1 provided the water electrolysis operates under a voltage lower than the thermo-neutral voltage. This phenomenon is due to that heat is absorbed from the environment. When the denominator in Equation 2-8 is 1.48 V, the electrolysis operates at the efficiency of 100%. No heat will be absorbed from or released to the environment.

In practice, if the potential drop caused by electrical resistance is 0.25 V and 0.6 V for the cathode and anode overpotentials at 25°C, respectively, the

Faradic efficiency is  $\frac{1.23 \times 100\%}{1.23 + 0.25 + 0.6} = 59\%$  and the thermal efficiency is

$\frac{1.48 \times 100\%}{1.23 + 0.25 + 0.6} = 71\%$ . The electrolysis cell is exothermic at cell potential

above 1.48V, and endothermic at cell potential below this value. The Faradic efficiency investigates the electrolysis reaction while the thermal efficiency takes the whole thermal balance into account.

Yet another means to compare and evaluate the efficacy of a water electrolysis systems is to consider the output of hydrogen production against the total electrical energy applied to the system, in both terms of hydrogen

production rate and energy (the high heating value of hydrogen) carried by the hydrogen produced.

$$\eta_{H_2 production rate} = \frac{r_{H_2 production rate}}{\Delta E} = \frac{V(m^3 m^{-3} h^{-1})}{Uit(kJ)} \quad 2-11$$

where the  $U$  is the cell voltage,  $i$  is the current,  $t$  stands for time.  $V$  is the hydrogen production rate at unit volume electrolysis cell. The physical meaning of Equation 2-11 is the hydrogen production rate per unit electrical energy input. It is a way for direct comparison of hydrogen production capacity of different electrolysis cells, or

$$\eta_{H_2 yield} = \frac{E_{useable}}{\Delta E} = \frac{283.8(kJ)}{Uit} \quad 2-12$$

where 283.8 kJ is the high heating value (HHV) of one mole hydrogen and  $t$  is for the time needed for one gram hydrogen produced.

An alternative expression of the energy efficiency is to subtract the energy losses from the total energy input as shown in Equation 2-13 below.

$$\eta_{H_2 yield} = 1 - \frac{E_{loss}}{E_{input}} \quad 2-13$$

where  $E_{loss}$  can be expressed in terms of the resistances discussed in Equation 2-14. Those resistances cause respective energy losses. By considering these resistances an analogous electrical unit, each of them can be calculated using the Joule's Law. Therefore,

$$E_{loss} = \sum E_{loss,i} = E_{loss,circuit} + E_{loss,anode} + E_{loss,O_2 bubble} + E_{loss,ion} + E_{loss,membrane} + E_{loss,anode} + E_{loss,H_2 bubble} \quad 2-14$$

Equation 2-14 identifies all the components of energy losses, which can then be rated, allowing the efficiency to be improved by targeting the key causes of energy loss components.

From the discussion above, we can conclude that there are two broad ways of energy efficiency improvement: one is to thermodynamically reduce the energy needed to split water to yield hydrogen, such as by increasing the operating temperature or pressure; the other is to reduce the energy losses in the electrolysis cell, which can be realised by minimising the dominant components of the resistances.

In addition to the thermodynamic analysis of water electrolysis, various system parameters such as electrode materials, electrolyte properties and reaction temperatures can affect the performance of electrochemical cells. It is necessary to discuss the kinetics of the electrode reactions.

### **2.1.5 Electrode Kinetics**

The rate of the electrode reaction, characterised by the current density, firstly depends on the nature and pre-treatment of the electrode surfaces. Secondly, the rate of reaction depends on the composition of the electrolytic solution adjacent to the electrodes. These ions in the solution near the electrodes, under the effect of electrode, form layers, known as *double layer* (Oldham and Myland, 1993), taking cathode for example, the charge layer formed by hydroxyl ions and potassium ions according to the charge of the electrodes. Finally, the rate of the reaction depends on the electrode potential, characterised by the reaction overpotential. The study of electrode kinetics seeks to establish the macroscopic relationship between the current

density and the surface overpotential and the composition of the electrolytic solution adjacent to the electrode surface (Newman, 1991).

The double layer is illustrated in Figure 2-4 (a). The accumulated ions form two mobile layers of solvent molecules and adsorbed species. The one nearer the electrode surface is relatively ordered, termed the inner Helmholtz layer (IHL). The other one with less order is called outer Helmholtz layer (OHL) (Pickett, 1979). The electrical charges on the surface of the electrodes are balanced by ionic counter-charges in the vicinity of the electrodes. The potential distribution is also plotted against the distance from the electrode surface in Figure 2-4 (b). It can be clearly seen that the interfacial potential difference exists between the electrode surface and the solution due to the existence of the double layer (Wendt and Kreysa, 1999).

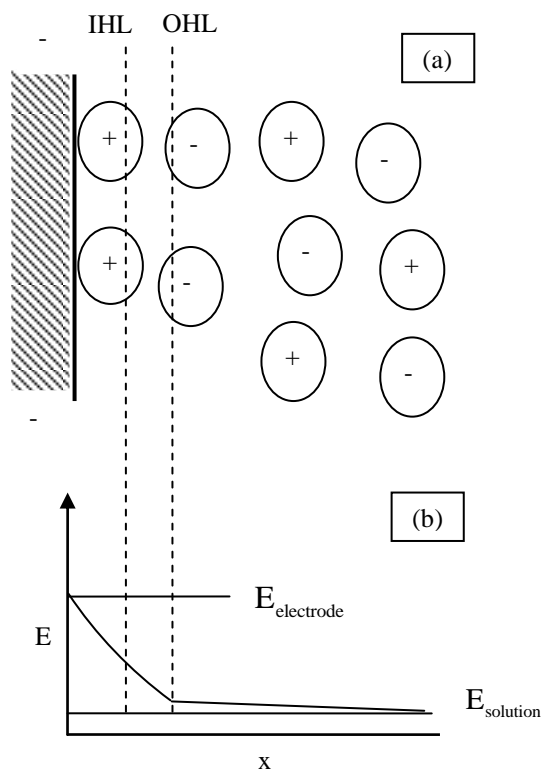


**Figure 2-4 A schematic illustrations of electrical double layer and the potential distribution near an electrode surface**

The phenomenon of the double layer formation is a non-faradic process (Wendt and Kreysa, 1999). It leads to the capacitive behaviour of the electrode reactions. This capacitor property of electrode surfaces should be taken into consideration in the kinetics.

According to the Faraday's law, the number of moles of the electrolysed species ( $\text{H}^+$  or  $\text{O}^{2-}$ ),  $N$ , is given by

$$N = \frac{Q}{nF} \quad 2-15$$

where  $Q$  is the total number of coulomb,  $n$  is the stoichiometric number of electrons consumed in the electrode reaction ( $n=2$  for both reactions R(2-1) and R(2-2)),  $F$  is the Faraday constant. The rate of electrolysis can be expressed as

$$Rate = \frac{dN}{dt} \quad 2-16$$

$\frac{dQ}{dt}$  can be noted as Faradic current  $i$  (Bard and Faulkner, 2001).

Generally the surface area at which the reaction takes place needs to be taken into account. The rate of the electrolysis reaction can be expressed as

$$Rate = \frac{i}{nFA} = \frac{j}{nF} \quad 2-17$$

where  $j$  is the current density.

The rate constant of a chemical reaction can be in general expressed by the Arrhenius equation.

$$k = Ae^{-E_A/RT} \quad 2-18$$

where  $E_A$ , stands for the *activation energy*,  $\text{kJ}\cdot\text{mol}^{-1}$ ,  $A$  is the *frequency factor*.  $R$  is the gas constant, and  $T$  is reaction temperature. Although the equation is oversimplified, it reveals the relationship between the activation energy and the rate constant.

For one-step, one-electron reaction, through the relationship between the current and the reaction rate, the dependence of the current density on the surface potential and the composition of the electrolytic solution adjacent to the electrode surface is given by the Butler-Volmer equation (Bard and Faulkner, 2001):

$$i = i_{cathode} - i_{anode} = FAk^0(C_O(0,t)e^{-\alpha f(E-E^0)} - C_R(0,t)e^{f(1-\alpha)(E-E^0)}) \quad 2-19$$

where  $A$  is the electrode surface area through which the current passes,  $k^0$  is the *standard rate constant*,  $\alpha$  refers to the *transfer coefficient* its value lies

between 0 and 1 for this one electron reaction,  $f$  is the  $F/RT$  ratio.  $t$  and  $0$  in the bracket are, respectively, the specific time at which this current occurs and the distance from the electrode. For the half reaction R(2-1),  $C_o(0,t)$  stands for the concentration of reaction species at cathode in the oxidised state, the hydrogen ions ( $H^+$ ), while  $C_R(0,t)$  is the concentration of reaction product hydrogen  $\frac{1}{2}H_2$ , which is in the reduced state.

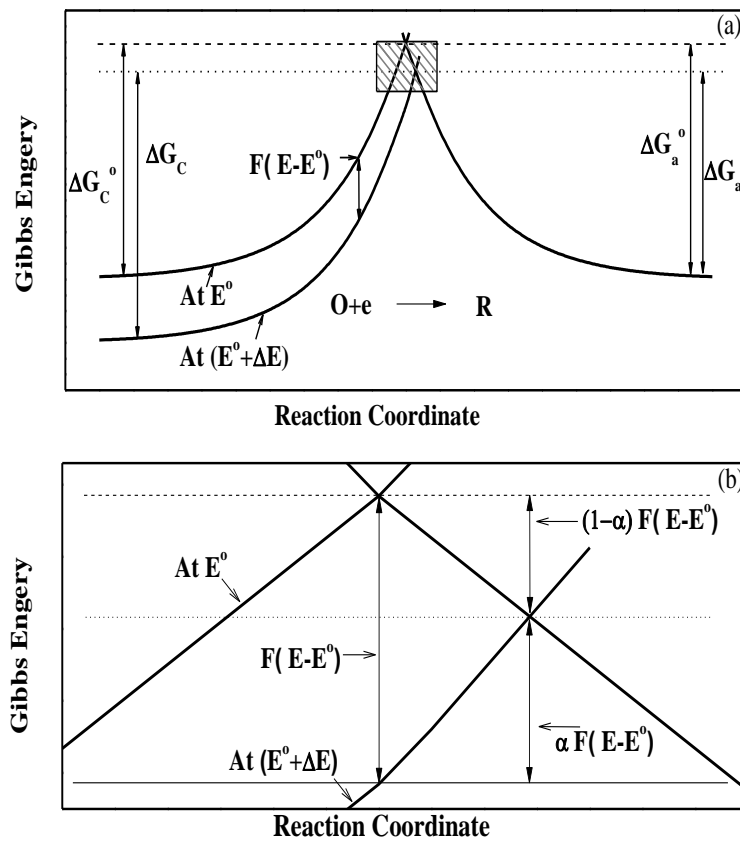


**Figure 2-5 Effect of potential change on Gibbs energy energies: (a) the overall relationship between energy change and state of reaction and (b) Magnified picture of shaded area of (a)**

Equation 2-19 is derived using the transition-state-theory (Bard and Faulkner, 2001). The theory describes a set of curvilinear coordinates in the reaction path as shown in Figure 2-5 (a). The potential energy is a function of the independent positions of the coordinates in the system. When a potential increase by  $\Delta E$ , it will cause the relative energy of the electron to

decrease by  $F(E-E^\circ)$  as illustrated in Figure 2-5 (a). The decrease in turn reduces the Gibbs free energy of the hydrogen ions in the hydrogen evolution reaction by  $(1-\alpha)(E-E^\circ)$  and, on the contrast, increases the Gibbs free energy of hydrogen by  $\alpha(E-E^\circ)$ , respectively. Therefore, provided that there is no mass transfer limitation, the Butler-Volmer equation can be derived from Equations 2-17 and 2-18 using the Gibbs free energy changes in Figure 2-5.

The Butler-Volmer equation can be simplified as:

$$i = i_0 (e^{-\alpha f \eta} - e^{(1-\alpha) f \eta}) \quad 2-20$$

where  $i_0$  is known as the exchange current density (Rieger, 1987), which is the current of the reversible water splitting reaction. From the simplified equation above, we can derive the over-potential at each electrode, respectively. In the absence of the influence of mass transfer and at the large overpotentials ( $> 118\text{mV}$  at  $25^\circ\text{C}$ ), one of the terms in Equation 2-20 can be neglected. For example, at large negative overpotential,  $e^{-\alpha f \eta} > e^{(1-\alpha) f \eta}$ . the relationship between  $i$  and  $\eta$  can be written in the Tafel equation (Abouatallah *et al*, 2001):

$$\eta = a + b \log i \quad 2-21$$

$$\text{where } a = \frac{2.3RT}{\alpha F} \log i_0 \text{ and } b = \frac{-2.3RT}{\alpha F}$$

The linear relationship between the overpotential and the logarithm of current density is characterised by the slope  $b$  and exchange current density  $i_0$ . The slope is also known as Tafel slope. Both parameters are commonly used as kinetic data to compare electrodes in electrochemistry and therefore

are also adopted as the main parameters for comparing and evaluating the electrode reactions and electrode materials in this thesis.

From the above analysis, the rate of the electrolysis can be expressed by the current or current density. Furthermore the current can be reflected by  $i_0$ , which is the current associated with the reversible reaction on the surface of the electrodes. The rate of the reaction is also directly determined by the overpotential, which depends on a number of factors. One of the important factors is the activation energy,  $E_A$ , which is strongly influenced by the electrode material, thus a focus of continuing research effort. To reduce the activation energies of the electrode reactions, or reduce the overpotential, it is therefore necessary to consider how they are related to the electrode materials and surface configurations.

#### 2.1.5.1 Hydrogen Generation Overpotential

The mechanism of the hydrogen evolution reaction is widely accepted (Bockris *et al*, 1981) to be a step involving the formation of adsorbed hydrogen



which is followed by either chemical desorption



or electrochemical desorption



where the subscript *ads* represents the adsorbed status.

The overpotential of hydrogen is generally measured by the Tafel equation

$$\eta_{cathode} = 2.3 \frac{RT}{\alpha F} \log \frac{i}{i_0} \quad 2-22$$

In this equation,  $i_0$ , the exchange current density of the reaction, which can be analogized as the rate constant of reaction, is a function of the nature of the electrode (cathode) material (Newman, 1991). The overpotential of the hydrogen production means extra energy barrier in the process of hydrogen formation.

The overpotential on the cathode is directly related to the formation of hydrogen in the vicinity of the electrode. The formation of hydrogen is intrinsically determined by the bond between hydrogen and the electrode surface. Pd has the lowest heat of adsorption of hydrogen ( $83.5 \text{ kJ}\cdot\text{mol}^{-1}$ ) as compared to  $105 \text{ kJ}\cdot\text{mol}^{-1}$  for Ni (Trasatti, 1971). Meanwhile, the hydrogen formation is also influenced by the electrode properties, the type and concentration of electrolyte and temperature. By comparing the kinetic data including the exchange current density and Tafel slope, the relationship between these factors can be revealed. Table 2-1 compares the kinetic parameters, represented by the current density and Tafel slope, of the hydrogen evolution reactions on different metal electrode materials.

**Table 2-1 Kinetics parameters of hydrogen production on different electrode metals**

Metal	Heat of adsorption $\text{kJ}\cdot\text{mol}^{-1}$	$\text{H}_2$ Electrolyte	T $^{\circ}\text{C}$	$i_0$ $\text{A}\cdot\text{m}^{-2}$	Tafel slope mV
Ni (Krstajic <i>et al</i> , 2001b)	105	1M NaOH	20	$1.1 \times 10^{-2}$	121
Fe (De Chialvo and Chialvo, 2001)	109	2M NaOH	20	$9.1 \times 10^{-2}$	133
Pb (Lee, 1971)	N/A	6N NaOH	25	$4 \times 10^{-2}$	121
Zn (Lee, 1971)	N/A	6N NaOH	25	$8.5 \times 10^{-6}$	124
Co(Correia <i>et al</i> , 1999)	N/A	0.5M NaOH	25	$4.0 \times 10^{-3}$	118
Pt (Bockris <i>et al</i> , 1981)	101	0.1N NaOH	22	4.0	105
Au (Bockris <i>et al</i> , 1981)	N/A	0.1N NaOH	25	$4.0 \times 10^{-2}$	120

For hydrogen evolution reaction, it is necessary to identify the rate determining step. If the hydrogen adsorption, Reaction R(2-4), is the rate determining step, electrode material with more edges and cavities in its surface structure which favour easy electron transfer will create more electrolysis centres for hydrogen adsorption. If the hydrogen desorption, Reaction R(2-5) and R(2-6), are the rate determining step, physical properties such as surface roughness or perforation will either increase the electron transfer by adding reaction area or preventing the bubbles from growing, which in turn increase the rate of electrolysis.

Increasing the overpotential could lead to a mechanism change. In other words, the rate determining step will alter within different potential ranges. When the potential is low, the electron transfer is not as fast as desorption. The hydrogen adsorption will be the rate determining step. On the contrast, when the potential is high enough to enable the hydrogen adsorption rate to be greater than the desorption rate, the hydrogen desorption will be the rate determining step.

### 2.1.5.2 Oxygen Generation Overpotential

The mechanism of oxygen evolution reaction is more complex compared to the pathways suggested for the hydrogen evolution reaction. There are a number of theories presented and discussed in the literature and the most generally accepted mechanism involves the following steps:



One of the charge transfer steps is rate controlling. The dependence of transfer coefficients  $\alpha$  in Equation 2-19 and Tafel slope variations can be used to identify the rate determining step. For example, a slow electron transfer step (R(2-7)) determines the reaction at low temperatures, on the contrast, a slow recombination step (R(2-9)) controls at high temperatures on nickel electrode. The different Tafel slopes between the steps can be used to judge the mechanisms (Pickett, 1979, Choquette *et al*, 1990).

The overpotential of oxygen evolution reaction is generally measured by the Tafel equation

$$\eta_{anode} = 2.3 \frac{RT}{(1-\alpha)F} \log \frac{i}{i_0} \quad \text{2-23}$$

The reaction rate decreases with increasing activation energy, so reducing the activation energy is always favoured for more efficient water electrolysis. Furthermore, the activation energy increases with increasing current density and can be lowered by using appropriate electrocatalysts. Table 2-2 below compares the kinetic parameters, again represented by the

current density and Tafel slope, of oxygen evolution reactions on different metal electrode materials.

**Table 2-2 Kinetic parameters of oxygen production on different metals**

Metal	Electrolyte	Temperature °C	$i_0$ $A \cdot m^{-2}$	Tafel slope mV
Pt (Miles <i>et al</i> , 1978)	30% KOH	80	$1.2 \times 10^{-5}$	46
Ir (Damjanov.A <i>et al</i> , 1966)	1 N NaOH	N/A	$1.0 \times 10^{-7}$	40
Rh (Damjanov.A <i>et al</i> , 1966)	1 N NaOH	N/A	$6.0 \times 10^{-8}$	42
Ni (Miles <i>et al</i> , 1976)	50% KOH	90	$4.2 \times 10^{-2}$	95
Co (Miles <i>et al</i> , 1978)	30% KOH	80	$3.3 \times 10^{-2}$	126
Fe (Miles <i>et al</i> , 1978)	30% KOH	80	$1.7 \times 10^{-1}$	191

Generally speaking, the overpotential of oxygen evolution is more difficult to reduce than that of hydrogen evolution, owing to the complex mechanism and irreversibility. Alloys of Fe and Ni have been found to be able to reduce the overpotential to some extent (Potvin and Brossard, 1992).

### 2.1.5.3 Cell Overpotential

As shown above, the hydrogen and oxygen overpotentials can be expressed by Equations 2-22 and 2-23. A typical plot in Figure 2-6 is the Tafel plot as a function of Equation 2-21 in water electrolysis. The parameters used to compare the electrode kinetics are the exchange current  $i_0$  and the Tafel slope. A higher exchange current density and lower slope indicate a higher electrode activity.

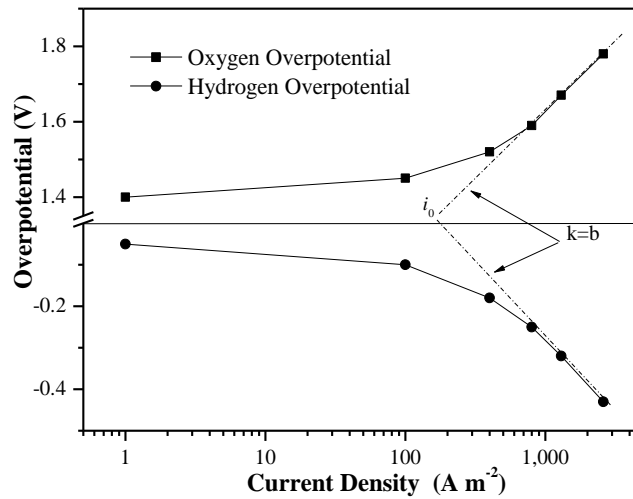


**Figure 2-6 Typical Tafel plots for both hydrogen and oxygen evolution**

Since the cell potential contains both anode and cathode reactions, identifying the contributions of each of anode and cathode to the cell voltage and factors influencing them are necessary to understand the overpotential resistance. The typical effect of temperature on the overpotential is summarised by Kinoshita (Kinoshita, 1992). As shown in the Figure 2-7 an increase in temperature will result in a decrease in the overpotential at the same current density.

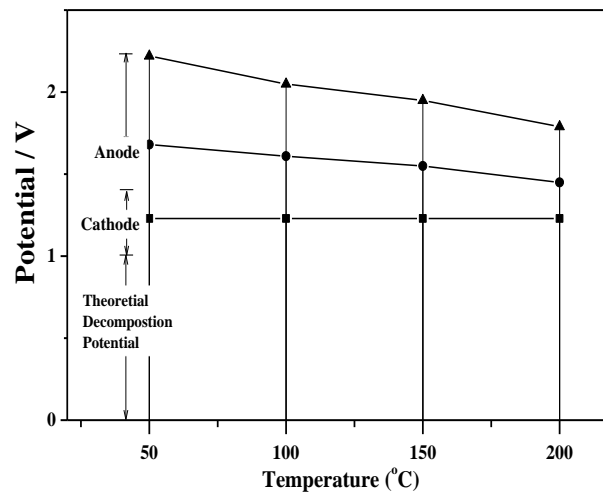


**Figure 2-7 An illustration of the contributions of anode and cathode polarisation to the cell voltage of an alkaline water electrolysis cell**

The overpotential is not only a function of temperature but also a function of current density (Leroy, 1983). As can be seen from Figure 2-8, the overpotentials from hydrogen and oxygen evolutions are the main sources of the reaction resistances. The other obvious resistance at high current densities is the Ohmic loss in the electrolyte, which includes resistances from the bubbles, diaphragm and ionic transfer. Understanding these resistances opens up opportunities to enhance the efficiency of the water electrolysis.

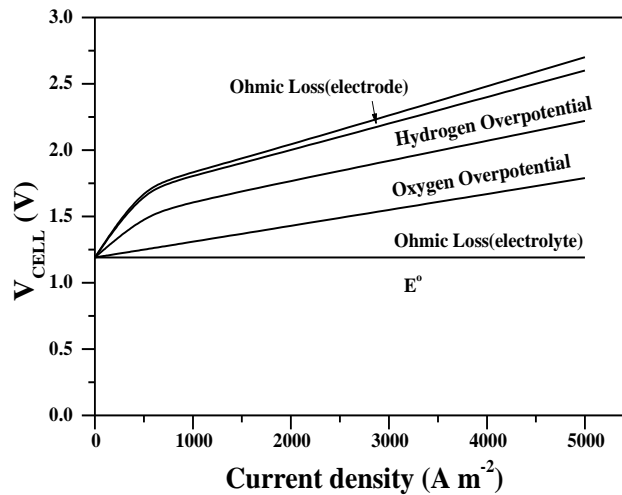


Figure 2-8 Compositions of the typical cell voltage of an alkaline water electrolysis cell

## 2.1.6 Electrochemical Reaction Resistances

### 2.1.6.1 Electrical Resistances

The electrical resistances are the direct reasons of heat generation which leads to the wastage of electrical energy in the form of heat formation according to the Ohms law. The electrical resistances in a water electrolysis system have three main components: (1) the resistances in the system circuits; (2) The mass transport phenomena including ions transfer in the

electrolyte; (3) The gas bubbles covering the electrode surfaces and the diaphragm.

The resistances of electrodes and connection circuits are determined by the types and dimensions of the materials, preparation methods, and the conductivities of the individual components. It can be expressed as follows:

$$R = \sum \frac{l}{A\kappa_g} \quad 2-24$$

where  $\kappa$  is the electrical conductivity and has the unit of  $\Omega^{-1} \cdot \text{m}^{-1}$ , subscript  $g$  stands for each component of the circuit, including wires, connectors and the electrode. This part of the resistance can be reduced by reducing the length of the wire, increasing the cross-section area and adopting more conductive wire material.

Ionic transfer within the electrolyte depends on the electrolyte concentration and separation distance between the anodes and cathodes, the diaphragm between the electrodes. Different from the conductance rate in the metallic conductor, the *Molar conductivity* is adopted to replace the conductivity and can be expressed as follows:

$$\Lambda = \frac{\kappa}{C} \quad 2-25$$

where  $\Lambda$  is the electrolyte concentration. The unit of the molar conductivity is  $\text{m}^2 \cdot \Omega^{-1} \cdot \text{mol}^{-1}$ . It is also a function of concentration and the mass transfer rate of the ions. As strong electrolytes are commonly applied in the water electrolysis, the empirical relationship between  $\Lambda$  and  $C$  is given in

$$\Lambda_c = \Lambda_0 - K\sqrt{C} \quad 2-26$$

where  $\Lambda_0$  is the mole conductivity extrapolated to infinite dilution which is known.  $K$  is the Kohlrausch coefficient, a proportionality constant of the linear relationship between molar conductivity and square root of concentration (Rieger, 1987). In terms of ionic resistance, improvements can be made by increasing the conductivity of the electrolyte by altering its concentration or adding appropriate additives.

The presence of bubbles in the electrolyte solution and on the electrode surfaces causes additional resistances to the ionic transfer and surface electrochemical reactions. One of the accepted theoretical equations to study the bubble effect in the electrolyte is given as follows (Crow, 1974):

$$\kappa_g = \kappa \times (1 - 1.5f) \quad 2-27$$

where  $\kappa$  is the specific conductivity of the gas-free electrolyte solution;  $f$  is the volume fraction of gas in the solution (Pickett, 1979). Quantitative illustration of the bubble resistance in terms of the bubble coverage on the surface and the bubble existence in the electrolytes needs to be considered. If we take bubble coverage into consideration, the bubble coverage is denoted as  $\theta$ , which represents the percentage of the electrode surface covered by the bubble. The electrical resistance caused by the bubble formation on the electrode surface can be calculated as follow (Hine and Murakami, 1980),

$$\rho = \rho_0 \times (1 - \theta)^{-3/2} \quad 2-28$$

where,  $\rho_0$  is the specific resistivity of the gas free electrolyte solution. If a diaphragm is used to separate the hydrogen and oxygen formed for collections, respectively, the presence of the diaphragm presents another

resistance to the ionic transfer. The resistive effect associated with the diaphragm is expressed by MacMullin (Macmullin and Muccini, 1956) for the apparent conductivity:

$$\kappa_d = 0.272 \frac{\kappa \times m^2}{p} \quad 2-29$$

where  $m$  is the hydraulic radius and  $p$  is the permeability. The effective resistance of a membrane frequently amounts to between three to five times more than the resistance of the electrolyte solution of the same thickness as that of the membrane (Pickett, 1979).

By dividing the overpotential by the current density, all of the resistances can be unified on the unit of ohm, which makes it possible to compare energy losses caused by different resistances as illustrated in Figure 2-9, where,  $E_{loss,electrolyte}$  includes energy losses due to the bubbles in the electrolyte and ionic transfer resistances. Figure 2-9 also shows that the energy losses caused by the reaction resistances increases relatively slowly as the current density increases. The energy loss in the electrical circuit is relatively small. However, the energy loss due to the ionic transfer resistance in the electrolyte becomes more significant at higher current density. The dot and dash lines are the bubble resistance and total resistance. The energy loss due to bubble coverage on the electrode surfaces, and thus the total energy loss are hypothetical, on the base of 50% electrode surface being covered by bubbles.

Figure 2-9 quantifies the major resistances that cause the energy loss. The bubble and electrode reactions are therefore the two main areas in this thesis.

The improved understanding of these resistances or the reduction of losses due to these resistances will help achieve the objectives of the thesis.

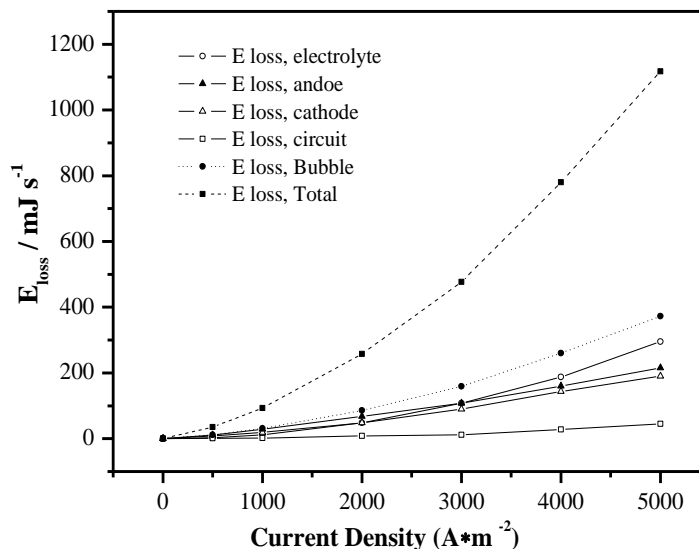


**Figure 2-9 A qualitative comparison of the energy losses caused by reaction resistances, ohmic resistance, ionic resistance and bubble resistance**

Although the relationship between the current density and energy loss in Figure 2-9 does not specify all of the resistances mentioned before, it approximately presents the relationships among the losses. More interestingly, the energy loss due to bubbles formed on the electrodes should be considered as the major contribution to the total energy loss. Therefore, minimising the bubble effect holds a key to the electrolyser efficiency improvement.

#### 2.1.6.2 Transport Resistances

Convective mass transfer plays an important role in the ionic transfer, heat dissipation and distribution, and gas bubble behaviour in the electrolyte. The viscosity and flow field of the electrolyte determine the mass (ionic) transfer, temperature distribution and bubble sizes, bubble detachment and rising

velocity, and in turn influence the current and potential distributions in the electrolysis cell. As the water electrolysis progresses the concentration of the electrolyte increases, resulting in an increase in the viscosity. Water is usually continuously added to the system to maintain a constant electrolyte concentration and thus the viscosity.

However, better mass transfer does not mean more hydrogen production. It is true that the mass transport leads to greater reaction rates, but the large number of gas bubbles formed, resulting from the increased reaction rate, can adversely hinder the contact between the electrodes and the electrolyte. The recirculation of electrolyte can be applied to mechanically accelerate the departure of the bubbles and bring them to the collectors.

The recirculation of the electrolyte is helpful in preventing the development of an additional overpotential due to the differences in electrolyte concentration in the cell. The velocity of fluid in the electrolyser can prompt the removal of the gas and vapour bubbles from the electrodes. On the other hand, the recirculation of the electrolyte can also help distribute the heat evenly within the electrolyte. At start-up, electrolyte circulation can be utilised to heat up the electrolyte to the operating temperature which is recommended to be 80-90°C (Dyer, 1985, Kinoshita, 1992).

### **2.1.7 Bubble Phenomena**

As electrolysis progresses, hydrogen and oxygen gas bubbles are formed on the surfaces of the anode and cathode, respectively, and are only detached from the surface when they grow big enough. The coverage of the electrode surfaces by the gas bubbles directly add to the electrical resistance of the

whole system, by reducing the contact between the electrolyte and the electrode, blocking the electron transfer, and increasing the ohmic loss of the whole system. Understanding the bubble phenomena is therefore an important element in the development of any water electrolysis systems. Mechanically circulating the electrolyte can accelerate the detachment of bubbles, providing a possible means to reduce the resistance due to gas bubbles. Alternatives are to consider the use of appropriate additives to the electrolyte solution to reduce the surface tension of the electrolyte and modifications of the electrode surface properties to make them less attractive to the gas bubbles.

Understanding the dynamics of the bubble behaviour is important in order to determine the conditions for the departure of the bubbles from the electrodes. The general thermodynamic condition for the three phase contact between the gas bubble, electrode and the electrolyte is a finite contact angle at the three phase boundary (Jones *et al*, 1999, Defay and Prigogine, 1966) as illustrated in Figure 2-10.

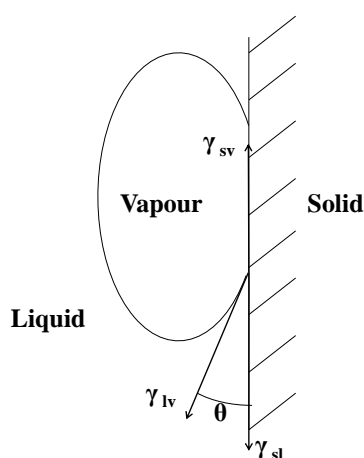


**Figure 2-10 An illustration of the contact angle at the three phase boundary of the gas bubble, electrode and the electrolyte**

The Young's equation defines the contact angle in terms of the three interfacial tensions (Adam, 1968),

$$\cos \theta = \frac{\gamma_{sv} - \gamma_{sl}}{\gamma_{lv}} \quad 2-30$$

Where  $\gamma_{sv}$ ,  $\gamma_{sl}$  and  $\gamma_{lv}$  are the surface tensions of the solid/vapour, solid/liquid and liquid/vapour interfaces, respectively. The Gibbs free energy change accompanying the replacement of the unit area of the solid/liquid interface by a solid/vapour interface

$$\Delta G = \gamma_{lv}(\cos \theta - 1) \quad 2-31$$

The detachment of the bubbles depends on the replacement of the electrolyte at the solid/solution interface, which is known as wettability (Kiuchi *et al*, 2006, Matsushima *et al*, 2003).

Two kinds of electrode surfaces can be defined according to the surface tension, namely, hydrophobic and hydrophilic. The electrode which favours water is hydrophilic, and the one does not is hydrophobic. Appropriate surface coating can therefore be applied to make the electrode surfaces more hydrophilic in order to reduce the surface coverage by the gas bubbles.

Therefore there are some broad approaches to manage the bubble phenomena. One is to treat the electrode surfaces to make them more hydrophilic so that water is more likely to take place of bubbles. Another is to use additives in the electrolyte solution to reduce surface tension so that bubbles are easy to depart from electrodes. In addition, controlling flow pattern to force bubbles to leave electrodes mechanically is also a means.

Intensive studies have been given to the bubble behaviour in the electrolysis systems (Vogt and Balzer, 2005, Kiuchi *et al*, 2006, Hine *et al*, 1975, Dejonge *et al*, 1982, Boissonneau and Byrne, 2000). It is a key issue to be resolved to overcome or reduce bubble resistance. Further detailed studies are necessary to further eliminate the negative effects of the bubbles.

## 2.2 Historical Development of Water Electrolysis

This section reviews the development of the water electrolysis over the past two hundred years since the discovery of the water electrolysis. From the discovery of the phenomenon of electrolytic split of water into hydrogen and oxygen to the development of various versions of industrial technique to meet the hydrogen demands of various applications, the water electrolysis development has gone through several landmarks. Some historical events of water electrolysis are listed in the Table 2-3.

**Table 2-3 Historical events of water electrolysis**

Year	Landmark Event
1800	Nicholson and Carlisle discovered the electrolytical splitting of water (Kreuter and Hofmann, 1998)
1920s	Several large 100 MW size plants were built worldwide (Leroy, 1983)
1948	First pressurized electrolyser was built by Zdansky/Lonza (Kreuter and Hofmann, 1998)
1966	First solid polymer electrolyte system was built by General Electric Company (Lu, 1979)
1970s	First solid oxide water electrolysis was developed (Spacil and Tedmon, 1969)

Those events in Table 2-3 promoted the development of this technology.

Generally, we may classify the developments of water electrolysis into five stages

1. The discovery and recognition of water electrolysis phenomena (1800s-1920s).

2. The technology became industrialised and mature for hydrogen production for industrial uses such as ammonia production and petroleum refining (1920s-1970s).
3. Systematic innovations were initiated to improve the net efficiency due to the fear of energy shortage and environmental considerations. The advancement in the space exploration drove the development of proton exchange membrane (PEM) water electrolysis, which is essentially the reverse of the PEM fuel cell operations, and military needs provoked the development of high pressure compact alkaline water electrolysis for submarine applications (1970s- present).
4. Rapidly evolving conceptual development to integrate water electrolysis with renewable energy technologies as a means for distributed energy production, storage and use as well hydrogen gas utilities, especially in remote communities (present).
5. Emergence of new water electrolysis concepts such as photovoltaic (PV) electrolysis that integrates the photoelectric effect and water electrolysis into one coherent operation, and steam electrolysis that employs a solid state electrolyte to effect the split of water molecules in steam (recent developments).

In the first stage, following the discovery of electricity, the phenomenon of water electrolysis was observed. Out of curiosity, the phenomenon was studied; the gases produced by electrolysis were finally identified to be hydrogen and oxygen (Kreuter and Hofmann, 1998), and gradually recognised for its potential applications. With the development of

electrochemistry, the proportional relationship between the electrical energy consumption and the amount of gases produced became established through the Faraday's law of electrolysis. Finally the concept of water electrolysis was scientifically defined and acknowledged (Rieger, 1987).

The second stage is the “golden” age for water electrolysis technology development. Most traditional designs were developed in this stage. Driven by the industrial need of hydrogen and oxygen, the knowledge established in the first stage was applied to the industrialisation of water electrolysis technologies. Stereotype of commercial water electrolysis developed at this stage contains some important technology components that are still being used today (Bowen *et al*, 1984).

One of the concepts still being applied in electrolyser is membrane. The function of membrane is to selectively allow the ions to pass through but not the gases. It realises the separation of the hydrogen and oxygen in the water electrolyzers with some inhibition on the ionic transfer. It was demonstrated that the benefits of being able to separate the hydrogen and oxygen gases outweigh the ohmic resistance brought about by the diaphragms. The first commercialised membrane is asbestos which was popular in the early stage. However, asbestos is not very resistant to corrosion due to the strong alkaline environment at elevated temperatures. More recently, due to its seriously adverse health effect, asbestos was gradually replaced by other materials (Rosa *et al*, 1995). Since the 1970s, the gas separation material has gradually shifted to polymers such as perfluorosulphonic acid, arylene ether and polytetrafluoroethylene (Hickner *et al*, 2004, Rosa *et al*, 1995).

Another significant development was the configurations of the electrolysis cells. As introduced before, they are monopolar and bipolar designs presented in the history. Typical conventional tank cells, with monopolar configuration, have the advantages of simplicity, reliability and flexibility. In contrast, filter press cells, with bipolar configuration, have the advantages of low ohmic loss and being more compact. High pressure electrolyzers using bipolar configuration would be hard to achieve with the monopolar cells. The disadvantages of bipolar cells are their structural complexity and requirement of electrolyte circulation and gas electrolyte separators.

The electrode material selection is based on a dedicated balance amongst the desires for the corrosion resistance, high conductivity, high catalytic effect and low price (Wendt and Kreysa, 1999). Stainless steel is a cheap electrode material with low overpotential, however, steel could not resist high concentration alkaline solutions. Other materials such as lead and noble metals are either not resisted to the alkaline or too expensive to be used as bulk materials for the electrodes. Nickel has been identified to be a very active material with better corrosion resistance to the alkaline than other transition metals. It became popular in the water electrolyzers during the electrolyser development. As compared in Table 2-1, nickel exhibits reasonable high hydrogen generation activity. Much research effort has been devoted to the understanding of the influence of physical property and the effects of the nickel-based alloys (Mauer *et al*, 2007, Bocca *et al*, 1998, Soares *et al*, 1992).

These developments stimulated the commercialisation of the electrolysis. The history of the commercial water electrolysis dates back to 1900, when

water electrolyser technique was still in its infancy. Two decades later, large size plants, rated at 100MW, were developed in Canada, primarily for the ammonia fertilisers (Leroy, 1983).

Electrolyser manufacturers all over the world made a great effort to build their own energy systems to meet different needs. By late 1980, Aswan installed 144 electrolysers with a nominal rating of 162 MW and a hydrogen generation capacity of  $32,400 \text{ m}^3 \cdot \text{h}^{-1}$ . Another highly modularised unit is the Brown Boveri electrolyser which can produce hydrogen at a rate of about 4 to  $300 \text{ m}^3 \cdot \text{h}^{-1}$ . A number of electrolyser companies and their water electrolysis units are listed and compared in Table 2-4:

**Table 2-4 Water electrolyser developers and cell operating conditions (Kinoshita, 1992)**

Parameter	De Nora S.A P	Norsk Hydro	Electrolyser Corp.Ltd.	Teledyne Energy systems	General Electric
Cell type	B-FP	B-FP	M-T	B-FP	B-FP
Anode	Expanded Ni-plated mild steel	Activated Ni-coated steel	Ni-coated Steel	Ni screen	PTFE-bonded noble metal
Cathode	Activated Ni-Plated steel	Activated Ni-coated steel	Steel	Ni screen	PTFE-bonded noble metal
Pressure (Mpa)	Ambient	Ambient	Ambient	0.2	0.4
Temperature °C	80	80	70	82	80
Electrolyte	29% KOH	25% KOH	28% KOH	35%	Nafion
Current density ( $\text{Am}^{-2}$ )	1500	1750	1340	2000	5000
Cell voltage (V)	1.85	1.75	1.9	1.9	1.7
Current efficiency (%)	98.5	98.5	>99.9	NR	NR
Oxygen purity (%)	99.6	99.3-99.7	99.7	> 98.0	> 98.0
Hydrogen purity (%)	99.9	98.9-99.9	99.9	99.99	>99.0

There are also some more companies not mentioned in this table. Stuart Cell (Canada) is the only monopolar tank-type cell manufacturer. Hamilton Sundstrand (USA), Proton Energy Systems (USA), Shinko Pantec (Japan) and Wellman-CJB (UK) are among the manufacturers of the latest PEM electrolyzers.

The key driver for the development of the water electrolysis technology in the first half the 20<sup>th</sup> century was the need of hydrogen for the production of ammonia fertilisers which was also facilitated by the low cost of hydroelectricity. As the massive hydrocarbon energy was increasingly applied in the industry, the economical advantage of water electrolysis gradually faded as coal gasification and natural gas reforming became able to produce hydrogen in large scales at much lower costs. This resulted in the cease of the progress of the water electrolysis technology as a means for hydrogen production. However, the oil crisis in the 1970s provoked a renewed interest in water electrolysis worldwide and hydrogen was considered as the future energy carrier (Bockris *et al*, 1981).

After the energy crisis in the 1970's, hydrogen as an energy carrier was considered a promising method to solve the energy security and sustainable energy supply problems, in the hydrogen economy ideology. Hydrogen production by water electrolysis received renewed interest and improving efficiency becomes a major goal. Some novel breakthroughs have been achieved at the cell system level with the emergence of pressurised electrolyzers and PEM electrolyser (Pletcher and Walsh, 1990).

Compact high pressure water electrolyzers have been utilised to produce oxygen on board of nuclear powered submarines as part of the life support

system. An important feature of the design is the elimination of gaskets between cells which necessitates high precision machining of the cell frames. The deficiency of high pressure electrolyser is the characteristic pressure of the system up to 3.5 MPa, posing a great demand for safety (Bockris *et al*, 1981).

For special energy need in the space area, a thin Nafion membrane was first applied by General Electric in 1966 (Pletcher and Walsh, 1990). The discovery of proton exchange membrane (PEM), realised the PEM water electrolysis, also named as solid polymer electrolysis (SPE). In an operation that reverses the PEM fuel cell, the PEM functions as the electrolyte to transfer the proton. Intensive studies have been carried out in order to reduce the cost of the membrane manufacturing. Subsequently, small scale PEM water electrolyzers were used for military and space applications in the early 1970s. However, the short durability of membrane makes PEM electrolyzers too expensive for general applications (Lu, 1979).

PEM water electrolysis systems offer several advantages over traditional alkaline water electrolysis technologies including greater energy efficiency, higher production rates, and more compact design (Marshall *et al*, 2007, Grigoriev *et al*, 2006). However, there are several disadvantages of the PEM electrolysis. PEM electrolyzers have more special requirements on the components, including expensive polymer membranes and porous electrodes, and current collectors (Barbir, 2005).

A comparison of typical alkaline and PEM electrolyzers are summarised in Table 2-5

**Table 2-5 A comparison of the two types of commercialised electrolyzers (Pletcher and Walsh, 1990)**

Parameter	Monopolar electrolyser	Alkaline	PEM electrolyser / Cell
Cell voltage	1.85		2V
Number of cells	N/A		7-51
Current density	0.25 A·cm <sup>-2</sup>		1.075 A·cm <sup>-2</sup>
Temperature	70°C		65°C (outlet)
Current	10kA		1kA (maximum)
Scale	200kW		N/A
Hydrogen production rate	42 m <sup>3</sup> ·h <sup>-1</sup>		0.42 m <sup>3</sup> ·h <sup>-1</sup>
Oxygen production rate	21 m <sup>3</sup> ·h <sup>-1</sup>		0.21 m <sup>3</sup> ·h <sup>-1</sup>
Hydrogen gas purity	H <sub>2</sub> >99.5%		H <sub>2</sub> >99.995%
Oxygen gas purity	O <sub>2</sub> >99%		O <sub>2</sub> >99%
Demineralized water conductivity	N/A		κ < 0.25 S·cm <sup>-1</sup>

## 2.3 Research Development and Trend

### 2.3.1 Electrode Material Searching

Metal electrodes are normally adopted in the gas evolving processes. As discussed in kinetics and the development of electrolyser sections earlier, the most widely used electrode material is nickel because of its stability and favourable activity. However, deactivation is a main problem of the electrode material even for nickel. The mechanism of the deactivation of the nickel electrodes is nickel the hydride phase formation at the surface of the nickel electrodes due to high hydrogen concentration. The iron coating prevents nickel hydride phase from forming and hence prevents deactivation of the electrode (Mauer *et al*, 2007). Dissolved vanadium species are also found to activate nickel cathodes during hydrogen evolution in the alkaline media (Abouatallah *et al*, 2001). Addition of iron to the manganese–

molybdenum oxides enhanced the stability of electrodes. The iron addition also enhanced the oxygen evolution efficiency. The formation of the nickel triple oxides seems responsible for the enhancement of both oxygen evolution efficiency and stability (Abdel Ghany *et al*, 2002). Therefore, electrocatalysts are the key to enhancing and stabilising the electrode activity.

Apart from material selection, electrode modifications in cell design are also important in water electrolysis. The electrode surfaces are commonly modified by slits and holes to facilitate the escape of gas bubbles. The holes must be appropriate to prevent the gas trapping. Typical diameters for electrode perforation in alkaline water electrolysis are 0.1 and 0.7 mm for hydrogen and oxygen, respectively (Wendt and Kreysa, 1999). Louvered, finned or slotted electrodes are also used to remove bubbles.

### 2.3.1.1 Electrocatalysts

To some extent, the electrode itself is a catalyst by affecting the activation energy of the electrochemical reaction. However, doping or coating more stable and active layer is always used in electrode design. Similar to catalysts, electrocatalysts facilitate charge transfer or chemical reaction, reducing the activation energy of the reaction. The obvious effect of an electrocatalyst is to reduce the overpotential of either or both of the two half reactions. The role of the electrocatalyst is affected by the electronic structure of the electrodes. In the hydrogen evolution reaction, Ni, Pd, Pt with  $d^8s^2$ ,  $d^{10}s^0$ , and  $d^9s^1$  electronic configurations, exhibiting minimum overvoltage values and Zn, Cd, Hg with  $d^{10}s^2$  electronic configuration showing maximum values. The spillover theory in electrocatalysis by

Bockris and Mchardy enables the understanding of the interaction between substances (Bockris *et al*, 1981).

Alloys, with different electronic distributions in the metal, are adopted to improve the activity of electrodes. For example, alloy of Mo and Pt was found to be a significant upgrade of the electrolytic efficiency in comparison with its individual components and conventional cathode materials (Stojic *et al*, 2006). More examples are listed in Table 2-6. The Tafel slope and exchange current density of the hydrogen evolution reaction in alkaline solutions at temperature near 70°C are used to compare the activities of Ni and Ni based alloy.

**Table 2-6 Tafel slopes of Ni alloys**

Material method	and Preparation	Electrolyte	Temperature °C	Tafel slope mV	$i_0$ A·cm <sup>-2</sup>	$\eta_{250}$ mV
Ni (wire) 1987)	(Huot and Brossard, 1987)	30% NaOH	70	99	$5.5 \times 10^{-5}$	362
Ni <sub>79</sub> Mo <sub>20</sub> Cd 1986)	(Conway and Bai, 1986)	1M NaOH	70	125	N/A	N/A
Ni <sub>70</sub> Mo <sub>29</sub> Si <sub>5</sub> B <sub>5</sub> (amorphous) (Huor <i>et al</i> , 1989)		30% KOH	70	118	$1.8 \times 10^{-6}$	489

The doping material could be chosen from a wide range of metals. Noble metals are commonly used as electrocatalysts. Ruthenium dioxide (RuO<sub>2</sub>), prepared by pyrolysis and calcinations, clearly shows the electrocatalytic activity for oxygen evolution reaction.(Ma *et al*, 2006). An anode electrocatalyst with the formula Ir<sub>x</sub>Ru<sub>y</sub>Ta<sub>z</sub>O<sub>2</sub> has been claimed to achieve overall voltage of 1.567V at 1A·cm<sup>-2</sup> and 80 °C, equating to an energy consumption of 3.75kWh·N·m<sup>-3</sup> H<sub>2</sub> and an efficiency of 94% with the total noble metal loading less than 2.04 mg·cm<sup>-2</sup> (Marshall *et al*, 2007). Non-

noble metals also find their electrocatalytic activities. The Li doping increases the electrical conductivity of these materials. The key to better performance is that the roughness factor increases with Li percentage up to 3% of Li, favouring oxygen evolution (Hamdani *et al*, 2004).

The physical properties of electrode materials also influence the electrocatalytic activity. Larger BET surface area and porosity of the oxide catalyst powder is found by the small La addition by Singh *et al* (2007). They observed a reduction in the charge transfer resistance for the oxygen evolution reaction on the electrode made of oxide powder.

Nanostructures have also received much attention as it enlarges the material surface area and enables a unique electronic property. The increased active area of the nanostructured electrode reduces the operating current density of the electrolyser. A 25% reduction in overpotential and 20% reduction in energy consumption were achieved by the use of the Ru nano-rod cathode compared to the planar Ru cathode. The improvement was attributed to the increased active area of the nanostructured electrode which reduces the operating current density of the electrolyser (Kim *et al*, 2006). Prashant V. Kamat (Kamat, 2007) also proposed different nanostructures for improving the performance of photoelectrolysis facilitating the charge transfer, which has the potential to be applied as electrodes for water electrolysis.

The preparation methods of electrodes are an important factor in terms of effecting electrode surface properties such as roughness. Coatings are another common technique in electrode preparation. For example composite of Ni, Fe and Zn prepared from the electrodeposition showed good stability for up to 200 h under the current density of  $1350 \text{ A}\cdot\text{cm}^{-2}$ . This material

showed good activity as well; in 28% KOH under 80 °C its overpotential is about 100 mV which is significantly lower than that of mild steel (400 mV) (Giz *et al*, 2000). A catalyst-coated membrane (CCM) with a five-layer structure was developed (Song *et al*, 2007). The five-layer CCM exhibits the highest performance and stability, attributed to the expansion of the triple-phase boundaries for electrochemical reactions and the improvement of contact and mass transfer resistance.

Table 2-7 and Table 2-8 list several electrocatalysts which are found helpful to reduce the overpotential or stabilise the electrodes of the industrial water electrolysis.

**Table 2-7 Oxygen overpotential of different electrode materials**

Composition	Method	T	Electrolyte	C	j	$\eta_{O_2}$	Reference
Formula		°C		mol·dm <sup>-3</sup>	A·m <sup>-2</sup>	mV	
Ni + Spinel type Co <sub>3</sub> O <sub>4</sub>	Thermo-decomposition	25	KOH	1	1000	235±7	(Singh <i>et al</i> , 2007)
Ni + La doped Co <sub>3</sub> O <sub>4</sub>	Thermo-decomposition	25	KOH	1	1000	224±8	(Singh <i>et al</i> , 2007)
MnOx Au	Modified Electro-deposition	25	KOH	0.5	100	300	(El-Deab <i>et al</i> , 2007)
Li10% Co <sub>3</sub> O <sub>4</sub>	doped Spray Pyrolysis	RT <sup>1</sup>	KOH	1	10	550	(Hamdani <i>et al</i> , 2004)
Ni	N/A	90	KOH	50wt%	1000	300	(Wendt <i>et al</i> , 1989)
La <sub>0.5</sub> Sr <sub>0.5</sub> CoO <sub>3</sub>	Spray-stiner	90	KOH	50wt%	1000	250	(Wendt <i>et al</i> , 1989)
Ni <sub>0.2</sub> Co <sub>0.8</sub> LaO <sub>3</sub>	Plasma Jet Projection	90	KOH	50wt%	1000	270	(Wendt <i>et al</i> , 1989)

Note: 1. Room temperature.

**Table 2-8 Hydrogen overpotential of different electrode materials**

Composition	Method	T	Electrolyte	C	j	$\eta_{H_2}$	Reference
Formula		°C		mol·dm <sup>-3</sup>	A·m <sup>-2</sup>	mV	
Ni-Fe-Mo-Zn	Co-deposition	80	KOH	6	1350	83	(Crnkovic <i>et al</i> , 2004)
Ni-S-Co	Electro-deposition	80	NaOH	28wt%	1500	70	(Han <i>et al</i> , 2003)
Ni50%-Zn	Electro-deposition	N/A	NaOH	6.25	1000	168	(Sheela <i>et al</i> , 2002)
MnNi <sub>3,6</sub> Co <sub>0,75</sub> Mn <sub>0,4</sub> Al <sub>0,27</sub>	Arc melting	70	KOH	30wt%	1000	39	(Hu, 2000)
Ti2Ni	Arc melting	70	KOH	30wt%	1000	16	(Hu and Lee, 1998)
Ni50% Al	Melting	25	NaOH	1	1000	114	(Los <i>et al</i> , 1993)
Ni75%Mo25%	Co-deposition	80	KOH	6	3000	185	(Raj, 1993)
Ni80%Fe18%	Co-deposition	80	KOH	6	3000	270	(Raj, 1993)
Ni73%W25%	Co-deposition	80	KOH	6	3000	280	(Raj, 1993)
Ni60%Zn40%	Co-deposition	80	KOH	6	3000	225	(Raj, 1993)
Ni90%Cr10%	Co-deposition	80	KOH	6	3000	445	(Raj, 1993)

To sum up, the physical modifications of electrodes help the removal of the gas from the electrodes. The electrode material influences the overpotential significantly. The electronic property and the surface property determine electrocatalytical performance of the coating or doping. Alloys, nano-structured materials, transition metals and noble metals could be used to improve the electrode activity. One of the specific objectives of this thesis is to reduce the electrode reaction resistance through electrode modification.

### 2.3.2 Electrolyte and Additives

Most commercial electrolyzers have adopted alkali (potassium or sodium hydroxide) solutions as the electrolyte. Energy consumption during the electrolysis of water was significantly reduced by small quantities of activating compounds by the effect of ionic activators (Stojic *et al*, 2007, Marceta Kaninski *et al*, 2004).

Ionic liquids (ILs) are organic compounds. At room temperature, they are liquids solely consisting of cations and anions, thus possessing reasonably good ionic conductivities and stability (Endres and El Abedin, 2006). Imidazolium ILs were used as an electrolyte for hydrogen production through water electrolysis. The current densities higher than  $200 \text{ A}\cdot\text{m}^{-2}$  and efficiencies greater than 94.5% are achieved using this ionic liquid in a conventional electrochemical cell with platinum electrodes at room temperature and atmospheric pressure. The catalytic activity of the electrode surface was not affected during the electrolysis mainly due to the chemical stability of the ILs (De Souza *et al*, 2006). However, the ILs normally have high viscosity and low water solubility which is not favoured for mass transport, resulting low achievable current densities and thus low hydrogen production rates. Therefore, more suitable ionic liquids with high conductivity and solubility are needed to facilitate electron transfer and water electrolysis, respectively.

Compared to the research on electrocatalysts, developmental effort on new electrolyte is relatively low. However, there is still a potential to improve the overall efficiency by using electrolyte additives to enhance ionic transfer by reducing the electrolyte resistance. On the other hand, the adoption of electrolyte additives could tune the affinity between electrolyte and electrodes and help to manage the bubble behaviour.

### **2.3.3 Bubble Management**

The bubble formation and its transportation are major causes of extra ohmic losses. Not only the dissolution of gas, but also the interface of gas between

electrodes and electrolyte lead to resistances to water electrolysis. An improved understanding of the bubble behaviour is critical to reduce the resistance caused by the bubbles, by bubble management.

The bubble behaviours are intensively studied (Jones *et al*, 1999, Vogt, 1989, Kiuchi *et al*, 2006) in the sense of electrochemistry, but no mechanisms or models have been applied to alkaline water electrolysis. Microgravity condition was used to study the bubble behaviours without the buoyancy effect. Water electrolysis under microgravity resulted in stable froth layer formation, and the accompanying ohmic resistance increased with the froth layer thickness. The contributions of electrode surface coverage by bubbles and electrolyte-phase bubble void fraction to the ohmic drop were also studied (Matsushima *et al*, 2003). Under territorial gravity, the bubble sizes are smaller. Therefore, reducing the residence time of bubble staying in the electrode is the key to minimising the bubble size and thus reducing the bubble resistance.

According to the theory of surface tension, a hydrophilic electrode prefers water rather than bubbles. It means the bubble sizes are not easy to grow. The mass transfer and ionic transfer between electrodes and electrolyte could be enhanced. Similarly, surfactant additive can be used to reduce the surface tension, which can minimise the bubble size or accelerate the departure of the bubbles and then achieve the same effect of hydrophilic materials. At the same time, these additives should be inert to the electrochemical reaction (Wei *et al*, 2007) and stable during the process.

Fluid mechanic means, by circulating the electrolyte solution to sweep the bubbles off the electrode surfaces can also be applied. To sweep the bubbles

off the electrode surface, the velocity of the fluid should be high enough, which in turn will benefit the mass transfer of the electrolyte and eliminate the concentration difference. Therefore, mechanically forcing the bubble to depart from the electrode surface is an alternative way to eliminate the bubble formed on the electrode surface.

## **2.4 Summary**

This Chapter examined the fundamentals of the water electrolysis. The gaps between current technology and the practical use are identified. The Chapter also reviewed the literature to identify the methodology, experimental techniques and approaches can be employed in this thesis.

Based on the thermodynamic and kinetic analyses of the alkaline water electrolysis, a number of resistances hindering the efficiency of the alkaline water electrolysis process have been identified. These include resistances due to bubbles, reaction activation energy, ionic transfer and electrical resistances in the circuit. The bubble resistance is suggested to be reduced by electrode modification and electrolyte additives. Reaction overpotential can be optimised by electrode material selection and preparation. In addition, transport-related resistances such as bubble resistance and electrolyte resistance can be reduced by improving mass transport such as bubble elimination by electrolyte circulation. By identifying the resistances causing extra energy losses, this study opens the opportunities to minimise the energy input especially at high current density.

Electrode kinetics is commonly used to compare the electrode reaction on water electrolysis. Tafel curve is commonly used and its parameters are normally used and will be presented in Chapter 3.

The specific objective of the present study are discussed as the further R&D efforts to improve the efficiency are needed to widespread the application of the alkaline water electrolysis. These include (1) identifying the resistances that cause the loss of energy efficiency and quantify them and find out the most significant ones for improvements by this research, (2) reducing electrochemical reaction resistance by modifying electrode preparation methods (3) reducing electrochemical reaction resistance by electrode surface profile modifications and surface coatings and (4) understanding bubble behaviour and managing the gas bubble resistances.

## **Chapter 3      Methodology,   Approaches   and Techniques**

### **3.1 Introduction**

To achieve the research aims and objectives outlined in Chapters 1 and 2, this thesis employs several experimental and analytical techniques. This chapter details experimental procedures and how the data was acquired. Then the analytical techniques and data analysis used in this thesis are also described. The justifications and limitations of these approaches and techniques are also discussed in this chapter.

Section 3.2 introduces the experimental techniques with three different experimental reactor designs and electrode preparation methods for the associated research objectives. Section 3.3 is concerned with various analytical techniques and data analysis. These techniques qualitatively or quantitatively characterise electrodes and the electrode reactions. Section 3.4 presents several data analysis techniques that enable the comparison of the electrode performances and the correlations between electrode, electrolyte, electrode reaction and bubble behaviour.

The research roadmap of the thesis regarding the experimental, analytical and modelling techniques is summarised and illustrated in Figure 3-1.

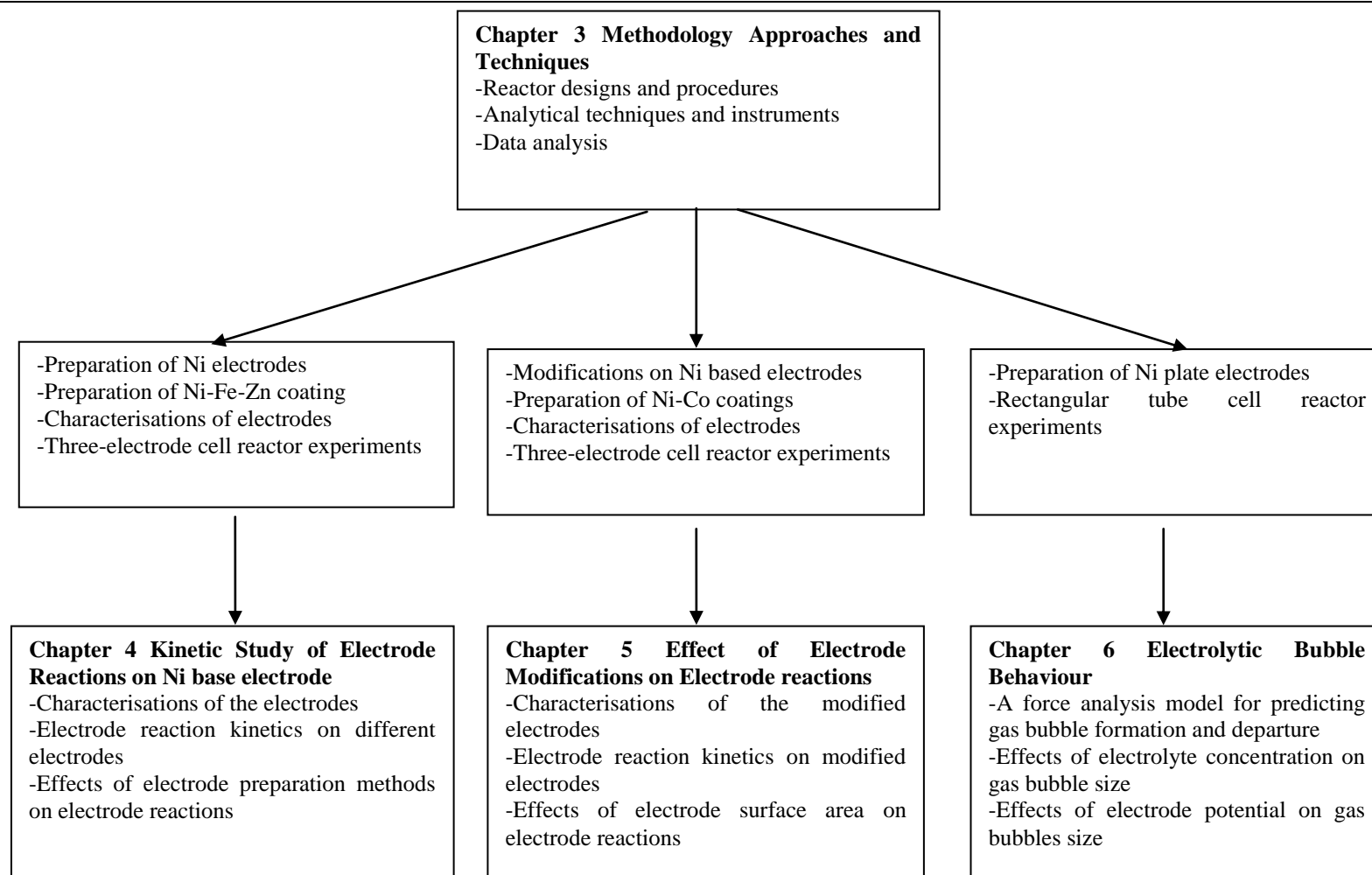


Figure 3-1 Research methodology map of the thesis structure

## **3.2 Experimental Designs and Materials**

As discussed in Chapter 2, the research aims of this thesis are: to evaluate the effects of electrode preparation methods on electrode reactions; to determine the effects of the electrode surface area on electrode reactions; to examine the behaviour and effects of electrolytic bubbles; to optimise a larger scale cell using the findings from the research objectives above. Therefore, two different experimental designs were designed and built for evaluating electrode reactions on Ni based electrodes, observing bubble phenomena and optimising the overall cell design, respectively. Although these reactors were for different purposes, they are presented in a similar flow. First, the reactor is presented, followed by electrode materials preparation and electrolytes preparation. Then, the experimental procedures are illustrated and explained. Finally, materials used in the experiment are listed.

### **3.2.1 Three-electrode Cell Reactor Experiments**

The three-electrode cell reactor was developed to evaluate electrode reactions on Ni based electrodes and is illustrated in Figure 3-2. It contains a lid and a Pyrex glass cell. The lid of the cell is made of plastic and moulded into several openings for inserting electrodes or other accessories such as thermometer. As shown in Figure 3-2 (a), the lid is able to accommodate three electrodes, a thermometer and a gas switch to import nitrogen or to vent the produced gases.

The cylindrical three-electrode cell reactor has a thermo-jacket layer and an inner layer. The thermo-jacket layer is for the circulation of water from a

water bath to keep the cell temperature constant. As shown in Figure 3-2 (b), two openings on the thermo-jacket layer are for the water inlet and outlet, respectively. The inner layer is for accommodating electrolyte with a maximum volume of 150ml. The electrolyte in the inner layer can be stirred with the help of a magnetic stirrer. The stirring provides a strong convection of the electrolyte solution to force the formed bubbles to detach from the electrode surfaces, minimising the bubble resistance. Figure 3-3 shows the actual picture of the three-electrode electrochemical cell.

The three-electrode cell system was used as the main reactor to evaluate the electrode reactions on various electrodes. The three electrodes were the working electrode, reference electrode and counter electrode, respectively. The reference electrode was not loaded with current, its potential was stable even under high current flowing in the cell (Bard *et al*, 2008). Therefore, the electrode potential could be accurately recorded.

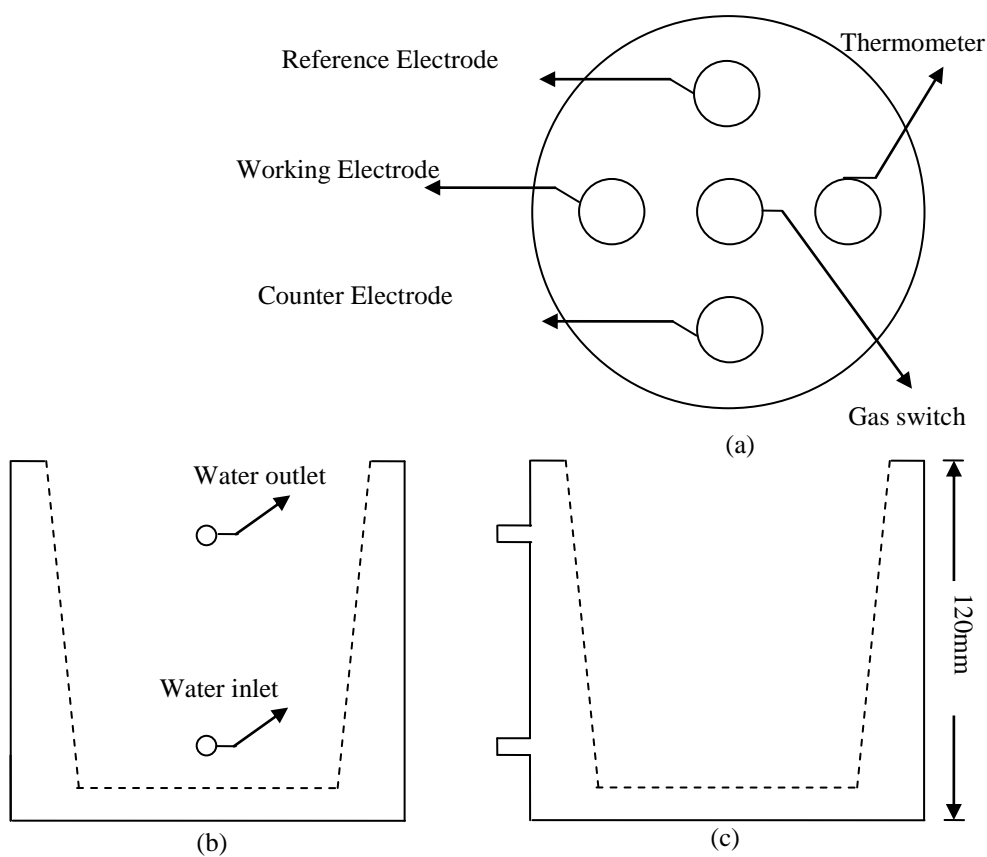


**Figure 3-2** An illustration of the three-electrode reactor. (a) the lid, (b) the main body (font view) (c) the main body (side view )



**Figure 3-3** The three-electrode electrochemical cell with the lid

### 3.2.1.1 Preparation of Ni Electrode and Ni-Fe-Zn Electrode

Ni electrodes were prepared by mounting a nickel disk onto the end of a copper rod of 2 mm in diameter using a silver conductive glue. The surface area of the nickel disk was  $3.14 \text{ mm}^2$ . The copper rod and silver conductive glue were used to provide a good electrical conduction for the nickel disk. The copper rod together with the mounted nickel disk was covered with two layers of epoxy resin and further two layers of plastic heat-shrunk tubes, leaving a length of 2 cm at the other end of copper rod uncovered for electrical connection. These resin coatings and heat-shrunk tubing layers were to prevent copper rod from contacting the electrolyte. By cutting and polishing off the excess resin and tube, only the face of the nickel disk of  $3.14 \text{ mm}^2$  was exposed to the electrolyte, serving as the base Ni electrode.

Similarly prepared Ni electrodes were then further polished with a serial of sandpapers made of silicon carbide with particle size from  $35\mu\text{m}$ ,  $18\mu\text{m}$  and  $10\mu\text{m}$  to  $5\mu\text{m}$ . Washing and ultrasound cleaning were applied after applying different sandpaper for polishing. The electrodes prepared with this procedure were denoted as Ni electrode.

Ni-Fe-Zn coated electrodes were prepared to alter the electrode surface structure (Solmaz *et al*, 2009, Giz *et al*, 2000, Mauer *et al*, 2007). The Ni-Fe-Zn electrodes were prepared with chemical deposition techniques using the Ni electrodes described above as substrates. The chemical deposition was performed in a Watt bath containing nickel sulphate  $300 \text{ g}\cdot\text{L}^{-1}$ , zinc sulphate  $0.7\text{g}\cdot\text{L}^{-1}$ , ferrous sulphate  $10 \text{ g}\cdot\text{L}^{-1}$ . The electrolysis time was 50 min under a current density of  $10\text{mA}\cdot\text{cm}^{-2}$ . After the deposition, the

electrode was treated by dipping electrode into a 6 M KOH solution for 6 hours.

#### **3.2.1.2 Mechanical Modification of Ni Electrode**

To mechanically modify electrodes to achieve different surface roughness, Ni electrodes prepared by mounting a nickel disk at the end of a copper rod served as the base Ni electrode. 3 sandpapers of different fineness, P400, P2000 and P4000, were applied to polish the three base Ni electrodes, respectively. The average grain sizes of these three sandpapers were 35, 10 and 5  $\mu\text{m}$ , respectively. The greater the sandpaper number, the smaller the sand grain size and thus the smoother the electrode surface after polishing. This allowed 3 Ni electrodes of different surface roughness to be prepared for further examination.

#### **3.2.1.3 Chemical Deposition of Ni-Co Coating**

Ni electrodes polished with the P4000 sandpaper were used as the substrates for cathode deposition of Ni and Co. When a cathodic potential is applied to a Ni electrode substrate, depending on the potential, the  $\text{Ni}^{2+}$  and  $\text{Co}^{2+}$  ions in the electrochemical deposition bath will be reduced, which forms a thin film on top of the Ni substrate (Fan and Piron, 1996). In this work, a cathodic current of  $30 \text{ mA}\cdot\text{cm}^{-2}$  was applied at room temperature. The electrochemical deposition bath contained 100ml of a solution of  $40\text{g}\cdot\text{L}^{-1}$   $\text{NiSO}_4$ ,  $4\text{g}\cdot\text{L}^{-1}$   $\text{CoSO}_4$ . and  $20\text{g}\cdot\text{L}^{-1}$   $\text{H}_3\text{BO}_3$ . To obtain Ni-Co coated electrodes and compare their activities, three coatings were prepared by varying the deposition duration, at 15, 30 and 60 minutes, respectively. The

resulting three electrodes were denoted as Ni-Co(1), Ni-Co(2) and Ni-Co(3), respectively.

#### **3.2.1.4 Three-electrode Cell Reactor Experimental Procedures**

A schematic illustration of the experimental three-electrode cell reactor system is illustrated in Figure 3-4. The three-electrode cell reactor experiments employed the prepared or the modified Ni electrodes to study the electrode reaction kinetics. The three electrodes were a Ni based electrode or modified Ni electrode as the working electrode, a silver/silver chloride electrode (SCE) as the reference electrode, and a Pt electrode of about 2 cm<sup>2</sup> in surface area serving as the counter electrode, respectively. 100ml of KOH electrolyte of different concentrations ranging from 0.5M to 4M were prepared and poured into the cell. Before each run, high purity nitrogen was purged into the cell through the gas switch to saturate the electrolyte solution with nitrogen. An actual image of the three cell reactor system is shown in Figure 3-5.

Water electrolysis was realised in the three-electrode cell. The temperature of the three-electrode cell was controlled by placing it in the water bath at 30±0.5°C. The electrolyte solution was stirred with a magnetic stirrer. Water electrolysis was realised by using potentiostat to apply potentials on the Ni based cathode against the SCE electrode, which will be further explained in the analytical approaches section. Then hydrogen evolution reaction and the oxygen evolution reaction occur on the Ni based electrode and the Pt electrode, respectively.

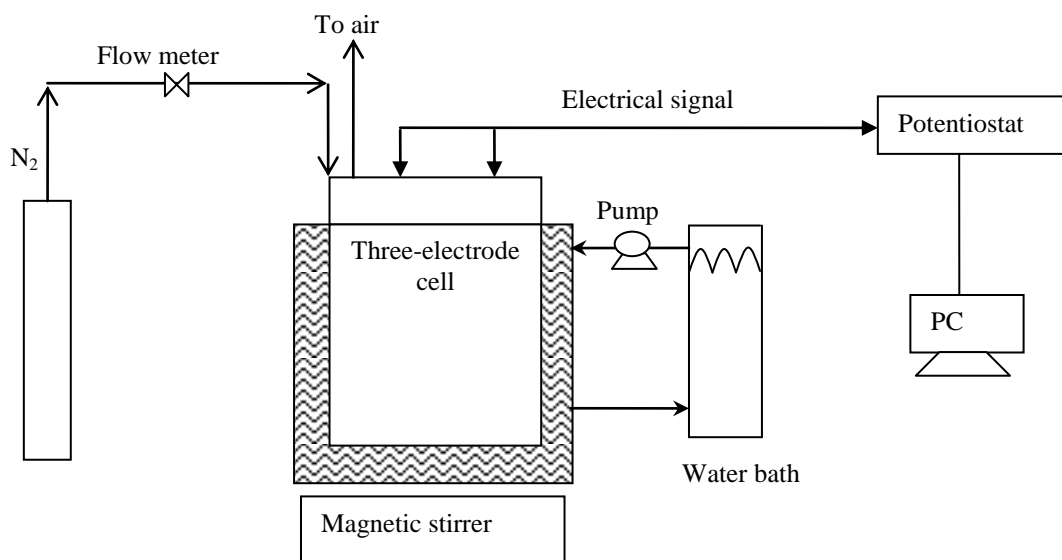


**Figure 3-4 A schematic illustration of the three-electrode reaction experimental setup**

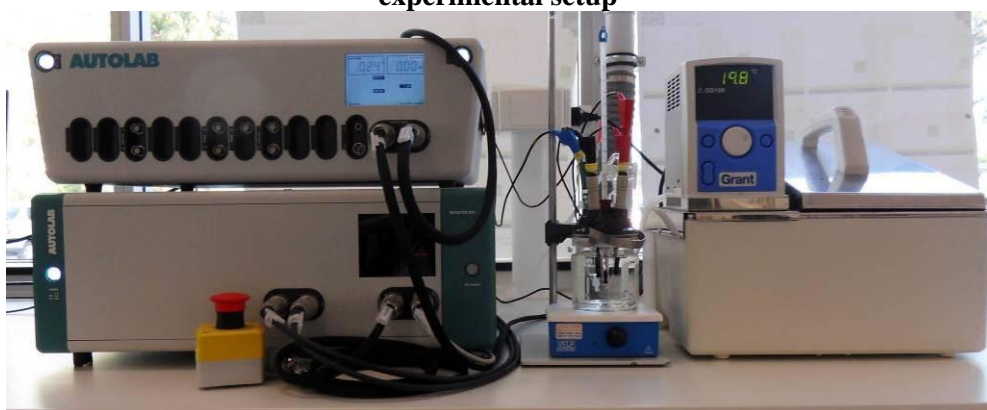


**Figure 3-5 An image of the experimental setup with three-electrode reactor, water bath and Autolab potentiostat**

### 3.2.2 Rectangular Tube Cell Reactor Experiments

The rectangular tube cell reactor was developed to observe bubble phenomena and is illustrated in the Figure 3-6. It contains a rectangular Pyrex tube cell. The both ends of the tube cell are cone tapered glass joints. As shown in Figure 3-6 (b), the top of the tube cell is connected to an electrode holder with two openings on both left and right sides for inserting anode and cathode respectively. The length of the tube cell is 200mm and

the inner width and depth of the tube are both 10mm. The actual image is shown in Figure 3-7.

Different from the three-electrode reactor design, the rectangular tube reactor was designed for observing the bubble behaviours. Therefore, it was designed in a rectangular configuration to minimise the image distortion that will occur in cylinder reactor. In this reactor design, although the detailed information regarding the potential of electrode reactions was missing, the design enabled the clear observation of the bubble growth.

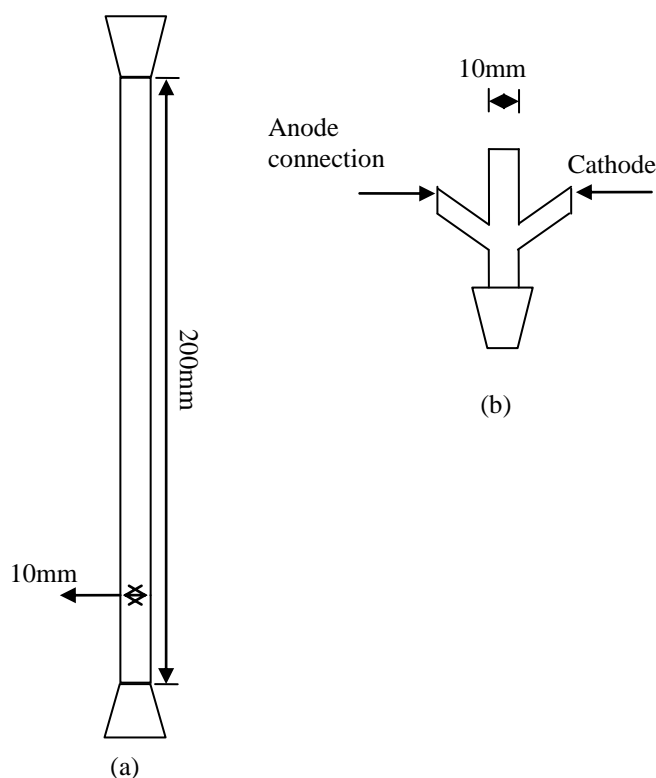


**Figure 3-6 An illustration of (a) rectangular tube cell and (b) the electrode holder**

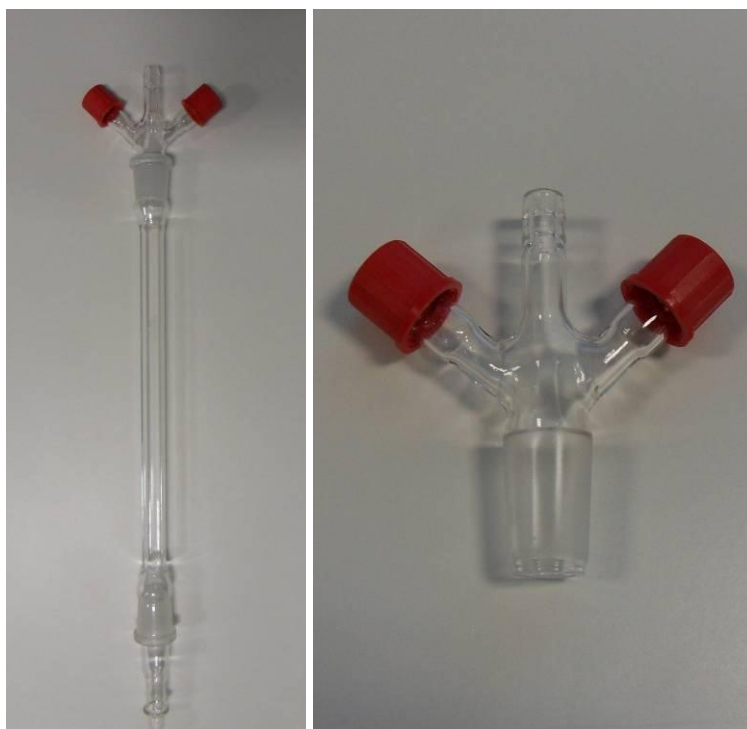


**Figure 3-7** An image of (a) rectangular tube cell and the electrode holder (b) the electrode holder

#### **3.2.2.1 Preparation of Ni Plate Electrodes**

The Ni plate electrode was prepared by cutting a nickel sheet into a square piece of 10mm×10mm. After polishing with P4000 sand paper and ultrasonic cleaning, the square nickel sheet was then soldered on a thin copper wire around 200mm long with a resistance less than 0.01Ω. The soldered side of the nickel sheet was then covered with epoxy resin. The resin was hardened in an oven at 110°C for ten minutes. Two Ni plates electrode were then glued together back to back using resin. Then another round of polishing and ultrasonic water washing was applied. The nickel plates prepared in such way was then used as anode or cathode.

#### **3.2.2.2 Rectangular Tube Cell Reactor Experimental Procedures**

A schematic of the rectangular tube cell reactor experimental system is illustrated in the Figure 3-8 and its image is shown in Figure 3-9. The rectangular tube cell reactor experiments employed the prepared Ni plate

electrodes as the anode and cathode to study the bubble behaviours. The electrodes were inserted in to the rectangular tube cell that both smooth nickel surfaces can be observed with a camera placed parallel to the rectangular tube cell.

The electrolytes were prepared at the desired concentrations and loaded in to the electrolyte container, respectively. Due to the difficulty of embracing a thermo-jacket in this design, all the electrolytes were kept in the water bath until it reached the desirable temperature. Then the electrolyte was pumped through the rectangular cell to circulate the electrolyte thus the desirable temperature can be achieved.

Water electrolysis was realised in the rectangular tube cell by using the potentiostat to apply potentials between anode and cathode, which will be further explained in the analytical approaches section.

To observe the electrolytic bubble behaviour, a CCD camera was used to record the growth and departure of the bubbles through the rectangular glass cell (Matsushima *et al*, 2009, Ma and Chung, 2001). The recorded videos can be used to extract frames to observe the sizes of the bubbles at a specific time, so that the size of bubble can be measured and compared.

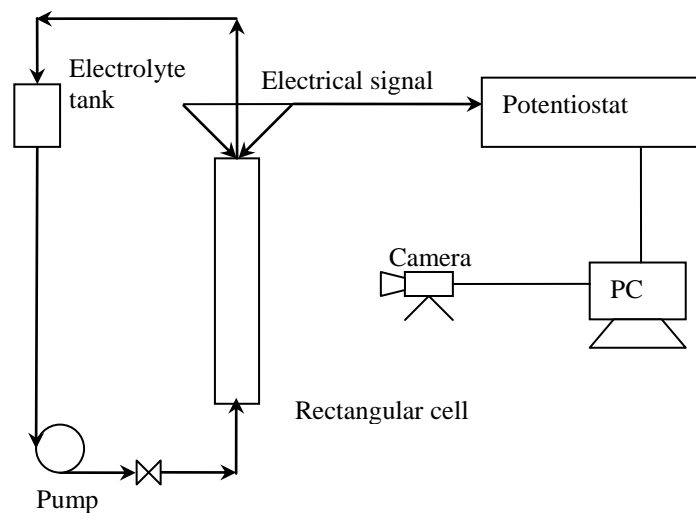


**Figure 3-8** A schematic illustration of rectangular tube cell experiments

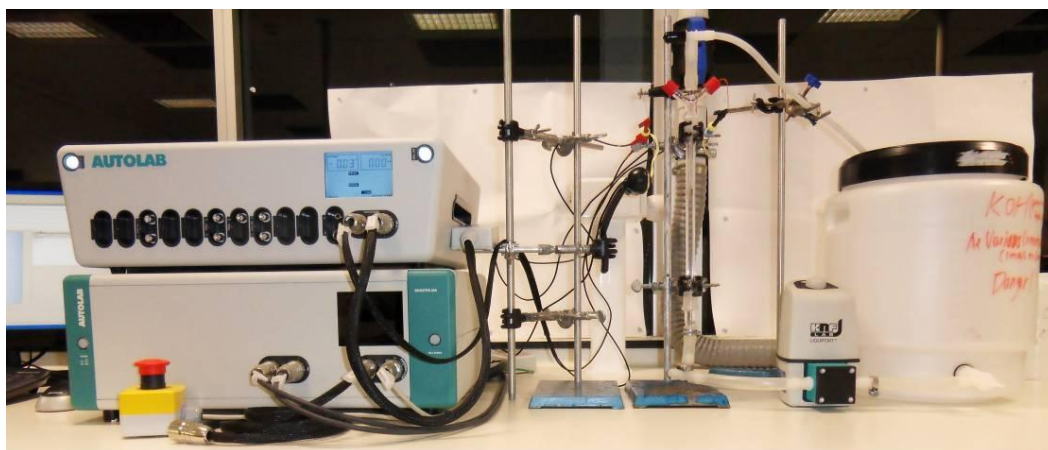


**Figure 3-9** A image of the rectangular tube cell experiments

### 3.2.3 Materials

The details of the chemicals and other materials used in this thesis are listed in Table 3-1.

**Table 3-1: Details and description of the chemical and other materials used in this thesis**

Item	Specifications	Company/Provider
Ni disk	$\Phi$ 1cm	Easycon
Copper Rod	$\Phi$ 1cm*10cm	Easycon
Silver conductive glue	-	Easycon
Epoxy resin	-	Easycon
Heat-shrink tube	-	Easycon
Sandpaper P400	35 $\mu$ m	Easycon
Sandpaper P2000	10 $\mu$ m	Easycon
Sandpaper P4000	5 $\mu$ m	Easycon
Ni Plate	Customised	
Ni <sub>2</sub> SO <sub>4</sub>	Nickel Sulphate	Ajax
Fe <sub>2</sub> (SO <sub>4</sub> ) <sub>3</sub>	Ferric sulphate	Ajax
ZnSO <sub>4</sub> ·7H <sub>2</sub> O	Zinc sulphate heptahydrate	Ajax
H <sub>3</sub> BO <sub>3</sub>	Boric Acid	Ajax
CoSO <sub>4</sub>	Cobalt sulphate hydrated	Ajax
KOH	Potassium hydroxide pellets	Ajax
Silver/Silver chloride reference electrode	-	Autolab
CCD camera	8M pixel	Logitech
KNF Corrosive resistance pump	0~3L·min <sup>-1</sup>	KNF
Tubing	Ø10mm	John Morris

### 3.3 Analytical Methods and Instrumentation

Several analytical techniques were used in the thesis which can be categorised into the following classifications which serve different purposes. Characterisation techniques are to enable the quantitative and qualitative analysis of the electrode surfaces profiles and compositions. Electrochemical techniques are to realise the quantitative comparison of the kinetics of electrode reactions on different electrodes or the cell performance. Image analysis technique is to provide a quantitative study of electrolytic bubble sizes.

### **3.3.1 Scanning Electron Microscopy (SEM)**

The electrode morphologies were examined using a ZEISS Scanning Electrode Microscopy (SEM) at the Centre for Microscopy, Characterisation and Analysis at The University of Western Australia. The Ni electrode samples were polished with sandpapers before SEM analysis. The surface profile and composition of the Ni electrodes with any further modification were examined right after modification. Images of all electrode samples were taken using Secondary Electron detector with appropriate accelerating voltages and magnifications for image collection.

### **3.3.2 Electron Dispersive X-Ray Spectroscopy (EDS)**

The composition of all the electrodes was determined using Electron Dispersive X-Ray Spectroscopy (EDS) equipped on the ZEISS SEM. The SEM was calibrated using Cu for the quantitative analysis of the electrode samples with appropriate accelerating voltages.

### **3.3.3 Potentiostatic Technique**

To characterise the electrode electrochemical activity, a potentiostatic technique was employed on an Autolab 302N electrochemical potentiostat at the Centre for Energy at The University of Western Australia.

The potentiostat is a unit to apply constant potential or current between electrodes. At the same time, current or potential signals could be recorded for future analysis. The corresponding current was recorded at the end of the each potential step. Potentiostatic techniques were used to characterise and compare electrode activities towards the electrode reactions (Crnkovic *et al*, 2004, Rami and Lasia, 1992). In this study, steady-state potentiostatic

techniques was also used to apply the potential between two electrode until the current reaches its equilibrium or stable state (Bard *et al*, 2008).

### **3.3.4 Electrochemical Impedance Spectroscopy (EIS)**

To obtain more detailed kinetic and impedance information of the electrode reactions, Electrochemical Impedance Spectroscopy (EIS) was employed at the same Autolab potentiostat. It also helps to interpret the electrochemical activity of the electrodes.

Electrochemical impedance spectrum has been widely used to characterise electrochemical reactions by means of impedance (Barsoukov and Macdonald, 2005). Generally, the EIS technique applies a set of sinusoid voltage signals with a range of frequencies on to a steady potential. The impedance is recorded as the ratio of the amplitudes of the sinusoid voltage signal to the current response (Bard *et al*, 2008). From the impedance study, detailed information such as double layer capacitor and solution resistance can be extracted (Orazem and Tribollet, 2008) and will be discussed in the associated discussion section of future chapter.

In this work, a set of sinusoid voltages of 5mV amplitude with the frequency ranging between 100kHz to 100mHz were applied on top of the three electrode potentials. These potentials were chosen within the linear part of the Tafel curves which will be demonstrated in the data presentation section.

## **3.4 Data Analysis**

This section is to provide a general guideline to illustrate how the data was processed and plotted in this thesis.

### 3.4.1 Polarisation Curve

The polarisation curve records the departure of cell potential from the equilibrium potential against the current density. Due to the fact that the process of water electrolysis contains both anodic and cathodic reactions, the cell voltage reflects the sum of resistance of hydrogen evolution reaction and oxygen evolution reaction, as well as the other resistances. The polarisation curve can be used as a direct measure of the total resistance of an electrolysis unit. A simple way to interpret the polarisation curve is to view voltage and current density as the energy requirement and hydrogen or oxygen generation rates, respectively. At a fixed current density, that is the fixed hydrogen or oxygen gas generation rate, the less cell voltage means less energy input for the electrolysis process.

All the data points were recorded at least three times to ensure the repeatability. The error bars represent the repeatability of each electrode reaction.

### 3.4.2 Tafel Curve

Tafel curves are obtained by plotting overpotential versus logarithm of current density, which is commonly used to characterise the activities of electrodes (Kaninski *et al*, 2009). The overpotential is calculated according to Equation 3-1

$$\eta_{H_2} = E - E^\circ - IR \quad 3-1$$

where  $E^\circ$  is the equilibrium potential (Bard *et al*, 2008) and  $IR$  is the ohmic loss (Zeng and Zhang, 2010) due to the solution resistance.

Several possible sources of resistances have been identified in the process of water electrolysis which is also applicable to other electrochemical processes. They are electrode reaction resistance, electric connection resistance, electrolyte resistance and resistance related to the mass transfer phenomena. All these resistances can be identified and examined individually when some of these resistances can be considered constant or negligible under the experimental conditions. To study one of the electrode reactions, the resistance of the other electrode reaction should be minimised. Therefore, a three-electrode set up was used. In this set up, the three electrodes were the working electrode, the counter electrode and the reference electrode, respectively. The target electrode reaction was studied on the working electrode while the other electrode reaction occurs on the counter electrode. The geometry area of the counter electrode was more than 30 times larger than that of working electrode. This minimised the resistance of the electrode reaction. The reference electrode has a stable potential and this ensures that the potential of the working electrode can be stably measured.

With the three-electrode set up and appropriate conditions, the electrode reaction can be considered to be dominated by a charge transfer controlled process, so the Tafel curve obtained represents the fundamental relationship between overpotential and current density. This relationship reveals the kinetics of the electrode reaction on a particular electrode.

### 3.4.3 Nyquist Plot and Bode Plot

Nyquist plot is a complex plot to characterise the impedance an electrochemical reaction. Each dot point on a Nyquist plot has a real part and an imaginary part. It represents the impedance of the electrochemical reaction corresponding to the frequency of the sinusoid perturbation of small amplitude. A Nyquist plot is typically a semicircle in shape.

The interpretation of measured impedance data on a Nyquist plot is carried out by the comparison between the data with the predictions of impedance based on the integration of all potential resistance and interfacial process such as the double layer, which will be fully detailed in the result discussion section.

Bode plot is another way to plot the impedance against frequency. It normally contains a combination of Bode magnitude plot and Bode phase plot. The interpretation of Bode plot is quite similar to that of Nyquist.

## 3.5 Summary

A detailed reactor design and experimental setup were employed for the investigation of the kinetics of electrode reaction. The SEM enabled the study of electrode surface profiles. The electrode preparation methods were also presented, these methods including alkaline leaching, mechanical and chemical modification. The electrochemical reactors then were then presented to study the kinetics of electrode reactions on the prepared electrodes. Finally, a rectangular electrochemical cell was employed to enable the observation of bubble behaviours and study the effect of experimental conditions on the bubble size and departure.

## **Chapter 4      Kinetics of Electrode Reactions on Ni Base Electrodes**

### **4.1 Introduction**

The purpose of this chapter is to present and compare the kinetics of hydrogen evolution reaction on Ni electrode and Ni-Fe-Zn electrode. The comparison also helps to unveil the effect of electrode surface and electrode preparation methods on the electrode kinetics.

In this chapter, Ni electrode was prepared by polishing with sandpapers. The Ni electrode prepared in such procedure was used as a base for Ni-Fe-Zn electrode. To examine the effect of the surface profile of electrode deposition, the kinetics of hydrogen evolution reaction was studied using a standard three-electrode reactor presented in Chapter 3. The surface profile of the electrodes was characterised under the help of SEM. The electrode activities were characterised using Tafel curves and electrochemical impedance spectroscopy.

### **4.2 Electrode Surface Characterisation**

The electrode surface profiles were examined using the SEM. SEM image in Figure 4-1 shows the surface morphologies of the base Ni. At the magnification of 5000 times, the base Ni electrode shows generally smooth surface with noticeable grooving due to the polish treatment. The EDX analysis confirmed that the compositions of the Ni electrodes were of  $99.8 \pm 0.1\%$  nickel.

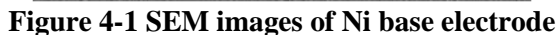


Figure 1 consists of two SEM images, (a) and (b). Image (a) shows the surface of the as-received sample, which appears relatively smooth with some small, dark, irregular particles scattered across it. A scale bar indicating 10 μm is located in the bottom right corner. Image (b) shows the surface of the etched sample, which is highly textured and porous, with many small, rounded features. A scale bar indicating 10 μm is also present in the bottom right corner. Both images include technical data at the bottom, such as magnification, voltage, and acquisition parameters.

The EDS result in Figure 4-3 also qualitatively confirms that all metal components present in the prepared Ni-Fe-Zn electrode. On the contrast, Zn disappeared in the EDS spectrum at the spots chosen for the Ni-Fe-Zn coated electrode after leaching. It can be reasonably concluded that the pore

and crack structures are formed by the leached zinc contents. This rougher structure potentially increases the surface area of the electrode.

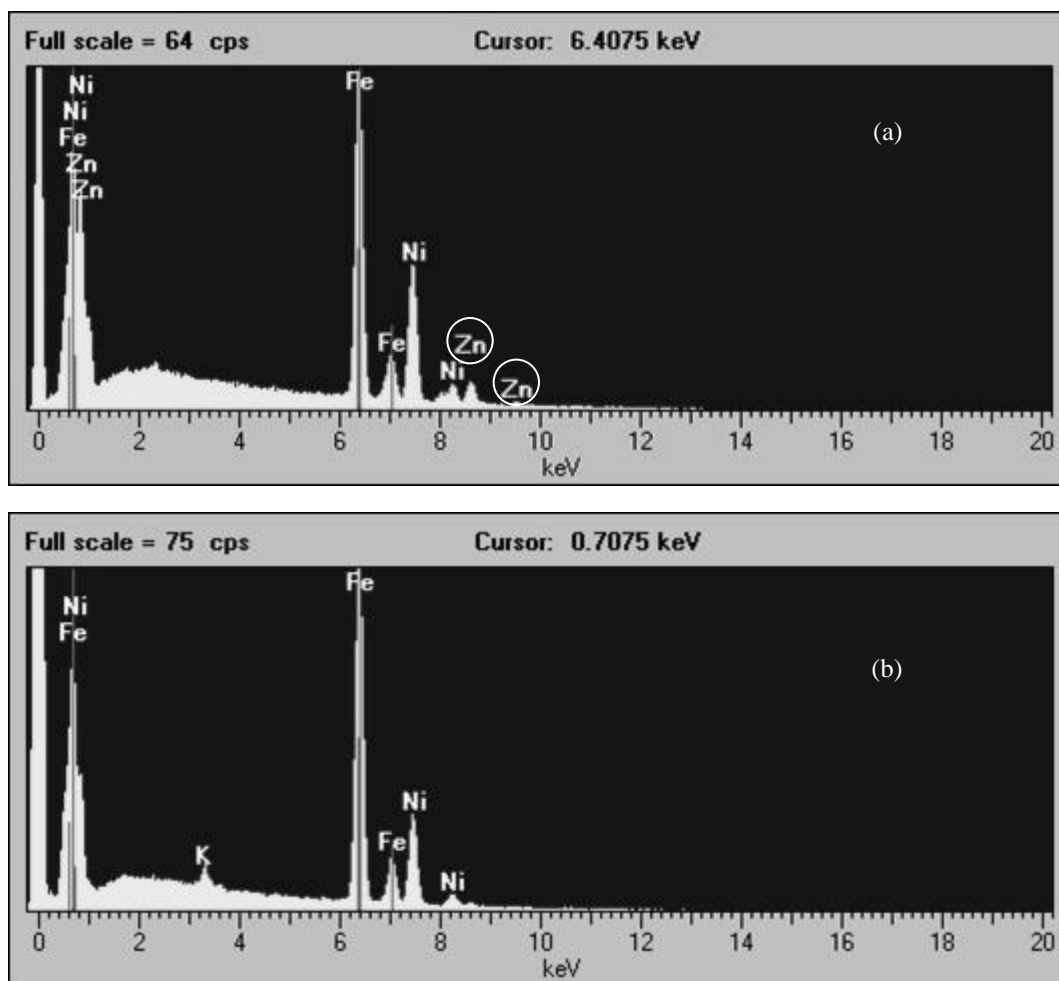


Figure 4-3 EDS of Ni-Fe-Zn (a) before and (b) after alkaline leaching

### 4.3 Kinetics of Hydrogen Evolution Reaction

Tafel curves were used to compare the activity of smooth electrode and Ni-Fe-Zn electrode towards hydrogen evolution reaction. The Tafel curves were extracted from corresponding steady-state polarisations by plotting the overpotential against the logarithm of current density. As shown in Figure 4-4, only a linear part of was present as Tafel curve. Within this region,

hydrogen evolution reaction can be considered as under kinetic control, and more importantly, of practical interest. Only one Tafel slope was found on both pure Ni and Ni-Fe-Zn coated electrodes. At a current density of  $100 \text{ mA}\cdot\text{cm}^{-2}$ , the overpotential was reduced by around 60 mV at Ni-Fe-Zn, which means the energy cost per unit hydrogen produced could be reduced. The kinetic parameters obtained from the steady-state Tafel curve are presented in Table 4-1, where  $j_0$  is the exchange current density of the electrode reaction. The larger the exchange current density an electrode shows, the better activity the electrode has. Although the Ni-Fe-Zn coated electrode has a larger Tafel slope, the exchange current density is an order of magnitude less than that of the Ni electrode. The Tafel equation of the hydrogen evolution reaction on a Ni electrode can be written as

$$\eta = 0.14 + 0.108 \log j \quad 4-1$$

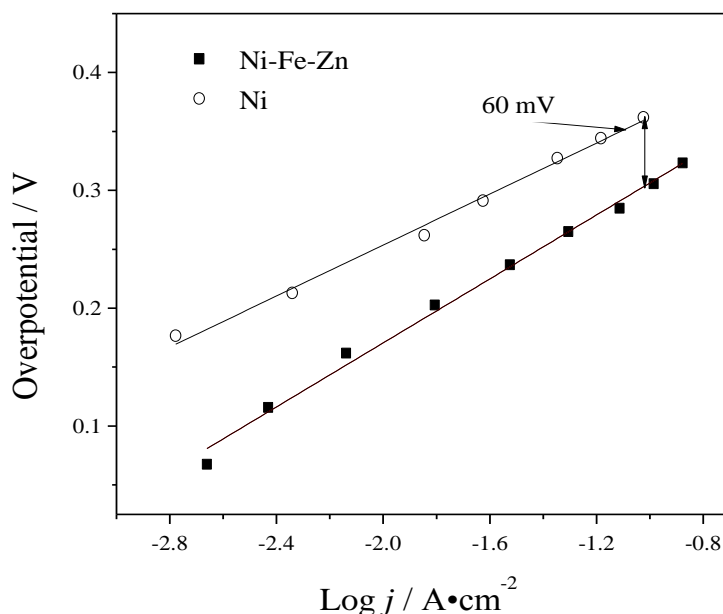


**Figure 4-4** The Tafel curves of hydrogen evolution reaction on both Ni and Ni-Fe-Zn electrodes

**Table 4-1 Tafel parameters extracted from Figure 4-4**

	Tafel slope / $\text{mV} \cdot \text{dec}^{-1}$	$j_0 / \text{A} \cdot \text{cm}^{-2}$
Ni	108	$4.5 \cdot 10^{-5}$
Ni-Fe-Zn	135	$5.6 \cdot 10^{-4}$

Comparing with other electrodes reported in the literature, the Ni-Fe-Zn coated electrode shows a relatively high electrode activity. Table 4-2 compares the kinetic parameters of the hydrogen evolution reaction on different electrodes. The reported experimental conditions, including reaction temperature and electrolyte solution have a significant effect on the kinetic parameters, especially the exchange current density. Under the same reaction temperature and electrolyte solution conditions, the Ni-Fe-Zn coated electrode still shows the highest exchange current density,  $5.6 \cdot 10^{-4} \text{ A} \cdot \text{cm}^{-2}$ , compared to that of the Ni, Ni/Zn, Ni-Co electrode. Two Ni-Co electrodes reported (Correia, Machado et al. 1999; Kaninski, Nikolic et al. 2009) show an exchange current density of  $2.9 \cdot 10^{-6} \text{ A} \cdot \text{cm}^{-2}$  and  $2.0 \cdot 10^{-4} \text{ A} \cdot \text{cm}^{-2}$ , respectively. This significant difference could be attributed to the different electrode preparation method and the different concentration of KOH solution used in the kinetic study. It has also been reported that a high exchange current density,  $5.4 \cdot 10^{-3} \text{ A} \cdot \text{cm}^{-2}$ , was achieved on a Ni-Mo electrode (Kubisztal, Budniok et al. 2007). However, a solution of 5M KOH was used as the electrolyte. The hydrogen evolution reaction could have not been under the kinetic control. Therefore, the data is not comparable to our measurements and the other literature reports.

**Table 4-2 Kinetics parameters for hydrogen evolution reaction on Ni-Fe-Zn electrode and other electrode materials reported in the literature**

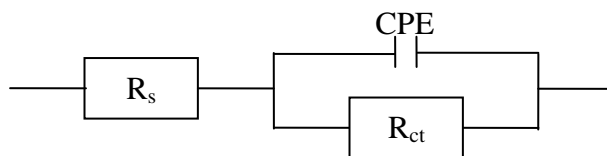
	Tafel slope /mV·dec <sup>-1</sup>	j <sub>0</sub> /A·cm <sup>-2</sup>	Temperature	Electrolyte Solution	Reference
Ni	108	4.5·10 <sup>-5</sup>	25°C	0.5M KOH	
Ni-Fe-Zn	135	5.6·10 <sup>-4</sup>	25°C	0.5M KOH	
Ni/Zn (50wt%)	119	3.9·10 <sup>-4</sup>	25°C	0.5M KOH	(Hitz and Lasia 2001)
Ni-Co	94	2.0·10 <sup>-4</sup>	Room temperature	1.0M KOH	(Kaninski, Nikolic et al. 2009)
Ni-Co-V	106	2.0·10 <sup>-4</sup>	Room temperature	1.0M KOH	(Kaninski, Nikolic et al. 2009)
Ni-Co	118	2.9·10 <sup>-6</sup>	25°C	0.5M KOH	(Correia, Machado et al. 1999)
Ni+Mo (46wt %)	154	5.4·10 <sup>-3</sup>	25°C	5.0M KOH	(Kubisztal, Budniok et al. 2007)
Pt	180	6.15·10 <sup>-5</sup>	22°C	5.0M KOH	(Angelo 2007)

## 4.4 Electrochemical Impedance Spectroscopy

The EIS is usually used for characterisation of electrode coatings and the behaviour of electrode reaction. In this study the EIS experimental data were collected when the hydrogen evolution reaction were carried out in a 0.5 M KOH solution at the temperature of 25°C. The potentials were chosen within the range of linear Tafel slope.

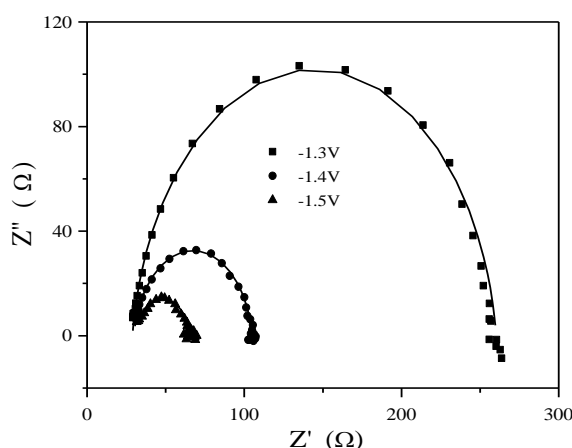
### 4.4.1 Electrode Kinetics on Ni Electrode

The following analogy circuit in Figure 4-5 is widely used to describe the hydrogen evolution reaction on smooth electrodes (Kaninski *et al*, 2009).



**Figure 4-5 An analogous circuit for describing the resistances of hydrogen evolution reaction on Ni electrodes**

$R_s$  is the solution resistance, representing the resistance due to the electrolyte resistivity.  $R_{ct}$  is the charge transfer resistance and it represents the resistance due to electrode reaction. Constant phase element is used rather than capacitor for better EIS fitting, and it is short for CPE. CPE is normally used when the Nyquist plot is not exhibiting perfect capacitive behaviour.



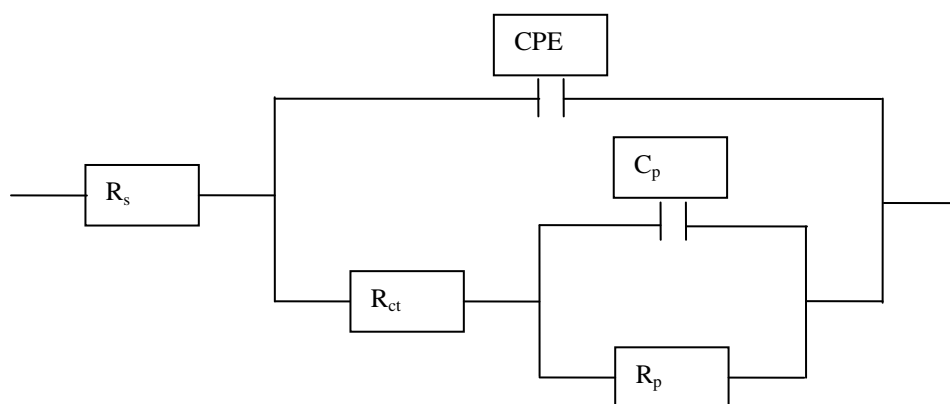
**Figure 4-6 The Nyquist plots for hydrogen evolution reaction on the Ni electrode polished with a sandpaper with 5 $\mu$ m grand size. The experiments were carried out at -1.3V, -1.4V and -1.5 V against Silver/Silver Chloride electrode (SCE), respectively. The dot points are experimental impedances and the continuous lines are the curves-fitted impedances.**

Figure 4-6 shows the Nyquist plot of hydrogen evolution on Ni electrode. In all cases, only one semi-circle was identified, which also indicates that the reaction is under kinetic control. The Nyquist plot also qualitatively illustrates the relationships between the electrode reactions at different overpotentials. All the semi-circles almost gathered at a point, which were

recorded at the highest frequencies. The impedance response at the high frequency can be approximated to  $R_s$ . It needs to be pointed out that this resistance includes the electrical contact wires. On the other hand, the impedance response at low frequency can be approximated to be the sum of  $R_s$  and  $R_{ct}$ , which is at the end point of the semi-circle. The imaginary part of this impedance, similar to that of the impedance at high frequency, also approaches zero. Therefore, the radius of the semi-circle presents the electrode reaction resistance. It can be seen from Figure 4-6 that the reaction resistance was decreased as the potential increased, while the solution resistance was independent to the potential.

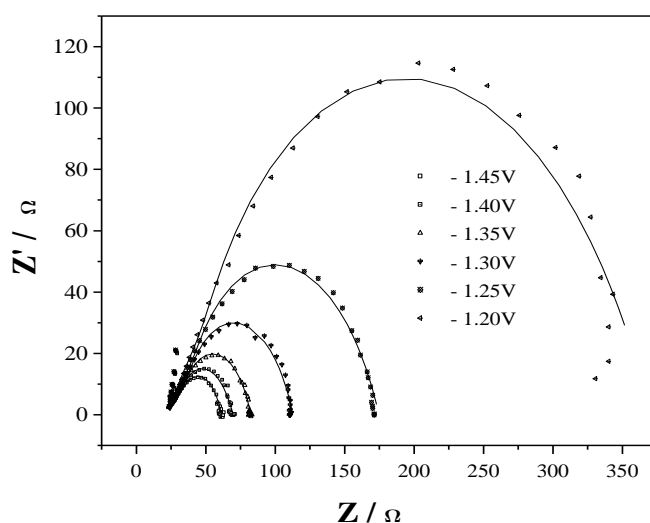
#### 4.4.2 Electrode Kinetics on Ni-Fe-Zn Electrode

The following analogy circuit in Figure 4-7 is widely used to describe the hydrogen evolution reaction on the porous electrodes (Hitz and Lasia, 2001). Similar to the Figure 4-5,  $R_s$  is the solution resistance. CPE replaces double layer capacitance for better EIS fitting.  $R_{ct}$  is the charge transfer resistance.  $C_p$  and  $R_p$  are pseudo-capacitor and pseudo-resistance respectively. These two pseudo-parameters present the effect of electrode porous structures.



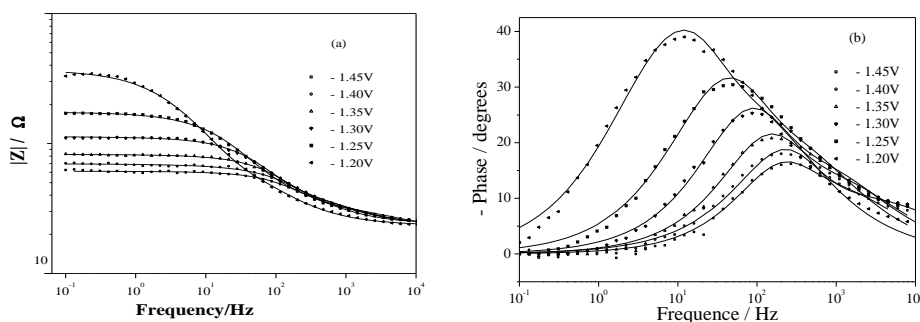
**Figure 4-7 The equivalent circuit employed for EIS data fitting for the Ni-Fe-Zn Electrode**

Figure 4-8 shows the Nyquist plot of hydrogen evolution on the Ni-Fe-Zn electrode. Similar to Figure 4-6, all the semi-circles almost shared a similar solution resistance,  $R_s$ , at the highest frequency. It also can be seen from Figure 4-8 that the reaction resistance was decreased as the potential increased, while the solution resistance was independent to the potential.



**Figure 4-8 The Nyquist plots for hydrogen evolution reaction on the Ni-Fe-Zn electrode at different potentials against SCE and corresponding fitting. The dot points are experimental impedances and the continuous lines are the curves-fitted impedances**

Quantitative data can be found on the Bode plot. As shown in Figure 4-9, the Bode modulus plot shows the resistance at both high and low frequency ends representing the  $R_s$  and  $R_s + R_{ct}$ , respectively. This can also be seen from the Bode phase where the phase angle drops towards zero at both ends. A maximum phase angle can be identified in all overpotentials, which indicates the capacitive behaviour of the electrode.



**Figure 4-9 The Bode modulus (a) and Bode phase (b) plots of EIS data and corresponding fitting. Scatters are experimental data; lines are EIS fitting using a non-linear regression procedure**

## 4.5 Effect of Electrode-Deposition

The values of all the components in Figure 4-7 were calculated with non-linear square fitting procedure. As presented in both Table 4-3 and Table 4-4, the fitted solution resistance remains steady. The charge transfer resistance reduces as the overpotential increases. The solution resistances are almost the same for the electrode reactions on both Ni and Ni-Fe-Zn electrodes, varying from 21.3 to 25.6  $\Omega$ .

The most significant different between Table 4-2 and Table 4-3 is the charge transfer resistance. This means that the Ni-Fe-Zn electrode has reduced the reaction resistance for the hydrogen evolution reaction significantly. The  $N$  values for Ni electrode is close to 1, this means that the electrode behaved like a capacitor and had a smooth surface. On the other hand, for Ni-Fe-Zn electrode, the  $N$  is less than 1 and  $T$  value is high than that of Ni electrode. These confirm that the Ni-Fe-Zn has a porous structure and has a larger surface area comparing to Ni electrode.

Since it was shown from the Tafel analysis that the charge transfer is the rate determining step within the range of potentials in the study, the linear

relationship between the overpotential and the logarithm of  $R_{ct}$  can be expected as Figure 4-10.

**Table 4-3 Estimated values of the electrical components by impedance fitting at various overpotentials on the Ni base electrode**

Overpotential/ $\eta$ mV	$R_s$ $\Omega$	$R_{ct}$ $\Omega$	T $\mu F \cdot s N^{-1}$	N
213	26.1	212.0	4.46	0.93
291	25.6	100.1	5.19	0.91
344	26.0	60.8	5.37	0.91

**Table 4-4 Estimated values of the electrical components at various overpotentials on the Ni-Fe-Zn coated electrode**

Overpotential/ $\eta$ mV	$R_s$ $\Omega$	$R_{ct}$ $\Omega$	T $\mu F \cdot s N^{-1}$	N
115	23.4	150.7	392	0.68
161	25.6	90.0	189	0.73
202	23.4	55.5	149	0.70
236	23.2	45.2	121	0.71
265	21.3	35.4	176	0.62

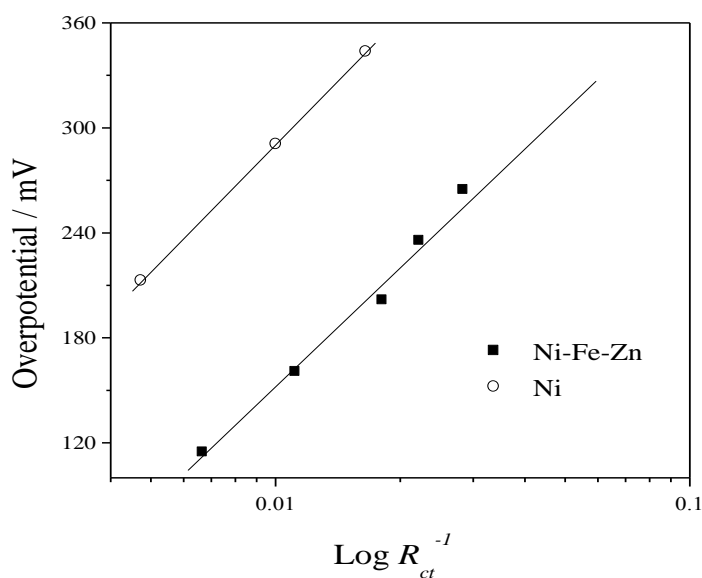


**Figure 4-10 Linear relationship between overpotential and  $\text{Log}(R_{ct}^{-1})$  of the hydrogen evolution reaction on Ni and Ni-Fe-Zn electrodes in 0.5M KOH at 298K.**

## 4.6 Summary

The SEM image analysis proved that the alkaline leaching treatment can provide a significantly enhanced porous structure. The nickel electrode with the Ni-Fe-Zn coating has been shown to offer a better activity towards the hydrogen evolution reaction than the pure Ni electrode. The electrode surface modification reduced the overpotential by 60 mV at the current density of  $100 \text{ mA}\cdot\text{cm}^{-2}$ . The activity enhancement on the Ni-Fe-Zn coated electrode can be attributed to the surface area increase. EIS shows that the resistance due to electrode reaction was significantly reduced when the Ni-Fe-Zn electrode was applied. It is also confirmed that the Ni-Fe-Zn electrode has got a larger surface area comparing to Ni electrode.

## **Chapter 5      Evaluating the Effect of Surface Modifications on Ni Based Electrodes for Water Electrolysis**

### **5.1 Introduction**

The purpose of this chapter is to further study the effect of electrode modifications on the electrode kinetics. By studying the kinetics of hydrogen evolution reaction on mechanically and chemically modified electrodes, the effect of surface area and electrode deposition were discussed.

In this chapter, Ni electrodes were prepared by polishing the electrodes with sandpapers of different grain sizes as presented in Chapter 3. The Ni electrode prepared in such procedure was used as a base for electrode deposition. To examine the effect of the surface profile of electrode deposition, the kinetics of hydrogen evolution reaction was studied using a standard three-electrode reactor presented in Chapter 3. The surface profiles of the prepared electrodes were characterised with the help of SEM. The electrode activity was characterised using Tafel curves and EIS technique.

### **5.2 Hydrogen Evolution Reaction on Ni electrodes**

Tafel curve presents the dependence of overpotential on current density, and is commonly used to characterise the electrode activity (Solmaz *et al*, 2009).

Previously, the current flow per unit electrode surface area was calculated according to Equation 5-1.

$$j = i / A \quad \quad \quad 5-1$$

Two kinds of surface areas, the geometric surface and effective surface area were analysed to present the effect of electrode modifications. The geometric surface area is the projected area of an electrode surface on a plane. The effective surface area is the area participating in the electrode reaction, which will be discussed in Section 5-3. Electrode activities characterised by the Tafel curves based on the geometric area and effective surface area, respectively, are noted as the apparent activity and intrinsic activity respectively.

The Tafel curves in Figure 5-1 characterise the apparent activities of electrodes modified by the mechanical polishing. The linearity of the Tafel curves suggests that the hydrogen evolution reaction was kinetically controlled (Navarro-Flores *et al*, 2005).

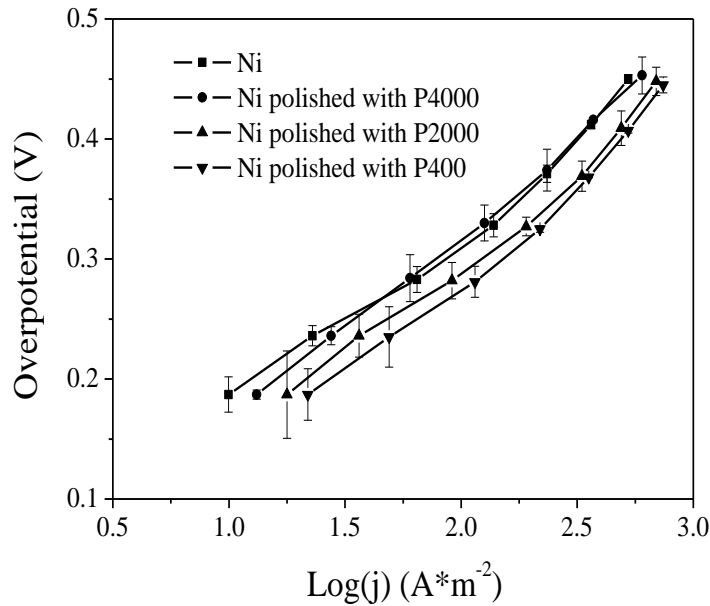


**Figure 5-1 Tafel curves of hydrogen evolution reaction illustrating the apparent activity of the Ni electrodes polished with different sandpapers**

Figure 5-1 also shows the Ni electrode polished with the P400 sandpaper achieved the best apparent activity by possessing the lowest overpotential of 422 mV at the current density of  $750 \text{ A}\cdot\text{m}^{-2}$ , followed by electrodes polished with the P2000 and P4000 sandpaper. This means that the mechanical polishing enhances the apparent activity by reducing the overpotential. The mechanical polishing resulted in larger electrode surface areas, thus, the current densities based on the geometric areas would have been overestimated, resulting in lower overpotential in the apparent activity (Kubisztal *et al*, 2007). Therefore, the best apparent activity is expected to occur on the Ni electrode with the largest surface area, in this case, the Ni electrode polished with the P400 sandpaper. It is furthermore speculated that if the effect of surface area can be isolated, these electrodes should share a same activity.

### 5.3 Relative Roughness Factor

SEM images in Figure 5-2 show the surface morphologies of the base Ni and mechanically polished Ni electrodes. It can be seen that the surfaces of electrodes became rougher as the grain size of the applied sandpaper increased. At the magnification of 5000 times, it is shown that the base Ni electrode shared a similar finishing to the Ni electrode polished with the P4000 sandpaper as in Figure 5-2 (a) and (b). The Ni electrode polished with the P2000 sandpaper showed a more obvious grooving while the Ni electrode polished with the P400 sandpaper showed an irregular grooving pattern as in Figure 5-2 (c) and (d). The EDX analysis confirmed that the compositions of the Ni electrodes were of  $99.8 \pm 0.1\%$  nickel.

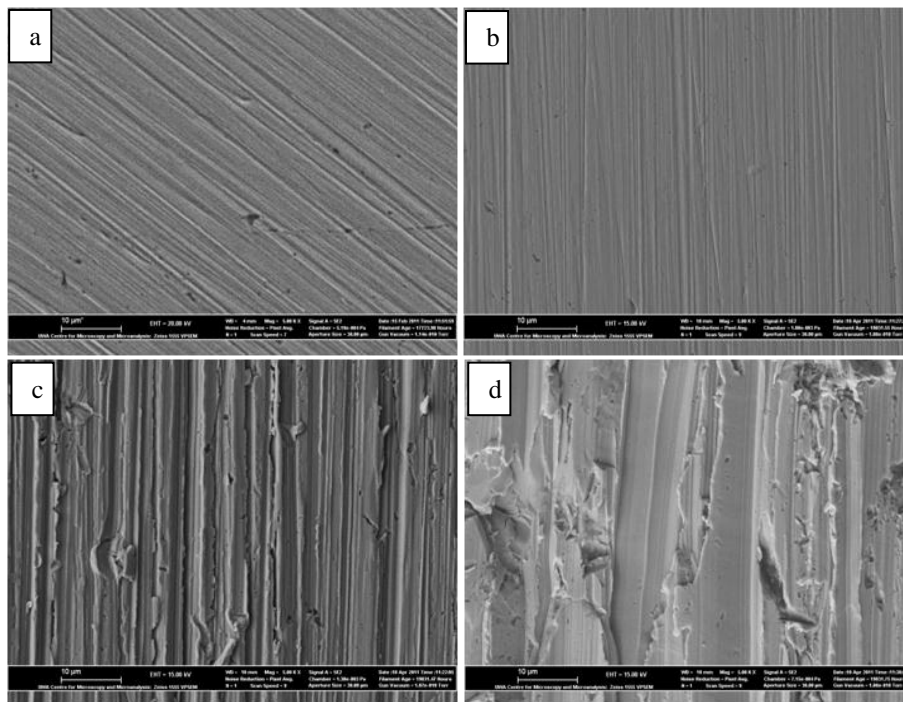


**Figure 5-2 SEM images of Ni electrodes at the magnification of 5000 times [(a) base Ni electrode, (b) Ni electrode polished with the P4000 sandpaper, (c) Ni electrode polished with the P2000 sandpaper and (d) Ni electrode polished with the P400 sandpaper]**

A more quantitative means to compare the surface roughness is by studying the double layer (Kubisztal *et al*, 2007) behaviour of the electrode surface. The double layer refers to two layers of charges, due to an electrical potential formed on the surface of electrode, which behaves like a capacitor (Bard *et al*, 2008). The double layer capacitance is proportional to the effective surface area of an electrode. Therefore, it has been used as a means to reflect the roughness of an electrode surface (Kubisztal *et al*, 2007).

To obtain the double layer capacitance, the EIS technique is commonly used (Bard *et al*, 2008), employing an imaginary analogous circuit to describe the impedance of an electrode reaction. The circuit always contains electrical components such as resistors and capacitors (Kaninski *et al*, 2009). Assigning an initial value for each electrical component incurs a theoretical value of impedance for the circuit (Barsoukov and Macdonald, 2005). By fitting the theoretical impedance with the experimental impedance, the values of all the electrical circuit components can be estimated (Orazem and Tribollet, 2008). Then, the double layer capacitance can be calculated.

The first step to obtain the impedance of hydrogen evolution reaction on the Ni electrode is to describe the impedance using an analogous circuit as shown in Figure 5-3. Due to the simplicity of the smooth Ni electrodes and sandpaper polished Ni electrodes, the analogous circuit contains less components than that of the alkaline-leached Ni-Fe-Zn electrode.  $R_{ct}$  is the charge transfer resistance, which is also noted as the reaction resistance. Constant phase element, short for CPE (Bard *et al*, 2008), is also used to replace the double layer capacitance for a better fitting when an electrode

does not behave as a pure capacitor (Shervedani and Madram, 2007). Figure 5-3 describes the impedance of hydrogen evolution reaction as a combination of a solution resistance  $R_s$ , in series with a parallel connection between  $R_{ct}$  and CPE. The physical meaning of this circuit is that the solution resistance only occurs in the solution. While the reaction resistance combined with the double layer capacitor in a parallel way because they coexist on the surface of electrode.

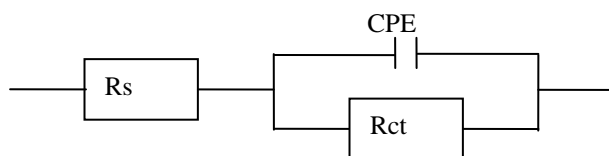


**Figure 5-3 An analogous circuit for describing the resistances of hydrogen evolution reaction on Ni electrodes**

After setting up the circuit, the impedance is experimentally recorded and commonly plotted in a complex plane, Nyquist plot (Bard and Faulkner, 2001). Figure 5-4 shows the Nyquist plots of the hydrogen evolution reaction on Ni electrodes at different potentials obtained in the present work. The Nyquist plots showed typical depressed semicircles for the impedances of hydrogen evolution reaction which validates the circuit in Figure 5-3.

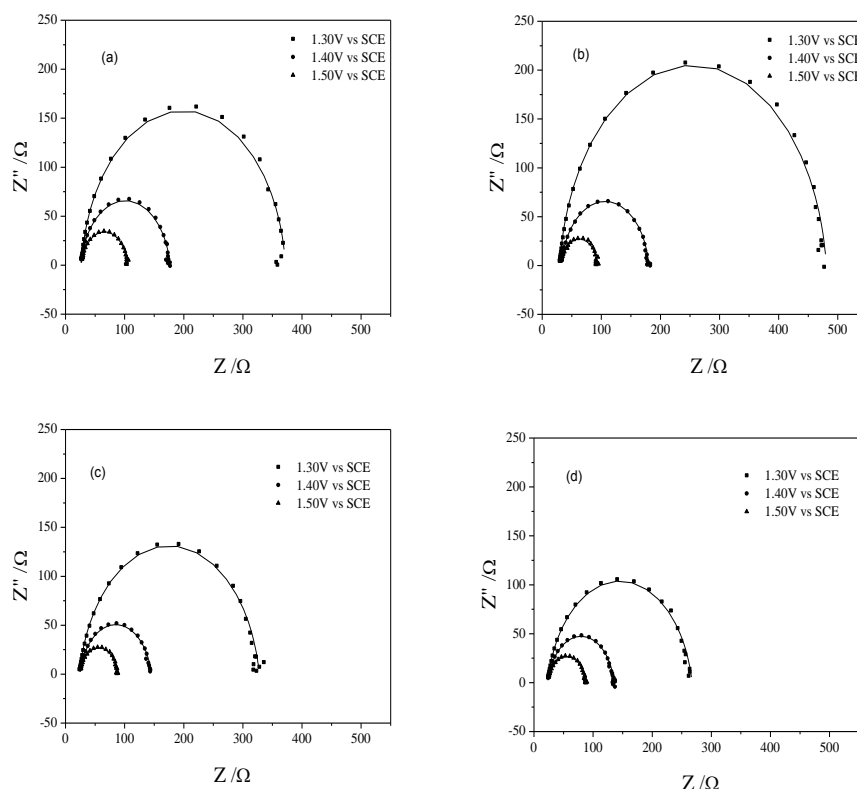


**Figure 5-4 The Nyquist plots for hydrogen evolution reaction on the Ni electrode polished with the sandpapers at the three selected potentials -1.3V, -1.4V and -1.5 V against SCE, respectively. (a) Ni electrode (b) Ni electrode polished with P4000 sandpaper, (c) Ni electrode polished with P2000 sandpaper (d) Ni electrode polished with P400 sandpaper. The dot points are experimental impedances and the continuous lines are the curves-fitted impedances.**

Combining the model and experimental results, the impedance fitting was performed following a non-linear square fitting procedure (Krstajic *et al*, 2001a), allowing the best values of the electrical components in the analogous circuit to be obtained with minimised deviations between the experimental and curve-fitted impedance data. The curve-fitted impedances are presented as the lines in Figure 5-4 and Figure 5-5. The curve fittings were in good agreement with the experimental data. It can be seen that the charge transfer resistance reduced as the electrode potential increases. At the potential of 1.50V against SCE, the electrode reaction on Ni electrode

polished with P400 sandpaper exhibited the lowest charge transfer resistance,  $64.7\Omega$ , among all the mechanically polished Ni electrodes.

Figure 5-5 shows the Bode plots for the impedances of hydrogen evolution reaction on Ni electrodes at different electrode potentials. For all electrodes, the magnitudes of the impedances reduced as the electrode potential increased. It is confirmed that the impedance of the electrode reaction reduced with the increase in the grain size of the sandpaper. When the electrode was polished with P4000 sandpaper, the magnitude of electrode reaction impedance was  $470\Omega$  at 1.30V against SCE, while it reduced to  $266\Omega$  when the P400 sandpaper was applied. It should also be noted that the phase shifts did not fit well with the experimental data at high frequencies. Due to the low magnitude of the impedance and lack of physical meaning, this part of data was ignored in the model choosing and fitting.

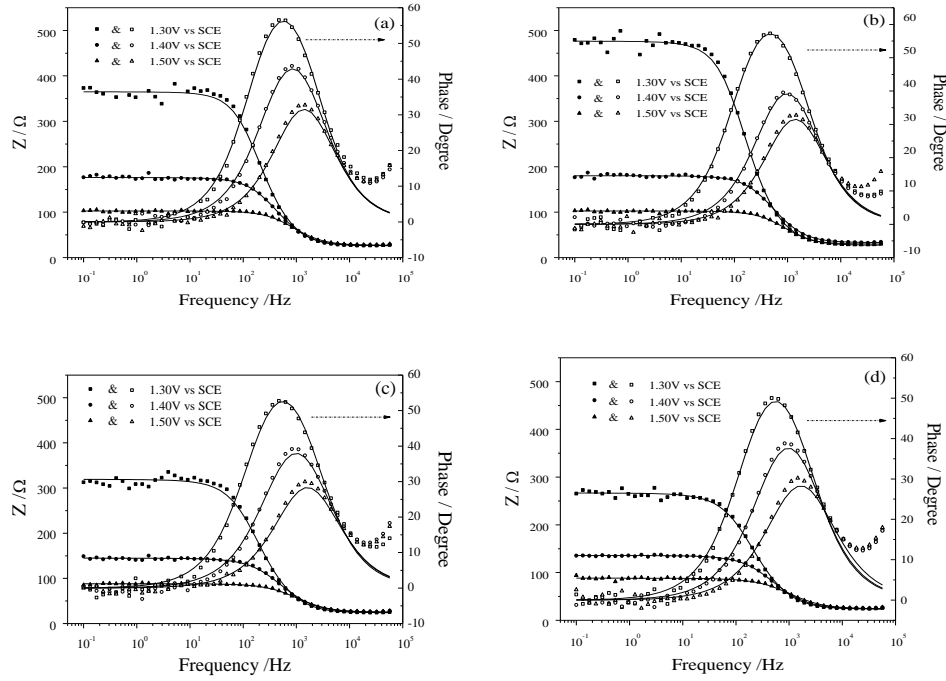


**Figure 5-5** The Bode plots for hydrogen evolution reaction on the Ni electrode polished with the sandpapers at the three selected potentials -1.3V, -1.4V and -1.5 V against SCE, respectively. (a) Ni electrode; (b) Ni electrode polished with P4000 sandpaper; (c) Ni electrode polished with P2000 sandpaper; (d) Ni electrode polished with P400 sandpaper. The dot points are experimental impedances and the continuous lines are the curves-fitted impedances.

With the impedance fitting, the parameters of the CPE, such as the admittance of the CPE,  $T$ , and the phase angle coefficient,  $N$ , can be estimated (Bard *et al*, 2008). The double layer capacitance values can then be calculated from the fitted values of the electrical components in the analogous circuit using Equation 5-2 (Kaninski *et al*, 2009).

$$C_{dl} = \left[ T \left( R_s^{-1} + R_{ct}^{-1} \right)^{-(1-N)} \right]^{1/N} \quad 5-2$$

The values of all these electrical components in the analogous circuit on different electrodes are presented in Table 5-1.

**Table 5-1 Estimated values of the electrical components by impedance fitting and double layer capacitances at various overpotentials on Ni electrodes**

Electrode	Voltage	$R_s$	$R_{ct}$	T	N	$C_{dl}$	$R_f$
	V SCE	vs $\Omega$	$\Omega$	$\mu F \cdot s^{N-1}$		$\mu F$	
Ni base electrode	130	26.8	345.0	3.94	0.94	2.25	3.6
	135	26.1	212.0	4.46	0.93	2.23	3.5
	140	25.6	150.9	5.19	0.91	2.23	3.5
	145	26.0	108.9	5.37	0.91	2.25	3.6
	150	26.8	78.3	5.18	0.91	2.17	3.5
P4000 polished	130	29.6	450.8	4.86	0.94	2.75	4.4
	135	31.2	240.5	4.61	0.94	2.54	4.0
	140	32.7	147.4	4.78	0.93	2.42	3.9
	145	32.1	89.1	3.91	0.95	2.43	3.9
	150	31.6	61.9	4.81	0.92	2.16	3.4
P2000 polished	130	23.6	304.1	7.59	0.91	3.09	4.9
	135	24.0	173.0	7.88	0.91	3.20	5.1
	140	24.5	120.6	8.27	0.89	2.88	4.6
	145	24.3	87.0	8.17	0.89	2.79	4.4
	150	24.5	63.7	7.69	0.90	2.74	4.4
P400 polished	130	23.2	244.1	9.09	0.90	3.42	5.4
	135	23.2	156.9	8.89	0.90	3.27	5.2
	140	23.5	112.1	8.70	0.90	3.17	5.1
	145	23.2	83.0	8.99	0.89	2.96	4.7
	150	23.4	64.7	8.94	0.88	2.64	4.2

With the double layer capacitance, the effective area can then be used to quantify the roughness of an electrode. The term relative roughness factor, denoted as  $R_f$ , is introduced and calculated by dividing the double layer capacitance of a rough electrode surface by the double layer capacitance of a smooth electrode surface, which approximates to  $20 \mu F \cdot cm^{-2}$  (Chen and Lasia, 1992). The relative roughness factor data obtained in this work, as shown in Table 5-1, suggest that the relative roughness factor increased as the sand grain size of the sandpaper applied in the polishing increased. This

also provides a quantitative comparison of the levels of roughness for electrodes with the mechanical polishing.

## 5.4 Intrinsic Activity of Ni Electrode

With the relative roughness factor, the effective surface area can be then calculated using the relation  $A' = A \cdot R_f$ , where  $A'$  is the effective surface area and  $A$  is the geometric surface area. The current density based on the effective surface area can then be obtained according to Equation 5-3 (Navarro-Flores *et al*, 2005),

$$j'' = i / A \cdot R_f \quad 5-3$$

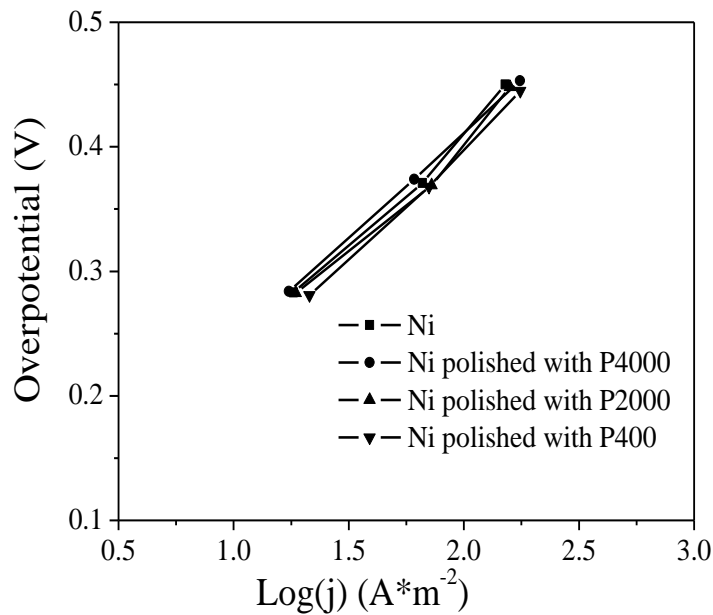


**Figure 5-6 Tafel curves of hydrogen evolution reaction illustrating the intrinsic activity of the mechanical polished Ni electrodes**

In contrast to the apparent activity, the intrinsic activity is based on the effective surface area rather than the geometric surface area. Figure 5-6 shows that the Tafel curves of Ni electrodes polished with different

sandpapers collapsed into a narrow band when the effective surface areas, in place of the geometric areas, were used in the current density calculations. These collapsed Tafel curves represent the intrinsic activity of Ni electrodes and may be described by Equation 5-4:

$$\eta = 0.02 + 0.191 \cdot \text{Log} j'' \quad 5-4$$

This finding also validates the relative roughness factor calculations as introduced in Section 5-2 above.

## 5.5 Hydrogen Evolution on Ni-Co Electrodes

To compare the apparent activities of Ni with Ni-Co electrodes, the same electrochemical tests were performed on the Ni-Co electrodes prepared with the electrochemical deposition method. Figure 5-7 shows the Tafel curves obtained, which characterise the apparent activities of Ni-Co electrodes. The Ni-Co(3) electrode exhibited an enhanced apparent activity by possessing lower overpotential than the Ni electrode. All three Ni-Co electrodes showed similar Tafel slopes, which implied that their intrinsic activities might collapse, as did the mechanically polished electrodes, when the relative roughness factor was applied.

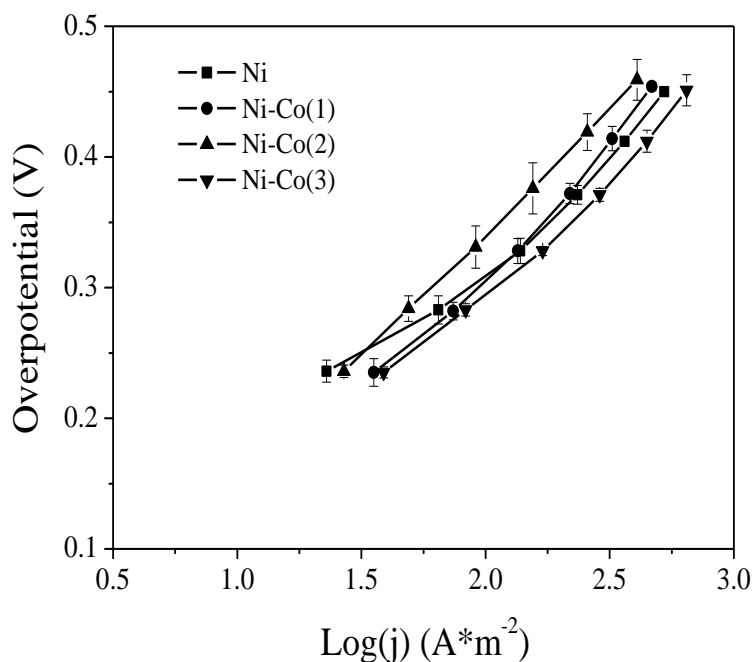


**Figure 5-7 Tafel curves of hydrogen evolution reaction illustrating the apparent activity of the Ni-Co electrodes**

Figure 5-8 shows the Bode plots of hydrogen evolution reactions on the prepared Ni-Co electrodes. The bode plots confirmed that Ni-Co (3) exhibits the best apparent electrode activity, followed by Ni electrode. The electrode reaction resistances on Ni-Co(3) and Ni electrode are generally less than those of Ni-Co(1) and (2).

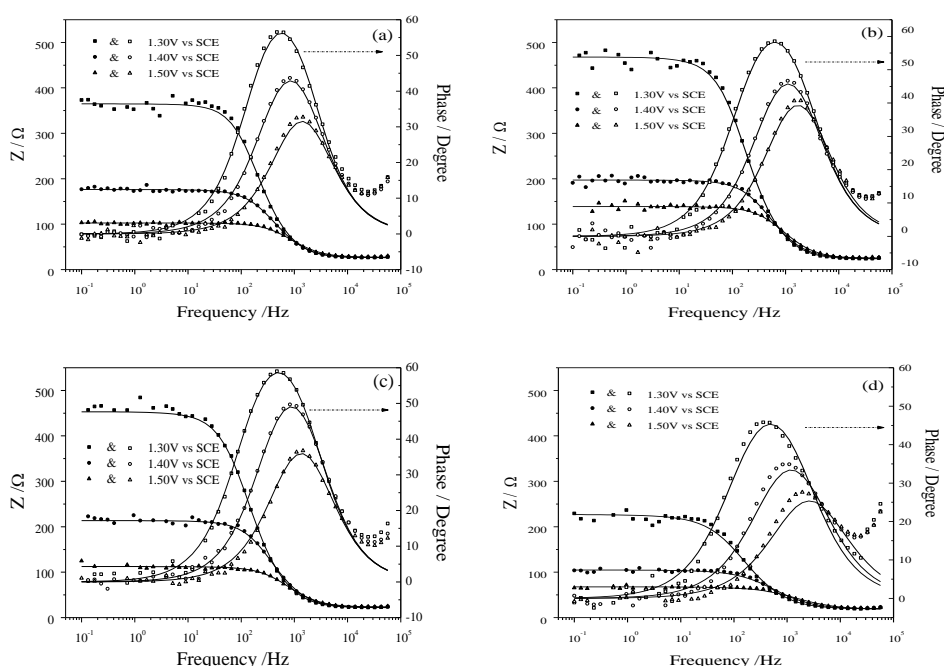


**Figure 5-8** The Bode plots for hydrogen evolution reaction on the Ni electrode and Ni-Co electrodes at the three selected potentials -1.3V, -1.4V and -1.5 V against SCE, respectively. (a) Ni electrode; (b) Ni-Co(1) electrode; (c) Ni-Co(2) electrode; (d) Ni-Co(3) electrode. The dot points are experimental impedances and the continuous lines are the curves-fitted impedances.

## 5.6 Intrinsic Activity of Ni-Co Electrodes

When the relative roughness factor calculation was applied to the Ni-Co electrodes, the corresponding double layer capacitances and relative roughness factors were calculated and are presented in Table 5-2. The relative roughness factor did increase slightly as the deposition duration increased. The intrinsic activities of these three Ni-Co electrodes are compared in Figure 5-9. Unfortunately, the Tafel curves for the Ni-Co electrodes did not collapse as expected. While the Ni-Co(1) and Ni-Co (3) electrodes showed slightly lower overpotential in the intrinsic activity than the Ni-Co(2) electrode, none of the Ni-Co electrodes showed an enhanced intrinsic activity than the Ni electrode. The difference in the Ni-Co electrode

intrinsic activities can only be attributed to the presence of Co, which altered the electrochemical characteristics of the Ni-Co electrode surfaces.

**Table 5-2 Estimated values of the electrical components by impedance fitting and double layer capacitances at various overpotentials on Ni-Co electrodes**

Electrode	Voltage e V vs SCE	$R_s$	$R_{ct}$	T	N	$C_{dl}$	$R_f$
		$\Omega$	$\Omega$	$\mu F \cdot s^{N-1}$		$\mu F$	
Ni	130	26.8	345.0	3.9	0.94	2.25	3.6
	135	26.1	212.0	4.5	0.93	2.23	3.5
	140	25.6	150.9	5.2	0.91	2.23	3.5
	145	26.0	108.9	5.4	0.91	2.25	3.6
	150	26.8	78.3	5.2	0.91	2.17	3.5
Ni-Co(1)	130	23.1	449.9	5.0	0.92	2.25	3.6
	135	23.7	227.5	4.8	0.92	2.23	3.6
	140	24.3	172.7	4.6	0.92	2.12	3.4
	145	24.8	134.1	4.3	0.93	2.07	3.3
	150	24.5	114.3	3.7	0.93	1.80	2.9
Ni-Co(2)	130	21.8	435.7	6.6	0.92	2.91	4.6
	135	22.6	281.3	5.3	0.93	2.72	4.3
	140	22.1	192.4	5.4	0.93	2.64	4.2
	145	22.2	122.8	5.6	0.93	2.74	4.4
	150	23.2	89.2	6.7	0.91	2.75	4.3
Ni-Co(3)	130	23.2	244.1	9.1	0.90	3.42	5.4
	135	23.2	156.9	8.9	0.90	3.27	5.2
	140	23.5	112.1	8.7	0.90	3.17	5.1
	145	23.2	83.0	9.0	0.89	2.96	4.7
	150	23.4	64.7	8.9	0.88	2.64	4.2

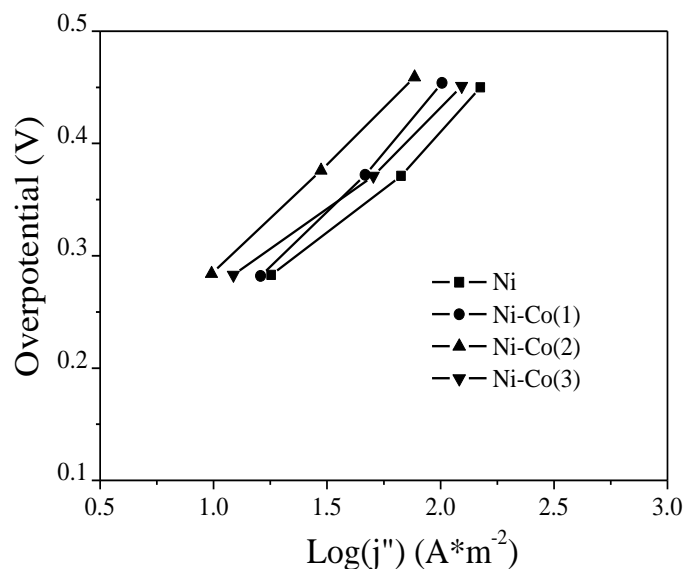


**Figure 5-9 Tafel curves of hydrogen evolution reaction illustrating the intrinsic activity of the Ni and Ni-Co electrodes**

Figure 5-10 shows the SEM images of the Ni-Co electrode surfaces and Table 5-3 presents their surface compositions from the EDX data, respectively. At the magnification of 5000 times, compared to the Ni electrode polished with the P4000 sandpaper (Figure 5-10 (a)), the Ni and Co co-deposition formed films with granular textures on the surfaces. The surface profiles of the three Ni-Co coated electrodes became notably rougher with increasing deposition duration as shown in Figure 5-10 (b), (c) and (d).

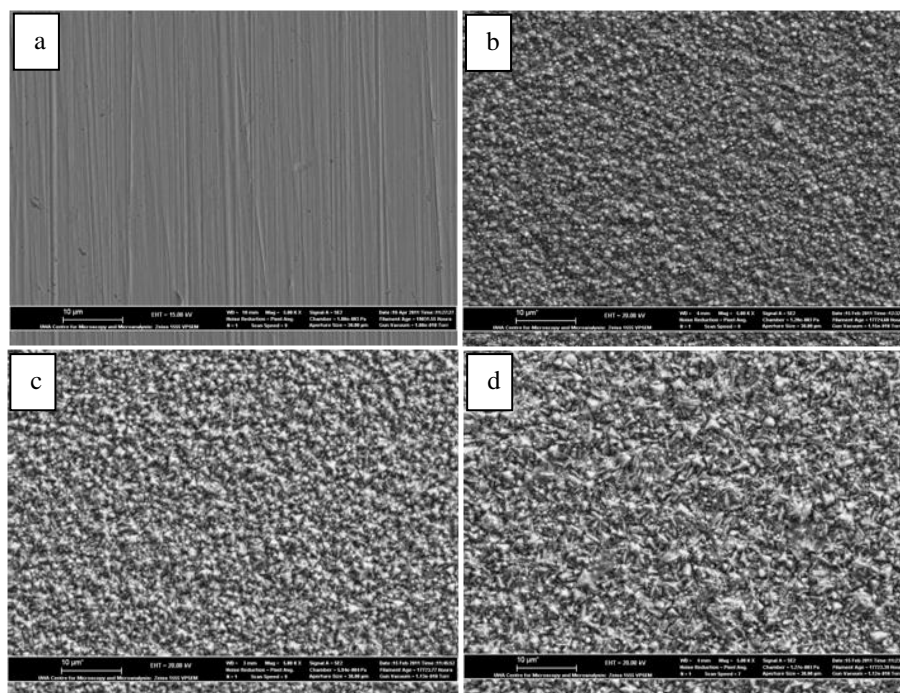


**Figure 5-10 SEM images of Ni-Co electrodes at the magnification of 5000 times [(a) Ni polished with P4000 sandpaper; (b) Ni-Co (1); (c) Ni-Co (2); (d) Ni-Co (3)]**

The EDX data in Table 5-3 show that the Ni contents on the Ni-Co(1) and Ni-Co(3) electrode surfaces were similar and higher than that on the Ni-Co(2) electrode. The variations in Ni-Co electrodes can be correlated with their intrinsic activities, respectively. The Ni-Co(1) and Ni-Co(3) electrodes shared a similar intrinsic activity as their electrode compositions were similar, as shown in Figure 5-9. In contrast, the Ni-Co(2) electrode showed a downgraded intrinsic activity due to the electrode composition difference. This observation is consistent with the finding that the activity of the Ni-Co electrodes is dependent on their Ni-Co composition (Lupi *et al*, 2009).

**Table 5-3 Surface compositions of the Ni-Co coatings at different deposition times as determined in the EDX analysis**

Deposition	Deposition time	Ni composition	Co composition
	Minutes	%	%
Ni-Co(1)	15	37.3±1.1	62.1±0.9
Ni-Co(2)	30	33.2±0.8	66.3±0.8
Ni-Co(3)	60	35.3±1.6	63.8±1.7

Furthermore, the Ni-Co electrodes did not show an enhanced intrinsic activity than the Ni base electrode, as also observed by Correia et al (Correia *et al*, 1999). It may be attributed to the fact that Ni and Co are both from the right hand side of transition metal series. Therefore, the synergism does not arise for the hydrogen evolution reaction (Jaksic, 1984). The increase in the apparent activity of Ni-Co electrode can only be attributed to the increase in the surface area.

Figure 5-9 shows that, the Ni-Co coated electrode is less active than the Ni electrode. On the other hand, Figure 4-10 show that the Ni-Fe-Zn coated electrode has less resistances for the charge transfer, which indicated that the Ni-Fe-Zn coated electrode is more active than the Ni electrode, namely, the Ni-Fe-Zn coated electrode has a better activity for hydrogen evolution reaction than the Ni-Co coated electrode. The following reasons are considered: 1) Figure 5-10 shows that the prepared Ni-Co coating does not have the porous structure as revealed in Figure 4-2 for the Ni-Fe-Zn coated electrode. 2) The electrode combination of Ni, Fe and Zinc has a synergic effect for hydrogen evolution reaction which does not exist in the Ni-Co coated electrode (Jaksic 1984).

## 5.7 Summary

Surface modifications to Ni based electrodes by means of mechanical polishing and electrochemical deposition have been performed and their activities towards hydrogen evolution reaction examined. The Ni electrodes modified by mechanical polishing show enhanced apparent activities than the base Ni. The rougher the Ni electrode surface after the mechanical polishing, the better the electrode activity by exhibiting the lower overpotential. The Ni electrodes, polished with sandpaper P400 with relative roughness factor of 5.2, shows the lowset overpotential of 422 mV at current density of  $750 \text{ A}\cdot\text{m}^{-2}$ .

The concepts of effective surface area and relative roughness factor have been introduced and their values can be derived from the electrochemical impedance studies. When the effective surface area is applied, the Tafel curves of the Ni electrodes polished with different sandpapers collapsed into a narrow band which can be described by the equation  $\eta = 0.02 + 0.191 \cdot \text{Log} j$ ". The equation represents the intrinsic activities of Ni electrodes towards hydrogen evolution reaction and also validates the roughness factor for presenting intrinsic activity.

While the electrodes modified by electrochemical deposition of Ni-Co do change their apparent electrode activities, their intrinsic activities are different, depending on their surface Ni-Co compositions as varied with the deposition time.

## **Chapter 6      Evaluating   the   Behaviour   of Electrolytic Gas Bubbles and Their Effect on the Cell Voltage in Alkaline Water Electrolysis**

### **6.1 Introduction**

As identified in the literature review (Chapter 2), gas bubbles attached to the electrodes present one of the most significant resistances to the whole electrolysis process and their behaviour needs to be fully understood in order to further improve the efficiency of alkali water electrolysis process. Currently, the evolution of electrolytic gas bubble in solutions is a poorly understood complex phenomenon. The evolution of electrolytic gas bubble involves nucleation, growth and departure (Jones *et al*, 1999). The departure of the electrolytic gas bubbles is one of the most influential steps in determining the resistance effects of the gas bubbles. A thorough force analysis is critical to gain a better understanding and to forecast the electrolytic gas bubbles behaviour and their departing from the electrode. Some excellent literature reports examined the possible forces acting on a growing bubble in boiling (Thorncroft and Klausner, 2001, Van Helden *et al*, 1995, Klausner *et al*, 1993). In addition to the predictions of the critical departure diameters of electrolytic bubbles, force analysis was also used to correlate bubble coverage on the electrode with electrolyte flow (Vogt and Balzer, 2005, Eigeldinger, 2000).

This Chapter aims to study the behaviour of gas bubbles and their effect on the cell voltage in water electrolysis theoretically and experimentally. A fundamental force analysis was performed for a single gas bubble on a vertical electrode. The force analysis was then used to predict the critical diameter for the departure of the electrolytic gas bubbles. The predictions were correlated with the observations from a laboratory setup of water electrolysis cell. The resistances of these gas bubbles were also characterised using the Tafel relation between the cell voltages and the cell currents.

As illustrated in Chapter 3, several factors to be considered are electrolyte concentration, cell voltage, temperature, gas property and solid property. For comparison, electrolyte concentration and cell voltage can be varied to examine their effects, while temperature, gas property and electrode surface property are maintained constant or considered unchanged during operation. On the other hand, the lift and drag forces will affect the departure diameter by introducing the electrolyte flow. Polarisation curves were plotted as the cell voltage against the current density. These polarisation curves were employed to characterise the resistance due to the gas bubbles.

## **6.2 Theoretical Analysis**

### **6.2.1 Force Analysis**

The force balance analysis was made, based on two types of electrolytic gas evolution models in this work. Both models were based on a vertical electrode: the first was an electrolytic gas bubble evolution model simply

involved the bubble formation on an electrode and was noted as the *stagnant model*; and the second was a model involves electrolyte flow, by adding an upward electrolyte flow over the electrode and this bubble evolution model was noted as the *flow model*.

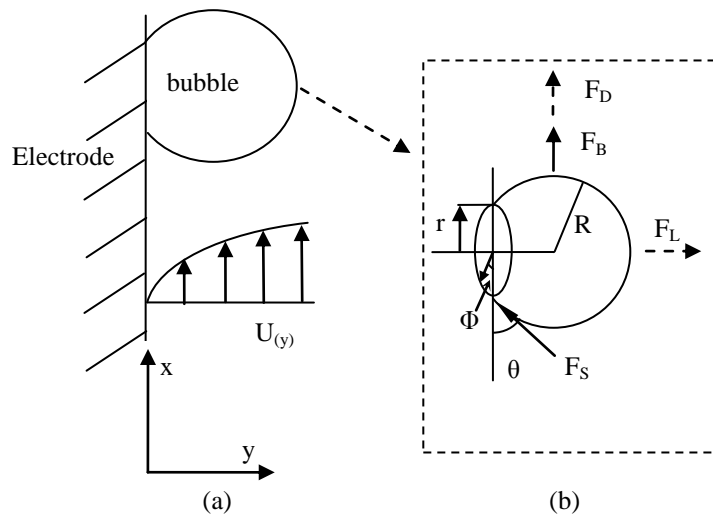


**Figure 6-1 A schematic diagram of a gas bubble on an electrode surface (a), and the forces acting on the bubble (b)**

Figure 6-1 (a) shows a gas bubble on an electrode surface in the stagnant model. In the flow model, the gas bubble experiences an upward electrolyte flow. The  $x$  coordinate is in the direction against gravity, and  $y$  coordinate is normal to the  $x$  coordinate and pointing away from the electrode, respectively. The electrolyte flows in the direction of the  $x$  coordinate,

Figure 6-1 (b) shows the forces acting on the gas bubble originated from various sources. The buoyancy and surface tension exist due to the density difference between liquid and gas and the property of the solution, respectively (Kulkarni and Joshi, 2005). In the presence of the electrolyte flow, a drag force and a lift force also come to play (Cole *et al*, 1980). In

this work, the force incurred by the temperature field effect is neglected by maintaining the temperature of the electrolyte constant.

The forces acting on a gas bubble can be decomposed into components along the x and y coordinates, resulting in possible movements of gas bubbles in the corresponding directions. These movements are noted as departure and lift-off, respectively.

### 6.2.2 Buoyancy

The buoyancy,  $F_B$ , is composed of the force from the pressure and the gravity on the mass of the gas bubble, which is expressed by Equation 6-1

$$F_B = \int_{A_B} p_L(x) dA + \int_{A_C} p_B dA - \int_{V_B} \rho_B g dV \quad 6-1$$

where  $A_B$  and  $A_C$  are the surface area of the gas bubble contacting the electrolyte and the contact area between the gas bubble and the electrode, respectively.  $p_L$  and  $p_B$  are the pressures of liquid and gas bubble, respectively.  $V_B$  is the gas bubble volume and  $\rho_B$  is the gas bubble density. The gravitational force on the gas bubble mass is assigned negative as it acts in the opposite direction of the x coordinate.

After rearrangement and integration (Van Helden *et al*, 1995), the buoyancy can be simplified (Eigeldinger, 2000) as Equation 6-2)

$$F_B = (\rho_L - \rho_B) g V_B e_x + [(\rho_B - \rho_L) g R + 2\sigma / R] \times \pi r^2 e_y \quad 6-2$$

where,

$$V_B = 1/3 \pi R^3 (1 + \cos \theta)^2 (2 - \cos \theta) \quad 6-3$$

$\rho_L$  is the density of the liquid.  $\sigma$  is the surface tension between the gas and the electrolyte liquid.  $\theta$  is the contact angle between the liquid-gas and liquid-solid interface,  $R$  and  $r$  are the diameter of the gas bubble and its circular contact area with the electrode, respectively, as shown in Figure 6-1 (b).

### 6.2.3 Expansion Force

Due to the growth of the gas bubble with the gas production, the pressure of the bubble experiences a dynamic change, which can be described by the well known Rayleigh equation (Van Helden *et al*, 1995). The gas bubble radius can be expressed as a function of time by  $R(t) = k \cdot t^{1/2}$  (Zeng *et al*, 1993), where,  $k$  is an empirical coefficient. There is a force present due to the expansion of the bubble which is estimated by  $F_G = -2\pi\rho_L R^2 \dot{R}^2$  (Van Helden *et al*, 1995, Thorncroft and Klausner, 2001), where,  $\dot{R}$  denotes the growth rate of radius with respect to time,  $\dot{R}(t) = 1/2 \cdot k \cdot t^{-1/2} = k^2 / 2R$ , so the expansion force can be simplified as Equation 6-4

$$F_G = -\pi\rho_L \cdot k^4 e_y \quad 6-4$$

where the coefficient  $k$  is a constant determined experimentally.

### 6.2.4 Interfacial Tension Force

The interfacial tension force exerted on the gas bubble exists along the circular contact area where the gas, liquid and solid phases are in contact with each other. It can be expressed by Equation 6-5 (Van Helden *et al*,

1995, Klausner *et al*, 1993) in the directions of x and y coordinates, respectively

$$F_s = r\sigma \int_0^{2\pi} \cos \theta \cos \phi d\phi e_x - r\sigma \int_0^{2\pi} \sin \theta d\phi e_y \quad 6-5$$

where  $\phi$  is the circumferential angle as in Figure 6-1 (b).

The equation includes the situation where the gas bubble experiences an inclination due to the buoyancy during its growth, where the contact angle  $\theta$  is a function of  $\phi$ . In this simplified model, the electrolytic gas bubble is assumed to grow symmetrically. The interfacial tension force can be expressed as  $F_s = -2\pi r\sigma \sin \alpha e_y$ , where  $\sigma$  is the surface tension between the electrolyte liquid and the gas.

The surface tension and the contact angle are the two key components determining the interfacial tension force. However they have been approximated as the properties of liquid. Due to the fact that the origin of the interfacial tension is from the contact of the three phases, more factors need to be considered in modelling the bubble behaviour in water electrolysis, for example, the electrode potential (Kaninski *et al*, 2011) and surface roughness of the electrode.

Equations 6-6 to 6-9 show that the surface tension can be found as a function of electrolyte concentration gradient (Weissenborn and Pugh, 1995), pressure gradient, (Lubetkin, 2002) temperature gradient (Van Helden *et al*, 1995), and voltage gradient (Lubetkin, 2002), respectively.

$$\sigma = \sigma_1 + k_1 \Delta c \quad 6-6$$

$$\sigma = \sigma_2 + k_2 \Delta p \quad 6-7$$

$$\sigma = \sigma_3 + k_3 \Delta T \quad 6-8$$

$$\sigma = \sigma_4 + k_4 \Delta U \quad 6-9$$

All these empirical equations provide quantitative information of the trend of interfacial tension force for the prediction of the critical diameter.

### 6.2.5 Drag and Lift Forces

Due to the flow velocity distribution shown in Figure 6-1 (a), the drag and lift forces acting on a bubble attached to a wall can be derived. By definition, they are in the directions of x and y coordinates (Van Helden *et al*, 1995) and can be expressed as  $F_D = 1/2 \cdot \zeta_D \rho_L v^2 A_a e_x$  and  $F_L = 1/2 \cdot C_L \rho_L v^2 A_a e_y$ , respectively, where  $\zeta_D$  and  $C_L$  are the drag and lift coefficients, respectively.  $v$  is the velocity of flow.  $A_a$  is the projected area of the bubble on the horizontal plane, that is, the maximum bubble cross section perpendicular to the flow direction,  $A_a = \pi R^2 [1 - (\theta - \cos \alpha \sin \theta) / \pi]$  (Eigeldinger, 2000).

## 6.3 Bubble Departure Diameter Predictions

When the gas bubble is attached to the electrode surface as shown in Figure 6-1, both  $\sum F_x = 0$  and  $\sum F_y = 0$  are satisfied. Once one of these conditions is broken, the gas bubble departs or lifts off from the electrode, respectively.

In the stagnant model, when the gas bubble attaches on the electrode surface,  $\sum F_x = F_b > 0$ . Therefore, the buoyancy force is not balanced with the sum of the other forces. This unbalance will force the bubble tilts upwards to reach a new force balance and then departs when the bubble can no longer tilts after sufficient growth in size.

The upward tilting of the bubble causes so-called advancing and receding angles (Van Helden *et al*, 1995), which are denoted as  $\alpha$  and  $\beta$  in Figure 6-2. Therefore, there will be an interfacial tension force in the x coordinate direction. This force will be balanced with the buoyancy force to maintain the bubble attachment on the electrodes.

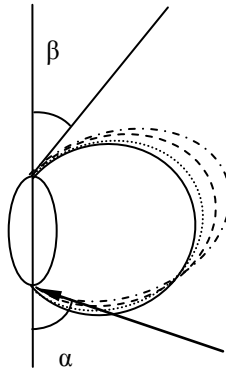


**Figure 6-2 Advancing and receding angles of a gas bubble attached to a vertical electrode surface**

Assuming a linear relationship between the contact angles and the circumferential angle (Klausner *et al*, 1993), that is  $\theta = \beta + (\alpha - \beta) \cdot \phi / \pi$ , substitution of  $\theta$  into the interfacial tension force equation results in

$$F_{s,x} = -2r\sigma \frac{\pi(\alpha - \beta)}{\pi^2 - (\alpha - \beta)^2} [\sin \alpha + \sin \beta] \quad 6-10$$

$$F_{s,y} = -2r\sigma \frac{\pi}{(\alpha - \beta)} [\cos \beta - \cos \alpha] \quad 6-11$$

Replacing Equation, 6-1), 6-2) and 6-4) in the force balance  $F_{B,x} + F_{S,x} = 0$ , yield Equation 6-12)

$$1/3(\rho_L - \rho_B)g\pi R^3(1+\cos\theta)^2(2-\cos\theta) - 2r\sigma \frac{\pi(\alpha - \beta)}{\pi^2 - (\alpha - \beta)^2} [\sin \alpha + \sin \beta] = 0 \quad 6-12$$

Therefore, the critical diameter of a gas bubble, above which the bubble departs, in the stagnant model can be approximated as Equation 6-13).

$$R = 2r = 2\sqrt{\frac{6\sin\theta\sigma(\alpha - \beta)[\sin \alpha + \sin \beta]}{(\rho_L - \rho_B) \cdot [\pi^2 - (\alpha - \beta)^2] \cdot g \cdot (1+\cos\theta)^2(2-\cos\theta)}} \quad 6-13$$

where,  $\rho_L$ ,  $\rho_B$  can be considered as constants.

The critical diameter for gas bubble departure can be expressed in Equation 6-14) by simplifying Equation 6-13).

$$R = k \cdot f(\theta, \alpha, \beta) \cdot \sqrt{\sigma} \quad 6-14$$

where,

$$f(\theta, \alpha, \beta) = 2\sqrt{\frac{\sin\theta(\alpha - \beta)[\sin \alpha + \sin \beta]}{[\pi^2 - (\alpha - \beta)^2] \cdot (1+\cos\theta)^2(2-\cos\theta)}} \quad 6-15$$

Combing Equations 6-6-6-9 with 6-15, it can be predicted that varying the electrolyte concentration and the cell voltage will alter the interfacial tension force and thus the critical diameter for the bubble departure. These changes can be estimated that the critical diameter for the bubble departure can be calculated. Experiment data can be recorded to verify the dependence of the

critical diameter on the parameters such as cell voltage and electrolyte concentration. The theoretical values can be then compared to validate the predictions.

To calculate the critical diameter for bubble departure, a few parameters in Equation 6-13 need to be analysed, such as contact angles and surface tension. The advancing and receding contact angles are usually measured through experimentation (Al-Hayes and Winterton, 1981). They characterise the flexibility of the gas bubble in distortion. It is determined by the surface tension, thus the surface defects (Drelich *et al*, 1996), and the property of the gas and liquid (Tadmor, 2004). Although the understanding of phenomenon is still poor, it can be assumed that the bubble size is a function of  $\theta$ ,  $\alpha$ ,  $\beta$  and the interfacial tension  $\sigma$ .

The contact angles for both hydrogen bubbles and oxygen bubbles had been experimentally determined by Matsushima (Matsushima *et al*, 2006) and extracted for our prediction. The average contact angle for hydrogen bubbles and oxygen bubbles were  $43^\circ$  and  $50^\circ$ , respectively. The advancing angle and the receding angle can be written as Equations 6-16) and 6-17) and  $\Delta\theta$  was reported with values not more than  $10^\circ$  (Yeoh *et al*, 2008), the critical diameter of the hydrogen bubble and the oxygen bubble can be calculated according to Equation 6-13.

$$\alpha = \theta + \Delta\theta \quad \text{6-16}$$

$$\beta = \theta - \Delta\theta \quad \text{6-17}$$

Take a 0.5M KOH solution for an example, its density is  $1.02\text{kg}\cdot\text{m}^{-3}$  at the temperature of  $20^\circ\text{C}$ , and its surface tension is  $72.4\text{mN}\cdot\text{m}^{-1}$ . Assuming  $\Delta\theta$

is  $6^\circ$ , the critical diameter for the departure of hydrogen and oxygen gas bubbles was predicted to be 0.50mm and 0.57mm, respectively.

Increasing the potential applied to the electrodes enhanced the wettability of the electrodes (Brussieux *et al*, 2011), which led to an increase in the surface tension and  $\Delta\theta$ . On the other hand, increasing electrolyte concentration led to an increase of electrolyte viscosity and surface tension. The increase in the electrolyte viscosity caused not only less coalescence of bubbles (Lumanauw, 2000) but also a reduction in  $\Delta\theta$ .

In the flow model, the drag force was added to the force balance so that

$$\frac{(\rho_L - \rho_B)g\pi R^3(1+\cos\theta)^2(2-\cos\theta)}{3} + \frac{\zeta_D \rho_L v^2 A_a}{2} - 2r\sigma \frac{\pi(\alpha - \beta)}{\pi^2 - (\alpha - \beta)^2} [\sin\alpha + \sin\beta] = 0 \quad 6-18$$

Therefore, applying electrolyte flow will bring down the critical diameter for bubble departure.

## 6.4 Dependence of Critical Diameter for Bubble Departure on Cell Voltage

Figure 6-3 shows typical images of hydrogen bubbles in 0.5M KOH at different current densities. To avoid the coalescences of bubbles, the current density applied was set at very low values so that the growth and detachment of a single bubble could be observed and analysed individually.

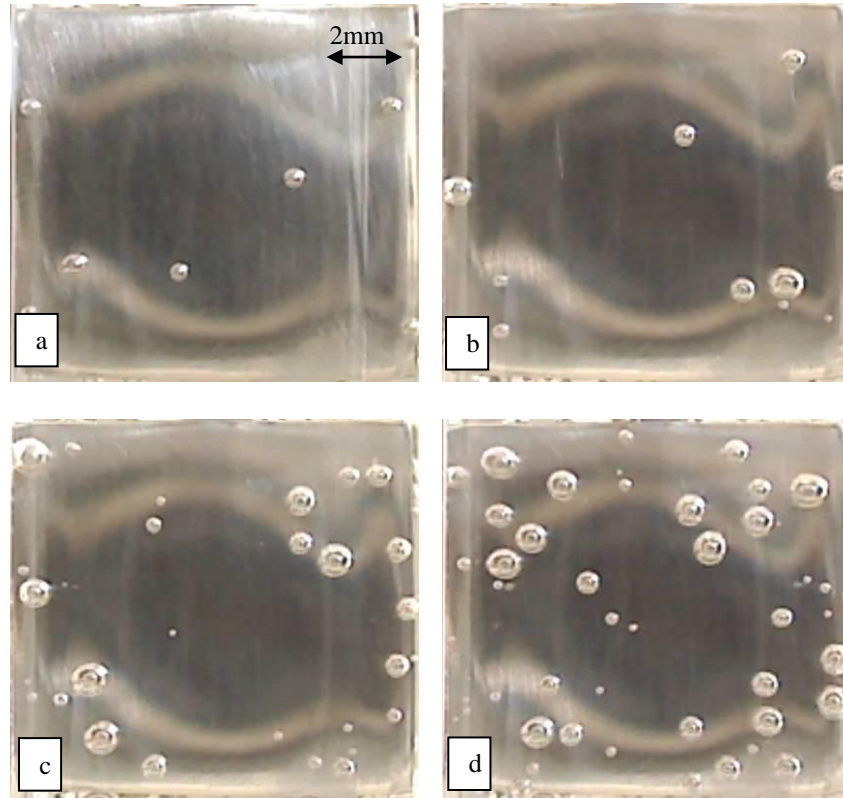


**Figure 6-3 Typical images of hydrogen bubbles in 0.5M KOH, at  $22\pm1^\circ\text{C}$ , at different current densities: (a)  $0.3\text{ mA}\cdot\text{cm}^{-2}$  (b)  $0.45\text{ mA}\cdot\text{cm}^{-2}$  (c)  $0.6\text{ mA}\cdot\text{cm}^{-2}$  (d)  $0.75\text{ mA}\cdot\text{cm}^{-2}$**

Each image of Figure 6-3 shows a number of individual hydrogen bubbles of different diameters. These bubbles were at different stages of growth. The images were extracted immediately before the largest bubble detached. Therefore, the largest bubble on each image represented the critical diameter under the particular current density.

The critical diameter for hydrogen bubble departure increased with increasing current density. When the current density increased from  $0.3\text{ mA}\cdot\text{cm}^{-2}$  to  $0.60\text{ mA}\cdot\text{cm}^{-2}$ , the critical diameter also increased from 0.59mm to 1.09mm. The number of hydrogen bubbles at a higher current density was also larger than that at a lower current density.

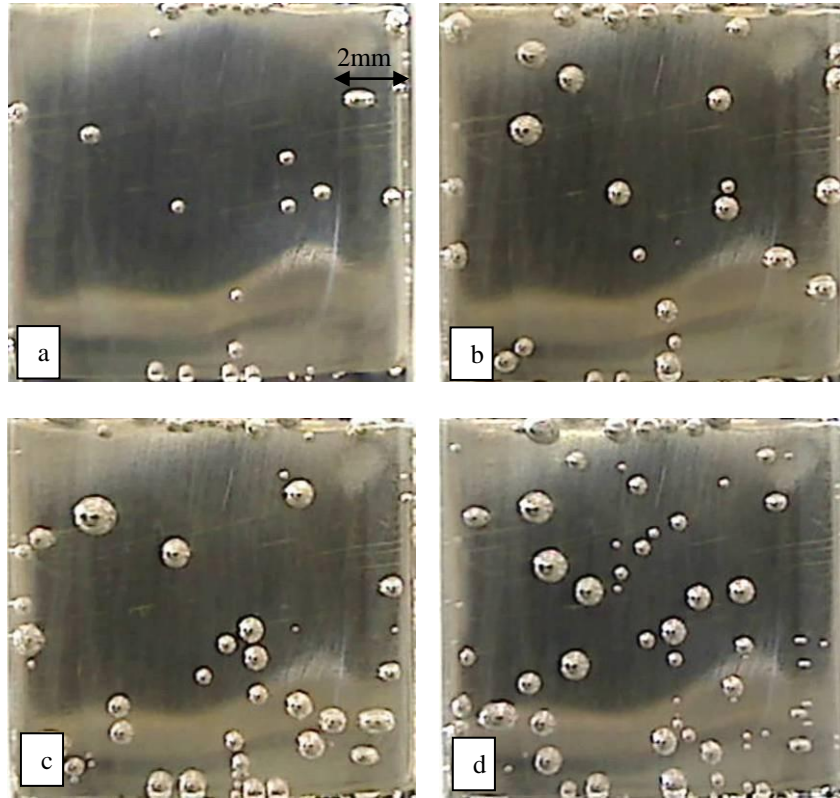


**Figure 6-4 Typical images of oxygen bubbles in 0.5M KOH, at  $22\pm1^{\circ}\text{C}$  at different current densities ( $\text{mA}\cdot\text{cm}^{-2}$ ): (a) 0.3 (b) 0.45 (c) 0.6 (d) 0.75**

Figure 6-4 shows typical images of oxygen bubbles in 0.5M KOH at different current densities. Note that the critical diameter for oxygen gas bubble departure increased from 0.60 mm to 1.08 mm when the current density increased from  $0.3\text{mA}\cdot\text{cm}^{-2}$  to  $0.60\text{mA}\cdot\text{cm}^{-2}$ .

The dependence of the critical diameters on cell voltage for hydrogen and oxygen bubbles departure is presented in Table 6-1. The trend of increasing the critical diameters with increasing cell voltage can be explained by the increased interfacial tension at higher electrode potentials (Lubetkin, 2002). At a higher current density, the cell voltage was also higher and therefore the interfacial tension force in the x coordinate direction was greater. Furthermore, the bubble buoyancy force had to be large enough to overcome the interfacial tension by increasing bubble diameter.

However, at the highest current density of  $0.75\text{mA}\cdot\text{cm}^{-2}$ , the critical diameter for both hydrogen and oxygen bubbles decreased a little. This could also be attributed to the higher current density. In this case, high current densities can lead to two possible changes. The first one is that the high voltage applied would result in local heating due to high ohmic loss. The localised heating will cause temperature gradient on the electrode surface. The second change is the number of gas bubbles. More bubbles formed and departed in high current density as in Figure 6-3 (d) and Figure 6-4 (d). Both the temperature field and the bubble movement will result in natural convection or micro-convection of the electrolyte. This may cause some bubbles depart prematurely.

It should be noted that the critical diameter concept can only be applied to ideal situations where the temperature throughout the electrolysis cell is uniform, the electrolyte is stagnant and the electrode surfaces are smooth so that the physical properties of the nucleation sites (such as the surface roughness) for the bubble growth are uniform for all bubbles. In experimentation and practical water electrolysis systems, it would be rather difficult to attain the ideal situation and, as such, the observed bubble departure may not be uniform.

**Table 6-1 The critical diameters for hydrogen and oxygen bubble departure at different cell voltages in 0.5M KOH at 22±1°C**

Current density	Cell voltage	Critical diameter (hydrogen)	Critical diameter (oxygen)
$\text{mA}\cdot\text{cm}^{-2}$	V	mm	mm
0.30	1.72	0.59	0.60
0.45	1.83	0.88	0.89
0.60	1.88	1.09	1.08
0.75	1.93	1.03	0.96

It was interesting to note that, during the experiments at the high cell voltages, at  $0.75\text{mA}\cdot\text{cm}^{-2}$  for instance, some fine bubbles much smaller than the observed critical diameters for hydrogen and oxygen, respectively, also departed. It can also be explained that the natural convection of the electrolyte caused by the bubble movement and temperature field due to local heating. The natural convection may prevent the small bubbles at the nucleation site from growing. Therefore, small bubbles beyond the detection departed from the electrode.

## 6.5 Dependence of Critical Diameter for Bubble Departure on Electrolyte Concentration

Since the electrolyte concentration also plays an important role in the interfacial force, its effect on the critical diameter for bubble departure was also examined. Figure 6-5 shows the typical images of hydrogen bubbles at the current density of  $0.60\text{mA}\cdot\text{cm}^{-2}$  in the KOH solutions of different concentrations. It was found that increasing KOH concentration from 0.5M to 4M dramatically decreased the critical diameter for hydrogen bubble departure and the number of bubbles was reduced as well. A similar decrease in the critical diameter was also found for the oxygen bubbles.

At a given current density,  $0.60 \text{ mA}\cdot\text{cm}^{-2}$  in this case, an increase in the electrolyte concentration resulted in decreases in cell voltage from 1.88 to 1.77V and an increase in electrolyte surface tension from 73 to  $84\text{dyns}\cdot\text{cm}^{-1}$  (Dunlap and Faris, 1962), which would have opposite effects on the critical diameter according to Equation 6-6, 6-9 and 6-14. These two factors need to be examined separately for their effect on the critical diameter.

Table 6-2 lists the critical diameter for hydrogen bubbles and corresponding the cell voltages at all concentrations tested. The cell voltages decreased from 1.88 to 1.77V when the concentration of KOH varied from 1M to 4M. The decreasing trend of the critical diameter was in accordance with its dependence on the cell voltage. Assuming the decreasing cell voltage was the only cause of the bubble size reduction, the critical diameter should be located between 0.59 and 1.08mm according to Table 6-1. However, the critical diameter of the hydrogen bubbles was reduced dramatically when the electrolyte concentration increased. Therefore, it can be ruled out that the cell voltage change alone caused the reduction in the hydrogen bubble critical diameter.

On the other hand, as the KOH concentration increased, the viscosity of the electrolyte increased and the surface tension would have increased (Dunlap and Faris, 1962). The increase in surface tension would result in the increase of the critical diameter. However, the critical bubble diameter was decreased. This led to only one possibility that the increase in viscosity result an adverse effect. It is proposed that the change in viscosity led to the decrease in  $\Delta\theta$ . The increased viscosity made it harder for the bubble to tilt or stretch,

which would result the decrease in  $\Delta\theta$ . According to Equation 6-10, the interfacial force in the direction of x coordinate would also decrease. Ultimately, a decrease in the critical diameter for bubble departure as indicated in Equation 6-13.

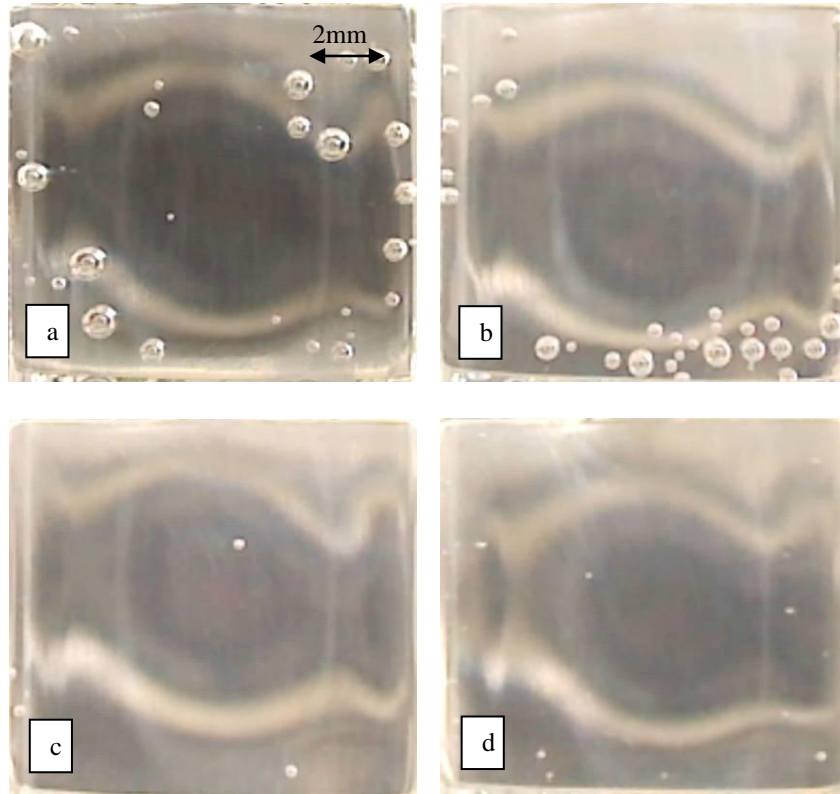


**Figure 6-5** Typical images of hydrogen bubbles at  $0.6\text{mA}\cdot\text{cm}^{-2}$  at  $22\pm 1^\circ\text{C}$  in KOH solutions of different concentrations (a) 0.5M (b) 1M (c) 2M (d) 4M

**Table 6-2** The critical diameters for hydrogen bubble in different KOH concentrations at  $22\pm 1^\circ\text{C}$  at current density  $0.6\text{mA}\cdot\text{cm}^{-2}$

KOH concentration	Cell voltage	Critical diameter (hydrogen)
M	V	mm
0.5	1.88	1.08
1.0	1.80	0.50
2.0	1.78	0.36
4.0	1.77	0.24

## 6.6 Bubble Behaviour at High Cell Voltages

The emergence of fine bubbles departing from the electrode had been identified for both hydrogen and oxygen bubbles when the cell voltage was

1.88V. It was reasonable to predict that more fine oxygen and hydrogen bubbles would be formed if the cell voltage increased further. As shown in Figure 6-6, as the cell voltage increased from 2.2V to 2.8V, more and more and increasingly smaller bubbles detached from the electrode. The diameters of these fine bubbles in Figure 6-6 (c) and Figure 6-6 (d) could not be detected by the current imaging technique.

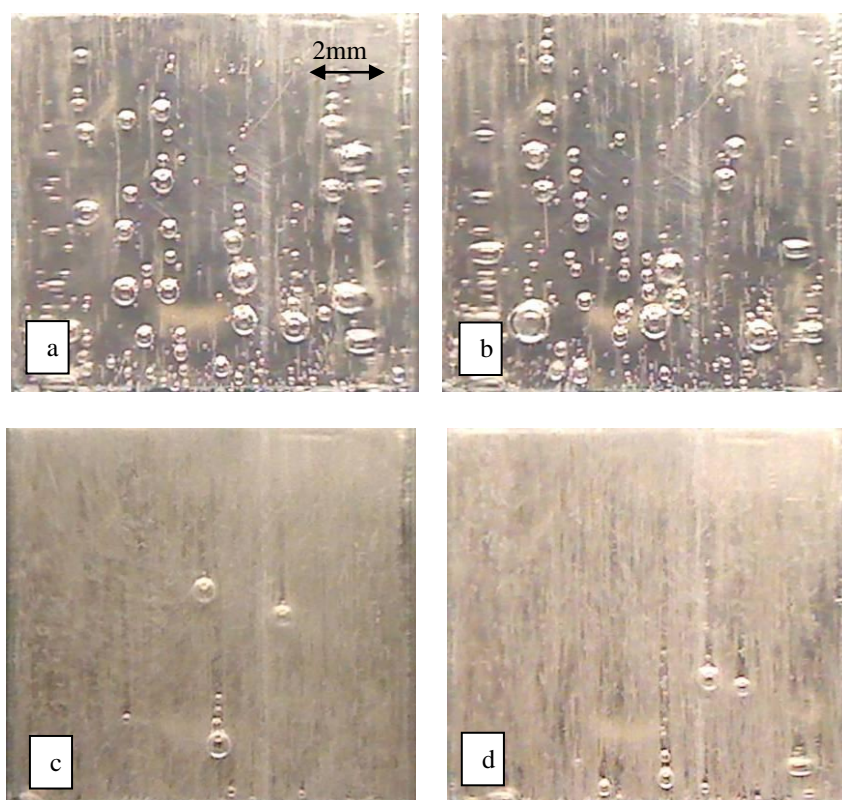


**Figure 6-6 Typical images of hydrogen bubbles in the water electrolysis at different cell voltage in 0.5M KOH electrolyte of  $22\pm1^{\circ}\text{C}$  (a) 2.2V (b) 2.4V (c) 2.6V (d) 2.8V**

One possible explanation to this phenomenon is that at high cell voltages, and therefore, high current densities, gases were produced at high rates. New gas bubbles repelled the gas bubbles formed earlier away from the electrode surfaces. In the meantime, the natural convections caused by the upward electrolyte motion due to the rapidly rising bubble and the

temperature field caused by the field localised heating would have also enhanced the departure of the rapidly forming gas bubbles (Iida *et al*, 2007).

## 6.7 The Effect of Electrolyte Circulation

The images in Figure 6-7 were also taken immediately before the largest bubble departed. Figure 6-7 (a) and Figure 6-7 (b) show the typical images of hydrogen bubbles in the 0.5M KOH electrolyte solution at the current density of  $0.75\text{mA}\cdot\text{cm}^{-2}$  without and with electrolyte circulation, respectively. The Reynolds number of the electrolyte flow was 2521. As can be seen, the diameter of the largest bubble departing the electrode was dramatically reduced as expected when the electrolyte circulation was applied due to drag and lift forces. At the current density of  $200\text{mA}\cdot\text{cm}^{-2}$ , it was found that the large amount of small gas bubbles were generated that the fine bubbles formed a bubble curtain on the electrode surface. The application of the electrolyte circulation did force most of bubbles departed before growing into critical diameter for departure. However, the bubble curtain was still on the surface of electrode which still posed a resistance barrier for water electrolysis.

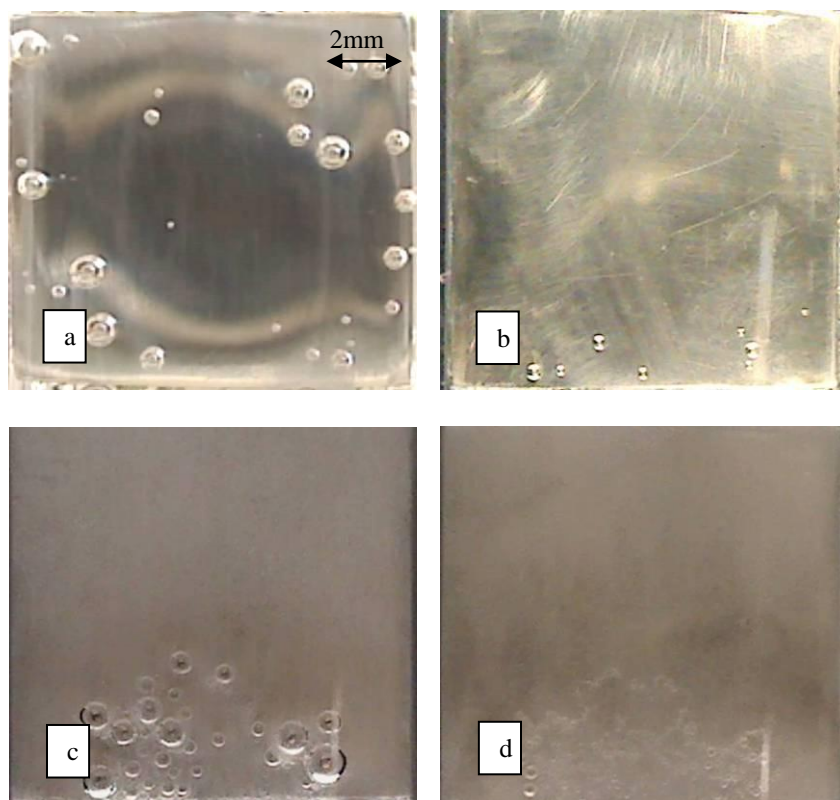


**Figure 6-7** Typical images of hydrogen bubbles in 0.5M KOH at the current density of  $0.75\text{mA}\cdot\text{cm}^{-2}$  (a) without circulation; (b) with circulation; and at the current density of  $200\text{mA}\cdot\text{cm}^{-2}$  (c) without circulation (d) with circulation The Reynolds number for both cases were 2521

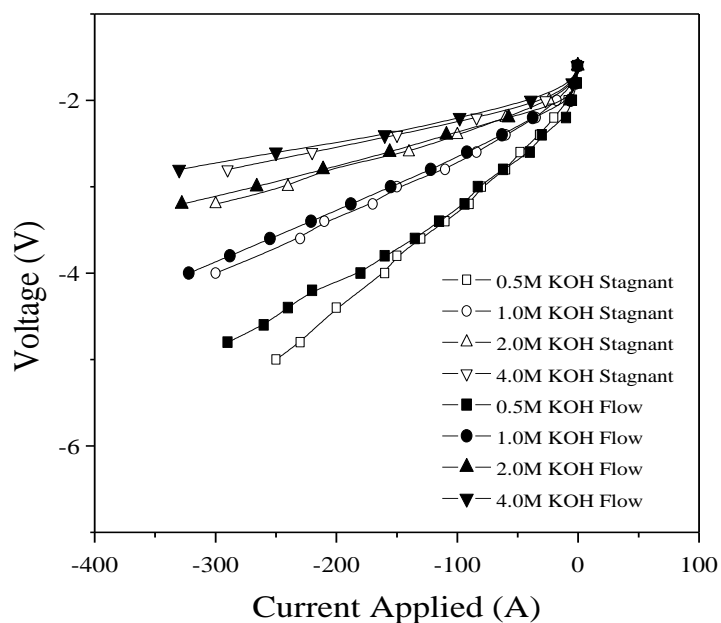


**Figure 6-8** Polarisation curves at different KOH concentrations with and without electrolyte circulation

Figure 6-8 shows the polarisation curves of water electrolysis in the stagnant and flow models at different KOH concentrations. The flow rate was controlled at  $1.6 \text{ L}\cdot\text{min}^{-1}$  and the Reynolds number were 2521, 2548, 2447 and 2002 for 0.5M, 1.0M, 2.0M and 4.0M KOH, respectively. The polarisation curves with hollow dot points were recorded in different electrolyte concentrations without electrolyte flows. The polarisation curve in 4.0M KOH showed the lowest cell voltages, followed by the polarisations curves in 2.0M and 1.0M and 0.5M KOH.

The polarisation curves with solid dot points were recorded with electrolyte flows in 0.5M, 1.0M, 2.0M and 4.0M KOH, respectively. There were small reductions in cell voltage in polarisation curves with electrolyte flows comparing those without electrolyte flow. This may be attributed to the removal of the grown bubbles at the electrode surface by the electrolyte circulation. However, due to the fact that bubble curtain still existed on the electrode especially at high current densities, it can be inferred that this bubbles forth layer represented the most of the resistance caused by bubble (Zeng and Zhang, 2010).

## **6.8 Comparison of Model Predictions with Experimental Observations**

The prediction of the critical diameter for bubble departure was based on Equation 6-13, where  $\sigma$ ,  $\theta$ ,  $\alpha$  and  $\beta$  were unknown parameters. The value or the range of these parameters was sourced from literature. Table 6-3 is a summary of the values used in predicting the critical diameter of bubble departure. The surface tension of the KOH solution was found 73.3, 78.5,

81.7 and 86.4 dyns·cm<sup>-1</sup> for solutions of 0.5, 1.0, 2.0 and 4.0M KOH, respectively (Dunlap and Faris, 1962). Due to the effect of electrode potential, the values of surface tension were increased accordingly. The contact angles for oxygen and hydrogen were independent of electrolyte and electrode potential, and were recorded 50° and 43° according to Matsushima (Matsushima *et al*, 2006).  $\alpha$  and  $\beta$  were assumed through Equation 6-16 and 6-17, where  $\Delta\theta$  was chosen in the range between 0° and 10° (Yeoh *et al*, 2008), and the value selection of  $\Delta\theta$  and  $\sigma$  were in agreement with the previous analysis of the effect of current density and KOH concentration.

**Table 6-3 A summary of parameters for predicting the critical diameter for bubble departure**

		$\sigma$ / dyns·cm <sup>-1</sup>	$\theta_{H_2}/^\circ$	$\theta_{O_2}/^\circ$	$\Delta\theta/^\circ$
<b>Current density/ mA·cm<sup>-2</sup></b>	0.30	84.0	50	43	6
	0.45	89.0	50	43	8
	0.60	94.0	50	43	9
	0.75	100.0	50	43	10
<b>Concentration/ M</b>	0.5	94.0	50	43	8
	1.0	94.0	50	43	4
	2.0	94.0	50	43	3
	4.0	94.0	50	43	1.5

With the predicted values for contact angle and surface tension, the critical diameter for bubble departure can be calculated. Figure 6-9 shows a comparison between the predicted and the measured critical diameters. A generally good agreement is evident for both hydrogen and oxygen gas bubbles. The predicted critical diameters were between 0.25mm to 0.90 mm. When the KOH concentration increased, the critical diameter dropped from 0.57mm, and the predicted critical diameter agreed with the measurement well. On the other hand, the potential increased, the predicted critical diameters were lower than that of measured values. This is due to the lack of

empirical data for the expansion force and the dependence of surface tension on electrode potential.

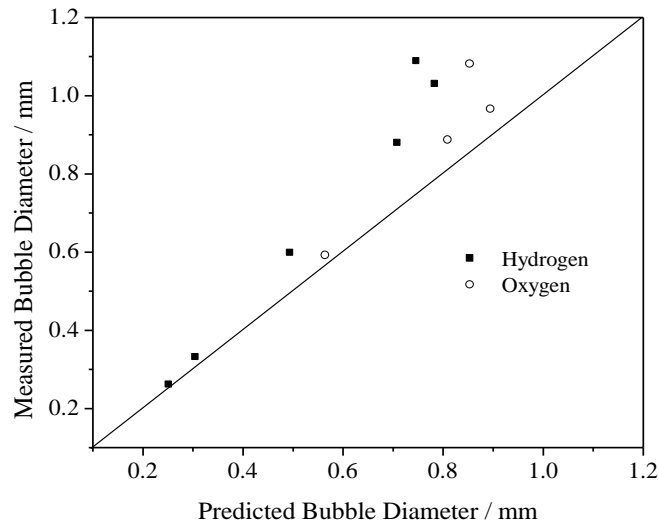


**Figure 6-9 Comparison of the predicted and measured critical diameters for hydrogen and oxygen gas bubbles**

Unfortunately, due to the lack of data, it was difficult to quantify the relationship between the drag and lift forces acting on bubble at the presence of the electrolyte circulation. Therefore, the predicted values were not presented in Figure 6-9. However, Figure 6-7 presented the significant decrease of bubble diameters in critical bubble diameter, which is also in agreement with the Equation 6-18.

## 6.9 Summary

A detailed force analysis was applied to analyse the behaviour and critical diameters of hydrogen and oxygen gas bubbles formed on smooth electrode surfaces during alkaline water electrolysis. It was found that, at the current densities below  $1 \text{ mA}\cdot\text{cm}^{-2}$ , the critical diameter of electrolytic gas bubble was highly dependent on the factors affecting the interfacial tension force,

such as electrolyte concentration and cell voltage. Increasing cell voltage increased the critical diameter for hydrogen and oxygen bubble departure from 0.59 to 1.03 mm and from 0.60 to 1.08 mm, respectively. The critical diameter for hydrogen bubbles departure decreased to 0.27 mm as the KOH concentration increased. Similar findings also applied to oxygen gas bubbles. The predicted critical diameters were in good agreement with the measured values.

At the current densities of  $200 \text{ mA}\cdot\text{cm}^{-2}$ , due to the effect of temperature gradient and force convection, many bubbles departed prematurely and formed a layer of small bubbles on the electrode surface. On the other hand, as some bubbles grew and merged with other small bubbles, these bubbles could reach their critical bubble diameter. To study the effect of these bubbles, the electrolyte circulation was introduced. It was found that the application of electrolyte circulation prevented the growth of the bubbles. However, the layer of small bubbles still existed. The polarisation curves showed small reductions in the cell voltage when the electrolyte circulation was applied, which can be explained by that the layer of small gas bubbles on the electrode surface presented a significant energy barrier for alkaline water electrolysis.

## **Chapter 7      Evaluation      and      Practical Implications**

In this chapter, the results and important findings from the work detailed in Chapter 4 to Chapter 6 are integrated and evaluated, and their potential implications are assessed, with reference to the gaps identified and objectives set up as presented in Chapter 2. In evaluating the work, comparisons of the findings from the current studies with those from previous studies are also made correspondingly. Potential practical implications are also discussed using a hypo-theoretical distributed energy system as an example. The evaluation also identifies and highlights new gaps in knowledge, technology and practical uses to which future research should be directed.

In the literature review, it was identified that there are several energy barriers in the process of alkaline water electrolysis which turn energy to heat. These resistances included electrical resistances, electrochemical reaction resistances and transport-related resistances. To understand and minimise the effect of these resistances, the specific objectives of this thesis work included (1) identifying the resistances that cause the loss of energy efficiency and quantify them and find out the most significant ones for improvements by this research, (2) reducing electrochemical reaction resistance by modifying electrode preparation methods (3) reducing electrochemical reaction resistance by electrode surface profile

modifications and surface coatings and (4) understanding bubble behaviour and managing the gas bubble resistances. These objectives were achieved through the detailed study in Chapter 2, Chapter 4, Chapter 5 and Chapter 6 and will be discussed in the following sessions.

The important improvements in knowledge and potential innovations in technology achieved in this thesis are presented as follows:

- 1) For the first time, the resistances of an electrolysis process were generalised and defined using an analogy of electrical circuit, and these resistances were quantified using the existing data from the literature. This served as a guideline for improving of water electrolysis and other electrochemical reactions.
- 2) From the electrode kinetic study, the effect of surface area was discussed and the roughness factor was employed to quantify the effect of electrode modifications. The intrinsic activity of nickel electrode was determined as  $\eta = 0.02 + 0.191 \cdot \text{Log} j''$ .
- 3) A model of the behaviour of gas in water electrolysis was established using a fundamental force analysis. The experimental results were in good agreement with the prediction produced by the model. This can provide guidelines for managing the resistances caused by bubbles.

## **7.1 The Electrode Kinetics on Ni and Ni-Co**

Electrode material is one of the most important research areas in alkaline water electrolysis. The properties of the electrode surface influence or

determine the rate of the electrode reactions. Electrode preparation through electrode-deposition can enhance the activity of electrode reaction, which can be demonstrated from the kinetic parameters of Tafel curve, such as Tafel slope and exchange current density (Kaninski *et al*, 2009, Krstajic *et al*, 2008).

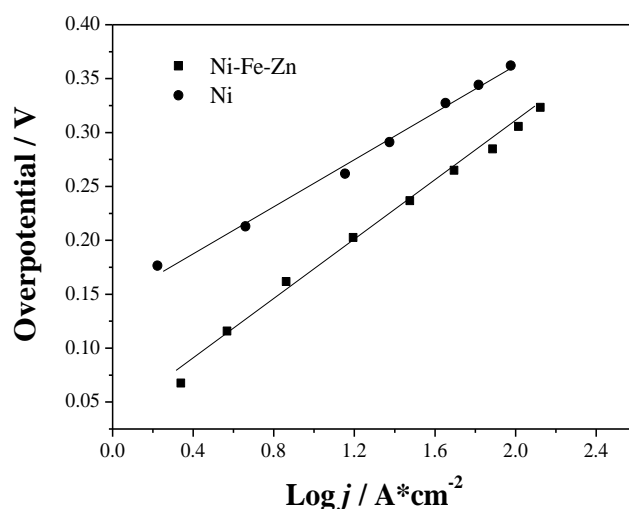


**Figure 7-1 The Tafel curves of hydrogen evolution reaction on both Ni and Ni-Fe-Zn electrodes**

It was found that the Tafel slope of the hydrogen evolution reaction on Ni electrode was  $108 mV \cdot dec^{-1}$  and the Tafel equation can be written as  $\eta = 0.14 + 0.108 \log j$  in Figure 7-1. The finding in the present experiment work is consistent with the literature values (Kaninski *et al*, 2009, Kubisztal *et al*, 2007), demonstrating the validity of the experimental technique. Detailed comparison can be found in Table 7-1. The difference between the kinetic parameters in the current study and previous studies can be attributed the different concentration. The selection of 0.5M KOH was to ensure that the electrode reaction was under the kinetic control. The linear relationship

between overpotential and the logarithm of current density confirmed the electrode reaction was under kinetic control.

**Table 7-1 A comparison of the experimental conditions and kinetic parameters of the hydrogen evolution reaction obtained in KOH**

	Temperature °C	KOH concentration M	Tafel slope/b mV·dec <sup>-1</sup>	Exchange current/j <sub>0</sub> A·cm <sup>-2</sup>
Kaninski et al.	25	1	115	$1 \times 10^{-5}$
Kubisztal et al.	N/A	5	121	$1.8 \times 10^{-4}$
Current study	25	0.5	108	$4.5 \times 10^{-5}$

The surface profiles of the Ni electrode and modified Ni electrodes were studied using SEM. Together with EDS, SEM technique presented the porous structure created by alkaline leaching process, and it was in accordance with previous study (Giz *et al*, 2000) that most part of the Zn was leached out from the electrode. These techniques were sufficient to represent the morphology and the composition after electrode preparation.

The alkaline leaching is a good way to produce porous structure (Solmaz *et al*, 2009). In this process, Zn was only used for the formation of the structure. First Zn was deposited on to electrode substrate with other active ingredients. Then, Zn was leached out by concentrated KOH, leaving the porous structure and larger surface area than that of before leaching. Although there was still residing Zn in the electrode after leaching (Giz *et al*, 2000), and this residing Zn might be consumed in the electrolysis, the high activity of these electrode deposited electrodes can still maintain high activity (Crnkovic *et al*, 2004).

It is worth mentioning that the stability test was not done on the prepared Ni-Fe-Zn electrode. There is a possibility that the porous structure might not

endure the corrosion caused by high temperature alkaline solutions. On the other hand, due to the limitations of the experimental setup, the kinetics of the electrode reaction was not studied under different temperatures, which can be used to derive the activation energy of the electrode reaction and would be strong and convincing evidence to our findings.

## **7.2 Electrode Modifications and Their Effect**

Our studies showed that through electrode modifications, the resistance of the electrode reactions can be reduced. Both mechanical and chemical modifications can alter the surface area and the activity of the electrode surface so that the apparent activity of the electrode can be improved. The effect of mechanical modification is determined by the final surface area of electrode. The surface areas of the modified electrode can be quantified using the surface roughness factor which was obtained from the impedance study of the electrode reaction (Kellenberger *et al*, 2007, Kubisztal *et al*, 2008). It was found that all the Ni electrodes after mechanical modification shared a similar Tafel relationship in Figure 7-2. This relationship was noted to govern the intrinsic activity of nickel electrode and can be expressed as  $\eta = 0.02 + 0.191 \cdot \text{Log} j$ ". This validated the method of calculating surface area, and the intrinsic activity was therefore can be used for comparing electrode activities. Further to this finding, the application of surface roughness factor should also be applicable to all other electrode metals, alloys or other material. Due to the time limitation, this work was not carried out.

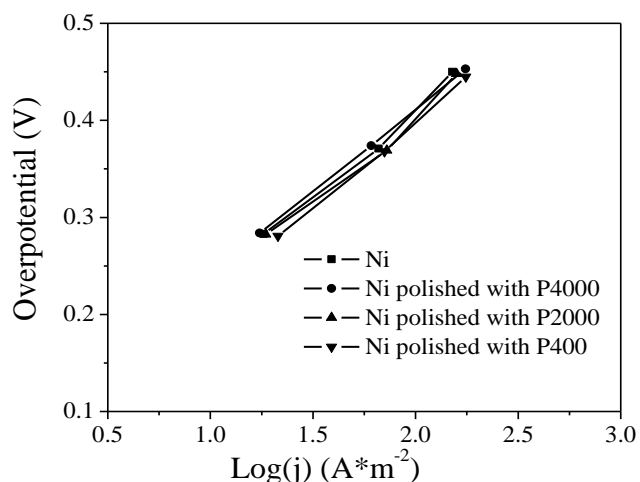


**Figure 7-2 Tafel curves of hydrogen evolution reaction illustrating the intrinsic activity of the mechanical polished Ni electrodes**

As previously reported that the Ni-Co-Zn electrode significantly reduced the overpotential of hydrogen evolution reaction with large roughness factor (Herraiz-Cardona *et al*, 2011), It was found that the Ni-Co deposits did not show large roughness factors, and their intrinsic activities were not better than that of Ni electrode. This confirmed the effect of porous structure in the electrode activity. A comparison between the current research and previous research by Herraiz-Cardona *et al* was made and shown in Table 7-2.

**Table 7-2 A comparison between the experimental conditions and roughness factor of current study and that of by Herraiz-Cardona *et al.*'s study**

	Electrode	T* <sup>1</sup>	C* <sup>2</sup> KOH	Tafel slope/b	Exchange current/j <sub>0</sub>	Roughness Factor/ R <sub>f</sub>
		°C		mV·dec <sup>-1</sup>	A·cm <sup>-2</sup>	
Herraiz-Cardona <i>et al.</i>	Ni-Co/Zn	30	30wt%	81	3.3×10 <sup>-3</sup>	1000
Current study	Ni-Co	25	0.5M	108	4.5×10 <sup>-5</sup>	4.3

\*1: Temperature

\*2: Concentration

Furthermore, it is worth mentioning that the compositions of Ni-Co electrodes significantly changed the performance of electrodes towards the hydrogen evolution reaction. This confirmed the importance of electrode deposition on the performance of electrode reaction. Although the trend of this change was not further investigated, it is indeed an exciting and worthwhile area for further exploration. A general trend or a regular pattern can be used as a guide for choosing electrode materials.

### **7.3 Electrolytic Bubble Behaviour and Their Effect**

Gas bubbles produced by electrode reaction also pose a significant energy barrier for alkaline water electrolysis as identified in Chapter 2. The gas bubbles on the electrode surface block the electrode reaction by occupying the surface of the electrode.

It was discussed that the force balance is critical in predicting bubble detachment diameter (Zeng *et al*, 1993, Thorncroft and Klausner, 2001). Both surface tension and buoyancy determined the growth and departure of the gas bubbles. It is also discussed in the Vogt's work that the electrolytic gas bubbles are different from boiling gas bubbles in many aspects (Vogt *et al*, 2004). One of the most important differences is the departure diameter. Our study confirmed the effect of electrode potential on the departure diameter. This could be considered in to the interfacial tension force between the electrode and gas bubbles.

Management of these bubbles can be achieved through the control of electrolyte concentration, temperature field or the addition of surfactant.

Such controls can help alter the bubble behaviour so that we can reduce the energy barriers caused by the formation of electrolytic gas bubbles.

The force analysis on a bubble confirmed that balance between buoyancy and surface tension determined the departure of the bubble. When buoyancy force exceeded the surface tension force on the vertical direction,  $\vec{F}_b > \vec{F}_s$ , the bubble will detach. A correlation between the critical diameter for the bubble departure and surface tension can be written in Equation 7-1, where  $\sigma$  is the surface tension, and  $\theta$  is the contact angle, and  $\alpha$ ,  $\beta$  are the advancing and receding angles of the bubble (Van Der Geld, 2004), respectively.

$$R = 2r = 2 \sqrt{\frac{\sin \theta (\alpha - \beta) [\sin \alpha + \sin \beta]}{[\pi^2 - (\alpha - \beta)^2] \times (1 + \cos \theta)^2 (2 - \cos \theta)}} \times \sqrt{\sigma} \quad 7-1$$

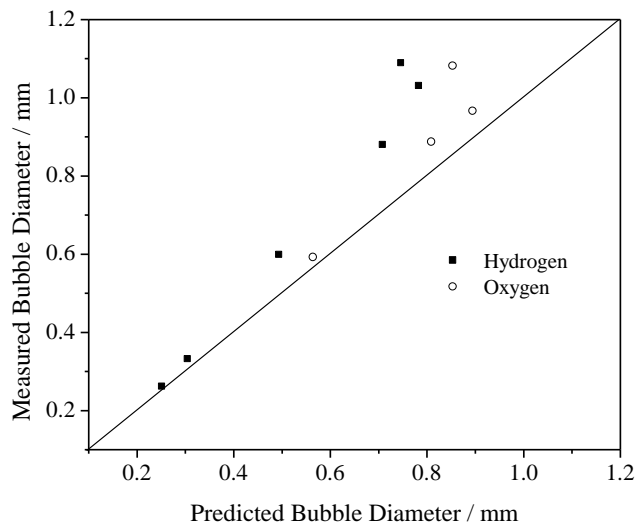


**Figure 7-3 Comparison of the predicted and measured critical diameters for hydrogen and oxygen gas bubbles**

With Equation 7-1 and the predicted values for the contact angle and surface tension, the critical diameter for bubble departure can be calculated. Figure

6-9 compares the predicted and the measured values of the critical diameters under different conditions. As can be seen from Figure 6-9, generally good agreement is evident for both hydrogen and oxygen gas bubbles.

We have found that only at low current densities, less than  $1\text{mA}\cdot\text{cm}^{-2}$ , bubbles can grow fully to the predicted critical diameter before departure. Higher current density will incur convection, which leads to small bubbles depart prematurely. Although these small gas bubbles tend to stay in the surrounding electrolyte, the finding gives some insights in controlling the effect of bubbles.

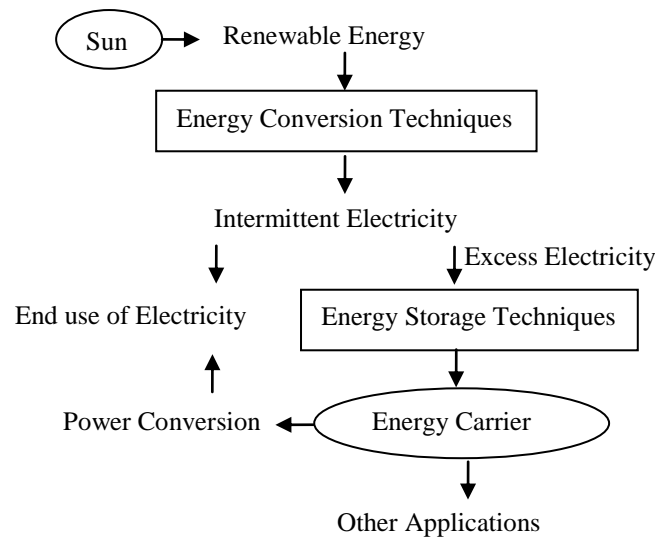
It was found in our study that the electrolyte concentration had an inhibition effect on the electrolytic bubble growth. It was explained by the advancing and receding of the bubble. This is in agreement of the findings of Deschenes (Deschenes *et al*, 1998).

Nevertheless, the current study only presented good prediction at the experimental conditions. Due to the complexity of the forces on electrolytic bubbles and the lack of experimental data, it is hard to predict the behaviour under the operating conditions of water electrolysis. In the present study the quantification of the force induced by convection has not yet been covered. It is suggested to study both the effect of temperature field and convection. It is also further suggested to study the effect of the electrode surface profile (Chien and Webb, 1998), which may also present different forces to give thorough understanding on the electrolytic gas bubble behaviour during operation conditions.

## 7.4 Practical Implications

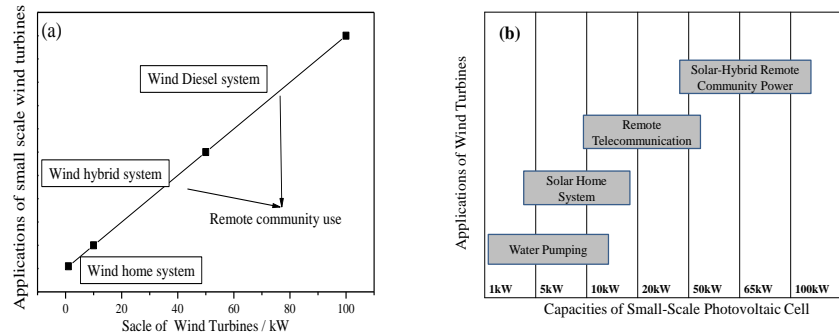
As an option of sustainable energy, renewable energy is attracting more and more attention with rapid growth. However, only a few percentage the renewable energy is currently deployed (Resch *et al*, 2008). Therefore, there is plenty potential in further exploiting renewable energy.

Figure 7-4 shows a conceptual distributed energy production, conversion, storage, and use system for remote communities. As can be seen from Figure 7-4, electrical energy can be produced from a renewable energy source such as wind or solar through appropriate energy conversion techniques. Then, the intermittent electricity can either be supplied to the users, or can be stored in the energy carrier when there is excess electricity. The energy carrier plays an important role in this system as an energy storage mechanism. It can either be transformed into electricity, when needed or can be used for other applications such as heating or fuel. Improvement and better understanding of the water electrolysis helps to facilitate the use of water electrolysis as an energy storage technique.



**Figure 7-4 A schematic illustration of a conceptual distributed energy system with energy storage technique playing an important role in utilisation of renewable energy**

One of the most important features of such a distributed energy system is its flexibility in scale. Take wind and solar energy for examples, the scale of the wind turbine varies from less than 1kW to 3-4 MW (Mathew, 2006), and a few kW to tens of GW for solar technology. The application of these systems can be used for different purposes including home use, small business and remote community use to power stations as shown in Figure 7-5 (Ackermann and Soder, 2000, T.Forsyth and Baring-Gould, 2007). When combined with all other techniques, such as battery and diesel, it might also serve the industrial needs.



**Figure 7-5 Range of power and applications for small scale wind turbines (a) and PV cells (b)**

The present thesis identified the barriers in alkaline water electrolysis. Several objectives were proposed to control or reduce the energy barriers thus to improve the efficiency of water electrolysis. Our studies advanced understandings of the role of electrode modification in electrode reactions, and improved fundamental understandings of the behaviour and the role of electrolytic gas bubbles in alkaline water electrolysis. Therefore, the high heat waste and low efficiency issues of current alkaline water electrolysis could be addressed or alleviated.

In potential practical applications, when preparing electrode materials, it is important to set two targets to achieve better electrode material. Firstly, larger electrode surface area is beneficial to better electrode performance. This can be done by choosing a porous material as the substrate or by using a preparation method that helps to gain a larger surface area. Secondly, electrode composition is another important influencing factor for the activity of the electrode. This requires experimental results to select appropriate electrode material taking the effect of surface area in to consideration.

On the other hand, bubble management can be realised by several factors that determine the departure of electrolytic bubbles. Increasing electrolyte concentration limits the growth of electrolytic bubbles. The increasing electrode potential helps bubbles grow to a larger size. When there is convection around electrodes, these bubbles tend to detach from the electrode prematurely. The detachment of these small gas bubbles can help reduce the resistance caused by the bubbles. However, these small electrolytic bubbles tend to stay in the electrolyte which still exhibits a high energy barrier for alkaline water electrolysis. These findings have various practical implications regarding the improving the efficiency of alkaline water electrolysis by controlling the behaviour of electrolytic gas bubbles.

#### **7.4.1 Feasibility Analysis**

Remote communities are always located far from major power grids, telecommunication stations and other major services. However, due to the low population density, the renewable energies are always available and sufficient to supply the energy needs in such remote areas.

It is argued that a continuous power of 2 kW for everyone would be sufficient to provide all with a high quality of life (Spreng, 2005). Assuming 100 people in a remote community, the total power need is around 200kW. Therefore, a 200kW wind turbine and/or PV cells are needed to supply the energy need.

Assuming a half of the electrical energy would be coming through the energy storage technique, that is 876MWh. Assuming the energy conversion

efficiency of the hydrogen fuel cell is 40%, the requirement in hydrogen production can be calculated through the higher heating value of hydrogen. That is 67393 kg hydrogen per year.

Assuming the energy conversion efficiency of the electrolyser is 60%, a gross hydrogen production of 1,509,609 m<sup>3</sup>/year is needed. The amount of hydrogen requires electrolysers to be capable of producing about 170 m<sup>3</sup> H<sub>2</sub>/hour. The Stuart Energy Systems offer electrolysers cable of producing about 15m<sup>3</sup>/hour (Young *et al*, 2007), so twelve such units will be sufficient to supply the hydrogen needs.

#### 7.4.2 Cost Analysis

Take hydrogen fuel cells as the power conversation technique in Figure 7-4, the estimated costs of the distributed energy system were listed in Table 7-3. The capital cost of each item was calculated on a basis of 20 years operation time. The capital cost of building a distributed energy system, not including other operation cost, is already higher than electricity produced from other conventional sources.

**Table 7-3 Estimated construction costs of a distributed energy system for a hypothetical remote community**

Unit	Price /\$	Capital Cost \$/kWh
Wind Turbine	500,000	0.029
Electrolyser	600,000	0.034
Hydrogen Fuel Cell	500,000	0.029

Although the cost of renewable energy is not competitive compared to fossil fuel for the next several decades (Moriarty and Honnery, 2012), further

research and development will help improve the renewable energy technologies and realise the utilisation of renewable energy in the future.

The technical potential of the proposed distributed energy system was achievable through the current technology of alkaline water electrolyser and hydrogen fuel cell. This system is capable of providing a stand-alone electricity supply for the remote communities.

The calculations presented in this study were on the basis of estimation of current technologies. There are still room for improvements of the technologies such as water electrolysis and hydrogen fuel cell.

## **7.5 Summary**

This Chapter evaluated the results and important findings in Chapter 4 to Chapter 6. By comparing the findings with those in previous studies, the effect of electrode modification, electrode surface area and electrolytic bubble behaviour was stressed and their research findings were compared with the literature data. Throughout the evaluation, new gaps in knowledge, technology and practical uses were discussed. Further studies are directed to understand or investigate the effect of electrode composition on electrode reactions and to further quantify the effect the force caused by convection to help better prediction the critical bubble diameter for bubble departure at the presence of convection.

Potential practical implications are also discussed using a hypo-theoretical energy distributed energy system as an example. To realise the potential of

renewable energy, a distributed energy system was proposed using alkaline water electrolysis as a means to produce hydrogen. Moreover, the implications of the findings in improving the efficiency of water electrolysis were discussed. Through analysing the needs in a hypothetical remote community, the requirement of electrolyser and fuel cell were achievable through currently available technologies. Although the cost of such a distributed system was high, it is believed that the future of the energy needs in remote community can rely on the distributed energy system.

## 8.1 Conclusions

The Tafel slope of the hydrogen evolution reaction on a smooth Ni electrode was found to be  $108\text{mV}\cdot\text{dec}^{-1}$  and the Tafel equation can be written as  $\eta = 0.14 + 0.108\text{Log}j$ . The linear relationship between the overpotential

and the logarithm of the current density confirmed the electrode reaction was under kinetic control.

The nickel electrode with the Ni-Fe-Zn coating showed an improved apparent activity towards the hydrogen evolution reaction than the pure Ni electrode. SEM image analysis proved that the alkaline leaching treatment realised a significantly enhanced porous structure. The apparent activity enhancement on the Ni-Fe-Zn coated electrode can be attributed to the increase in the surface area.

The alkaline leaching was confirmed as a good way to produce porous structure. In this process, Zn was only used for the formation of the structure. First Zn was deposited on to electrode substrate with other active ingredients. Then, Zn was leached out by concentrated KOH, leaving the porous structure and larger surface area than that of before leaching.

### **8.1.2 Electrode Modifications and Their Effect**

Both mechanical and chemical modifications altered the surface area and the activity of the electrode surface so that the apparent activity of the electrode was improved. The Ni electrodes modified by mechanical polishing showed enhanced apparent activities than the base Ni. The improvement of the apparent activities was found to be proportional to the increase in the surface area.

The concepts of effective surface area and relative roughness factor, derived from the electrochemical impedance studies, were introduced. When the effective surface area was applied, the Tafel curves of the Ni electrodes

polished with different sandpapers collapsed into a narrow band which can be described by the equation  $\eta = 0.02 + 0.191 \cdot \log j''$ . The equation represents the intrinsic activities of Ni electrodes towards the hydrogen evolution reaction and also validates the roughness factor for presenting intrinsic activity.

While the electrodes modified by electrochemical deposition of Ni-Co changed their apparent electrode activities, their intrinsic activities are different, depending on their surface Ni-Co compositions as varied with the deposition time. The effect of electrode composition on the electrode kinetics remained unknown and warrants further investigation.

### **8.1.3 Electrolytic Bubble Behaviour and Their Effect**

The force analysis on a bubble confirmed that balance between buoyancy and surface tension determined the departure of the bubble. This thesis work confirmed the effect of electrode potential on the departure diameter.

The critical diameter for electrolytic gas bubble departure was highly dependent on the electrolyte concentration and cell voltage at low current densities. The critical diameters for hydrogen and oxygen bubbles increased from 0.59 to 1.03mm and from 0.60 to 1.08 mm, respectively, as the electrode potential increased from 1.72 to 1.93V. The critical diameter for hydrogen bubble departure decreased to 0.27mm as the KOH concentration increased from 0.5M to 4M. Similar findings were also obtained for the oxygen gas bubbles. It was explained by the fact that an increase in the

electrode potential resulted in an increase in the interfacial tension, while an increase in the KOH concentration had an adverse effect by reducing  $\Delta\theta$ .

Predictions were made using the force analysis model employing the experimental data in the literature. Generally good agreement between the predicted and the measured values of the critical diameters under different conditions was obtained.

At high cell voltages or electrolyte flow, the corresponding convections induced by the upward flowing bubbles caused the other bubbles to depart prematurely. The application of electrolyte circulation dramatically reduced the bubble sizes. It was also found that only a small reduction in the cell voltage caused by the electrolyte circulation which means the gas bubble curtain formed on the electrode surface presented a significant energy barrier for alkaline water electrolysis.

## **8.2 Practical Implications**

The practical implications were discussed using a conceptual distributed energy production conversion, storage, and use system for remote communities as an example. To fully realise the potential of renewable energies, alkaline water electrolysis was proposed to produce pure hydrogen, which can serve as an energy carrier solving the intermittence problem of renewable energies.

The present thesis identified the barriers in alkaline water electrolysis that limited the application of water electrolysis. Several objectives were

proposed to control or reduce the energy barriers and these objectives were studied and presented in Chapter 4 to 6. The findings have the potential practical implications as follows:

To alleviate the resistance of the electrode reaction, alkaline leaching and electrode modifications are suggested for preparing electrodes with large surface areas. The use of the roughness factor is recommended for benchmarking and selecting electrode materials. Electrode composition is another important influencing factor for the activity of the electrode that needs to be taken in to account when selecting electrode materials.

This study also improved understandings of the behaviour and the role of electrolytic gas bubbles in alkaline water electrolysis. These findings have various practical implications regarding the improvement of the efficiency of alkaline water electrolysis by controlling the behaviour of electrolytic gas bubbles. Bubble management can be realised by several factors that determine the departure of electrolytic bubbles. Increasing electrolyte concentration limits the growth of electrolytic bubbles. Increasing electrode potential helps bubbles grow to a larger size. When there is convection around electrodes, these bubbles tend to detach from the electrode prematurely.

### **8.3 Recommendations for Future Work**

The Ni-Fe-Zn coated electrode shows a porous structure and a better activity than the Ni electrode in this thesis. Future work can be done to explore and evaluate other electrode preparation methods that can generate similar

porous electrode surface. For the electrode prepared by alkaline leaching, it is recommended to carry out a stability test to ensure the porous structure can endure the corrosive environment. On the other hand, the kinetics of the electrode reaction is recommended to be studied at different temperatures. This helps to derive the activation energy of the electrode reaction and would be a convincing criterion when comparing electrodes.

Furthermore, it was found that the compositions of Ni-Co coated electrodes significantly changed the performance of electrodes towards the hydrogen evolution reaction. Therefore, future studies are also recommended to investigate the influence of electrode composition on the performance of electrode reaction. A general trend or a regular pattern can be used as a guide for choosing electrode materials. As the Ni-Co coated electrode did not show the synergic effect which existed in the Ni-Fe-Zn coated electrode, it is also interesting and recommended to explore what are the possible metals, alloys or compounds that have such a synergic effect. This study will also serve as a guide in designing and preparing electrode materials. When comparing the activity the electrodes, it is recommended to compare both the apparent and the intrinsic activity of an electrode reaction on different electrode materials.

The behaviour of electrolytic bubbles is a complicated phenomenon and requires much more work to further understand the way the bubbles affect the cell voltage and the operation of an electrolysis unit. In the present study the quantification of the force induced by convection has not yet been

covered. Therefore, it is also further suggested to study both the effect of temperature field and convection on bubble behaviour which may also gain understanding and facilitate the prediction of electrolytic gas bubble behaviour during operation conditions.

It is also revealed that the layer of small bubbles near the electrode surface represents a significant resistance and it is therefore suggested that more work can be done to understand the formation of these small bubbles and remove these bubbles so that we can minimise the effect of these bubbles and the cell voltage can be reduced significantly.

There are also some more areas have not been explored to understand the electrolytic bubble behaviour in this thesis. It is suggested to study the effect of the electrode surface profile on bubble behaviour, which might have effects on the growth and departure of the electrolytic bubbles (Chien and Webb 1998). The selection of electrolyte solution also plays an important role in the bubble behaviour. Therefore, it is also suggested that more work can be done to understand the way the electrolyte affects the bubble growth so that further improvement can be made on the performance of a water electrolysis unit.

## References

- Abdel Ghany, N. A., Kumagai, N., Meguro, S., Asami, K. & Hashimoto, K., 2002, Oxygen evolution anodes composed of anodically deposited Mn-Mo-Fe oxides for seawater electrolysis, *Electrochimica Acta*, 48, (1), 21-28.
- Abouatallah, R. M., Kirk, D. W., Thorpe, S. J. & Graydon, J. W., 2001, Reactivation of nickel cathodes by dissolved vanadium species during hydrogen evolution in alkaline media, *Electrochimica Acta*, 47, (4), 613-621.
- Ackermann, T. & Soder, L., 2000, Wind energy technology and current status: a review, *Renewable & Sustainable Energy Reviews*, 4, (4), 315-374.
- Adam, N. K., 1968, The physics and chemistry of surfaces.
- Agbossou, K., Chahine, R., Hamelin, J., Laurencelle, F., Anouar, A., St-Arnaud, J. M. & Bose, T. K., 2001, Renewable energy systems based on hydrogen for remote applications, *Journal of Power Sources*, 96, (1), 168-172.
- Al-Hayes, R. a. M. & Winterton, R. H. S., 1981, Bubble diameter on detachment in flowing liquids, *International Journal of Heat and Mass Transfer*, 24, (2), 223-230.
- Barbir, F., 2005, PEM electrolysis for production of hydrogen from renewable energy sources, *Solar Energy*, 78, (5), 661-669.
- Bard, A. J. & Faulkner, L. R. 2001. *Electrochemical methods-fundamentals and applications*, New York, John Wiley & Sons.
- Bard, A. J., Inzelt, G. & Scholz, F. 2008. *Electrochemical Dictionary*, Berlin, Springer.
- Barreto, L., Makihiro, A. & Riahi, K., 2003, The hydrogen economy in the 21st century: a sustainable development scenario, *International Journal of Hydrogen Energy*, 28, (3), 267-284.
- Barsoukov, E. & Macdonald, J. R. 2005. *Impedance spectroscopy-theory, experiment, and applications*, Hoboken, Wiley-Interscience.
- Belmont, C. & Girault, H., 1994, Coplanar interdigitated band electrodes for synthesis Part I: Ohmic loss evaluation, *Journal of Applied Electrochemistry*, 24, (6), 475-480.
- Bird, R. B., Stewart, W. E. & Lightfoot, E. N. 2007. *Transport phenomena*, New York, John Wiley & Sons.
- Bloom, H. & Futmann, F. 1977. *Electrochemistry: The Past Thirty and the Next Thirty Years* New York Plenum Press.

- Bocca, C., Barbucci, A. & Cerisola, G., 1998, The influence of surface finishing on the electrocatalytic properties of nickel for the oxygen evolution reaction (OER) in alkaline solution, *International Journal of Hydrogen Energy*, 23, (4), 247-252.
- Bockris, J. O., 2002, The origin of ideas on a Hydrogen Economy and its solution to the decay of the environment, *International Journal of Hydrogen Energy*, 27, (7-8), 731-740.
- Bockris, J. O. M., Conway, B. E., Yeager, E. & White, R. E. 1981. *Comprehensive Treatise of Electrochemistry*, New York, Plenum Press.
- Bockris, J. O. M. & Veziroglu, T. N., 2007, Estimates of the price of hydrogen as a medium for wind and solar sources, *International Journal of Hydrogen Energy*, 32, (12), 1605-1610.
- Boissonneau, P. & Byrne, P., 2000, An experimental investigation of bubble-induced free convection in a small electrochemical cell, *Journal of Applied Electrochemistry*, 30, (7), 767-775.
- Bowen, C. T., Davis, H. J., Henshaw, B. F., Lachance, R., Leroy, R. L. & Renaud, R., 1984, Developments in Advanced Alkaline Water Electrolysis, *International Journal of Hydrogen Energy*, 9, (1-2), 59-66.
- Brussieux, C., Viers, P., Roustan, H. & Rakib, M., 2011, Controlled electrochemical gas bubble release from electrodes entirely and partially covered with hydrophobic materials, *Electrochimica Acta*, 56, (20), 7194-7201.
- Carter, T. J. & Cornish, L. A., 2001, Hydrogen in metals, *Engineering Failure Analysis*, 8, (2), 113-121.
- Chen, L. L. & Lasia, A., 1992, Study of the Kinetics of Hydrogen Evolution Reaction on Nickel-Zinc Powder Electrodes, *Journal of the Electrochemical Society*, 139, (11), 3214-3219.
- Chien, L.-H. & Webb, R. L., 1998, Measurement of bubble dynamics on an enhanced boiling surface, *Experimental Thermal and Fluid Science*, 16, (3), 177-186.
- Choquette, Y., Menard, H. & Brossard, L., 1990, Electrocatalytic performance of composite coated electrode for alkaline water electrolysis, *International Journal of Hydrogen Energy*, 15, (1), 21-26.
- Cole, R., Papazian, J. M. & Wilcox, W. R., 1980, Bubble departure radii at solidification interfaces, *International Journal of Heat and Mass Transfer*, 23, (2), 219-224.
- Conway, B. E. & Bai, L., 1986, H<sub>2</sub> evolution kinetics at high activity Ni-Mo-Cd electrocoated cathodes and its relation to potential

- dependence of sorption of H, *International Journal of Hydrogen Energy*, 11, (8), 533-540.
- Correia, A. N., Machado, S. a. S. & Avaca, L. A., 1999, Studies of the hydrogen evolution reaction on smooth Co and electrodeposited Ni-Co ultramicroelectrodes, *Electrochemistry Communications*, 1, (12), 600-604.
- Crnkovic, F. C., Machado, S. a. S. & Avaca, L. A., 2004, Electrochemical and morphological studies of electrodeposited Ni-Fe-Mo-Zn alloys tailored for water electrolysis, *International Journal of Hydrogen Energy*, 29, (3), 249-254.
- Crow, D. R. 1974. *Principles and Applications of Electrochemistry*, London, Chapman and Hall.
- Damjanov, A., Dey, A. & Bockris, J. O. M., 1966, Electrode Kinetics of Oxygen Evolution and Dissolution on Rh Ir and Pt-Rh Alloy Electrodes, *Journal of the Electrochemical Society*, 113, (7), 739-&.
- De Chialvo, M. R. G. & Chialvo, A. C., 2001, Hydrogen evolution reaction on a smooth iron electrode in alkaline solution at different temperatures, *Physical Chemistry Chemical Physics*, 3, (15), 3180-3184.
- De Souza, R. F., Padilha, J. C., Goncalves, R. S., De Souza, M. O. & Rault-Berthelot, J., 2007, Electrochemical hydrogen production from water electrolysis using ionic liquid as electrolytes: Towards the best device, *Journal of Power Sources*, 164, (2), 792-798.
- De Souza, R. F., Padilha, J. C., Goncalves, R. S. & Rault-Berthelot, J. L., 2006, Dialkylimidazolium ionic liquids as electrolytes for hydrogen production from water electrolysis, *Electrochemistry Communications*, 8, (2), 211.
- Defay, R. & Prigogine, I. 1966. *Surface tension and adsorption* London, Longmans
- Degiorgis, L., Santarelli, M. & Cali, M., 2007, Hydrogen from renewable energy: A pilot plant for thermal production and mobility, *Journal of Power Sources*, 171, (1), 237-246.
- Dejonge, R. M., Barendrecht, E., Janssen, L. J. J. & Vanstralen, S. J. D., 1982, Gas Bubble Behavior and Electrolyte Resistance during Water Electrolysis, *International Journal of Hydrogen Energy*, 7, (11), 883-894.
- Deschenes, L. A., Barrett, J., Muller, L. J., Fourkas, J. T. & Mohanty, U., 1998, Inhibition of bubble coalescence in aqueous solutions. 1. Electrolytes, *Journal of Physical Chemistry B*, 102, (26), 5115-5119.

- Drelich, J., Miller, J. D. & Good, R. J., 1996, The effect of drop (bubble) size on advancing and receding contact angles for heterogeneous and rough solid surfaces as observed with sessile-drop and captive-bubble techniques, *Journal of Colloid and Interface Science*, 179, (1), 37-50.
- Dunlap, P. M. & Faris, S. R., 1962, Surface Tension of Aqueous Solutions of Potassium Hydroxide, *Nature*, 196, (4861), 1312-1313.
- Dunn, S., 2002, Hydrogen futures: toward a sustainable energy system, *International Journal of Hydrogen Energy*, 27, (3), 235-264.
- Dyer, C. K., 1985, Improved Nickel Anodes for Industrial Water Electrolyzers, *Journal of the Electrochemical Society*, 132, (1), 64-67.
- Eigeldinger, J., 2000, The bubble coverage of gas-evolving electrodes in a flowing electrolyte, *Electrochimica Acta*, 45, (27), 4449.
- El-Deab, M. S., Awad, M. I., Mohammad, A. M. & Ohsaka, T., 2007, Enhanced water electrolysis: Electrocatalytic generation of oxygen gas at manganese oxide nanorods modified electrodes, *Electrochemistry Communications*, 9, (8), 2082-2087.
- Eliaz, N., Eliezer, D. & Olson, D. L., 2000, Hydrogen-assisted processing of materials, *Materials Science and Engineering A*, 289, (1-2), 41-53.
- Eliezer, D., Eliaz, N., Senkov, O. N. & Froes, F. H., 2000, Positive effects of hydrogen in metals, *Materials Science and Engineering A*, 280, (1), 220-224.
- Endres, F. & El Abedin, S. Z., 2006, Air and water stable ionic liquids in physical chemistry, *Physical Chemistry Chemical Physics*, 8, (18), 2101-2116.
- Fan, C. & Piron, D. L., 1996, Study of anomalous nickel-cobalt electrodeposition with different electrolytes and current densities, *Electrochimica Acta*, 41, (10), 1713-1719.
- Giz, M. J., Bento, S. C. & Gonzalez, E. R., 2000, NiFeZn codeposit as a cathode material for the production of hydrogen by water electrolysis, *International Journal of Hydrogen Energy*, 25, (7), 621-626.
- Granovskii, M., Dincer, I. & Rosen, M. A., 2006, Environmental and economic aspects of hydrogen production and utilization in fuel cell vehicles, *Journal of Power Sources*, 157, (1), 411-421.
- Grigoriev, S. A., Porembsky, V. I. & Fateev, V. N., 2006, Pure hydrogen production by PEM electrolysis for hydrogen energy, *International Journal of Hydrogen Energy*, 31, (2), 171-175.
- Hamdani, M., Pereira, M. I. S., Douch, J., Addi, A. A., Berghoute, Y. & Mendonca, M. H., 2004, Physicochemical and electrocatalytic properties of Li-Co<sub>3</sub>O<sub>4</sub> anodes prepared by chemical spray pyrolysis

- for application in alkaline water electrolysis, *Electrochimica Acta*, 49, (9-10), 1555-1563.
- Han, Q., Liu, K., Chen, J. & Wei, X., 2003, Hydrogen evolution reaction on amorphous Ni-S-Co alloy in alkaline medium, *International Journal of Hydrogen Energy*, 28, (12), 1345-1352.
- Hanley, N. & Nevin, C., 1999, Appraising renewable energy developments in remote communities: the case of the North Assynt Estate, Scotland, *Energy Policy*, 27, (9), 527-547.
- Herraiz-Cardona, I., Ortega, E., Vazquez-Gomez, L. & Perez-Herranz, V., 2011, Electrochemical characterization of a NiCo/Zn cathode for hydrogen generation, *International Journal of Hydrogen Energy*, 36, (18), 11578-11587.
- Hickner, M. A., Ghassemi, H., Kim, Y. S., Einsla, B. R. & Mcgrath, J. E., 2004, Alternative Polymer Systems for Proton Exchange Membranes (PEMs), *Chemical Reviews*, 104, (10), 4587-4612.
- Hine, F. & Murakami, K., 1980, Bubble effects on the solution IR drop in a vertical electrolyzer under free and forced convection, *Journal of the Electrochemical Society*, 127, (2), 292-297.
- Hine, F., Yasuda, M., Nakamura, R. & Noda, T., 1975, Hydrodynamic Studies of Bubble Effects on Ir-Drops in a Vertical Rectangular Cell, *Journal of the Electrochemical Society*, 122, (9), 1185-1190.
- Hitz, C. & Lasia, A., 2001, Experimental study and modeling of impedance of the HER on porous Ni electrodes, *Journal of Electroanalytical Chemistry*, 500, (1-2), 213-222.
- Hollmuller, P., Joubert, J. M., Lachal, B. & Yvon, K., 2000, Evaluation of a 5 kW(P) photovoltaic hydrogen production and storage installation for a residential home in Switzerland, *International Journal of Hydrogen Energy*, 25, (2), 97-109.
- Hu, W., 2000, Electrocatalytic properties of new electrocatalysts for hydrogen evolution in alkaline water electrolysis, *International Journal of Hydrogen Energy*, 25, (2), 111-118.
- Hu, W. & Lee, J.-Y., 1998, Electrocatalytic properties of Ti<sub>2</sub>Ni/Ni-Mo composite electrodes for hydrogen evolution reaction, *International Journal of Hydrogen Energy*, 23, (4), 253-257.
- Huor, J. Y., Trudeau, M., Brossard, L. & Schulz, R., 1989, Hydrogen evolution on some Ni-base amorphous alloys in alkaline solution, *International Journal of Hydrogen Energy*, 14, (5), 319-322.
- Huot, J. Y. & Brossard, L., 1987, Time-Dependence of the Hydrogen Discharge at 70-Degrees-C on Nickel Cathodes, *International Journal of Hydrogen Energy*, 12, (12), 821-830.

- Iida, T., Matsushima, H. & Fukunaka, Y., 2007, Water electrolysis under a magnetic field, *Journal of the Electrochemical Society*, 154, (8), E112-E115.
- Isherwood, W., Smith, J. R., Aceves, S. M., Berry, G., Clark, W., Johnson, R., Das, D., Goering, D. & Seifert, R., 2000, Remote power systems with advanced storage technologies for Alaskan villages, *Energy*, 25, (10), 1005-1020.
- Jaksic, M. M., 1984, Electrocatalysis of Hydrogen Evolution in the Light of the Brewer-Engel Theory for Bonding in Metals and Intermetallic Phases, *Electrochimica Acta*, 29, (11), 1539-1550.
- Janjua, M. B. I. & Leroy, R. L., 1985, Electrocatalyst Performance in Industrial Water Electrolysers, *International Journal of Hydrogen Energy*, 10, (1), 11-19.
- Jones, S. F., Evans, G. M. & Galvin, K. P., 1999, Bubble nucleation from gas cavities - a review, *Advances in Colloid and Interface Science*, 80, (1), 27-50.
- Kamat, P. V., 2007, Meeting the Clean Energy Demand: Nanostructure Architectures for Solar Energy Conversion, *J. Phys. Chem. C*, 111, (7), 2834-2860.
- Kaninski, M. P. M., Nikolic, V. M., Tasic, G. S. & Rakocevic, Z. L., 2009, Electrocatalytic activation of Ni electrode for hydrogen production by electrodeposition of Co and V species, *International Journal of Hydrogen Energy*, 34, (2), 703-709.
- Kaninski, M. P. M., Saponjic, D. P., Nikolic, V. M., Zugic, D. L. & Tasic, G. S., 2011, Energy consumption and stability of the Ni-Mo electrodes for the alkaline hydrogen production at industrial conditions, *International Journal of Hydrogen Energy*, 36, (15), 8864-8868.
- Kato, T., Kubota, M., Kobayashi, N. & Suzuoki, Y., 2005, Effective utilization of by-product oxygen from electrolysis hydrogen production, *Energy*, 30, (14), 2580-2595.
- Kellenberger, A., Vaszilcsin, N. & Brandl, W., 2007, Roughness factor evaluation of thermal arc sprayed skeleton nickel electrodes, *Journal of Solid State Electrochemistry*, 11, (1), 84-89.
- Kim, S., Koratkar, N., Karabacak, T. & Lu, T.-M., 2006, Water electrolysis activated by Ru nanorod array electrodes, *Applied Physics Letters*, 88, (26), 263106 1-3.
- Kinoshita, K. 1992. *Electrochemical oxygen technology*, New York, John Wiley & Sons.
- Kiuchi, D., Matsushima, H., Fukunaka, Y. & Kuribayashi, K., 2006, Ohmic resistance measurement of bubble froth layer in water electrolysis

- under microgravity, *Journal of the Electrochemical Society*, 153, (8), E138-E143.
- Klausner, J. F., Mei, R., Bernhard, D. M. & Zeng, L. Z., 1993, Vapor bubble departure in forced convection boiling, *International Journal of Heat and Mass Transfer*, 36, (3), 651-662.
- Kreuter, W. & Hofmann, H., 1998, Electrolysis: The important energy transformer in a world of sustainable energy, *International Journal of Hydrogen Energy*, 23, (8), 661-666.
- Krstajic, N., Popovic, M., Grgur, B., Vojnovic, M. & Sepa, D., 2001a, On the kinetics of the hydrogen evolution reaction on nickel in alkaline solution-Part I The mechanism, *Journal of Electroanalytical Chemistry*, 512, (1-2), 16-26.
- Krstajic, N., Popovic, M., Grgur, B., Vojnovic, M. & Sepa, D., 2001b, On the kinetics of the hydrogen evolution reaction on nickel in alkaline solution - Part II. Effect of temperature, *Journal of Electroanalytical Chemistry*, 512, (1-2), 27-35.
- Krstajic, N. V., Jovic, V. D., Gajic-Krstajic, L., Jovic, B. M., Antozzi, A. L. & Martelli, G. N., 2008, Electrodeposition of Ni-Mo alloy coatings and their characterization as cathodes for hydrogen evolution in sodium hydroxide solution, *International Journal of Hydrogen Energy*, 33, (14), 3676-3687.
- Kubisztal, J., Budniok, A. & Lasia, A., 2007, Study of the hydrogen evolution reaction on nickel-based composite coatings containing molybdenum powder, *International Journal of Hydrogen Energy*, 32, (9), 1211-1218.
- Kubisztal, J., Panek, J. & Budniok, A., 2008, ELECTROLYTIC Ni-BASED COMPOSITE COATINGS CONTAINING MOLYBDENUM AND SILICON FOR HYDROGEN EVOLUTION REACTION, *Carbon Nanomaterials in Clean Energy Hydrogen Systems*, 347-356.
- Kulkarni, A. A. & Joshi, J. B., 2005, Bubble formation and bubble rise velocity in gas-liquid systems: A review, *Industrial and Engineering Chemistry Research*, 44, (16), 5873-5931.
- Lattin, W. C. & Utgikar, V. P., 2007, Transition to hydrogen economy in the United States: A 2006 status report, *International Journal of Hydrogen Energy*, 32, (15), 3230-3237.
- Lee, T. S., 1971, Hydrogen Overpotential on Pure Metals in Alkaline Solution, *Journal of the Electrochemical Society*, 118, (8), 1278-&.
- Leroy, R. L., 1983, Industrial Water Electrolysis - Present and Future, *International Journal of Hydrogen Energy*, 8, (6), 401-417.
- Leroy, R. L., Bowen, C. T. & Leroy, D. J., 1980, The Thermodynamics of Aqueous Water Electrolysis, *Journal of the Electrochemical Society*, 127, (9), 1954-1962.

- Los, P., Rami, A. & Lasia, A., 1993, Hydrogen evolution reaction on Ni-Al electrodes, *Journal of Applied Electrochemistry*, 23, (2), 135-140.
- Lu, P. W. T., 1979, Advances in water electrolysis technology with emphasis on use of the solid polymer electrolyte, *Journal of Applied Electrochemistry*, 9, (3), 269.
- Lubetkin, S., 2002, The motion of electrolytic gas bubbles near electrodes, *Electrochimica Acta*, 48, (4), 357-375.
- Lumanauw, D. 2000. *Hydrogen bubble characterization in alkaline water electrolysis*. University of Toronto.
- Lupi, C., Dell'era, A. & Pasquali, M., 2009, Nickel-cobalt electrodeposited alloys for hydrogen evolution in alkaline media, *International Journal of Hydrogen Energy*, 34, (5), 2101-2106.
- Ma, H., Liu, C., Liao, J., Su, Y., Xue, X. & Xing, W., 2006, Study of ruthenium oxide catalyst for electrocatalytic performance in oxygen evolution, *Journal of Molecular Catalysis A: Chemical*, 247, (1-2), 7-13.
- Ma, Y. & Chung, J. N., 2001, A study of bubble dynamics in reduced gravity forced-convection boiling, *International Journal of Heat and Mass Transfer*, 44, (2), 399-415.
- Macmullin, R. B. & Muccini, G. A., 1956, Characteristics of Porous Beds and Structures, *AIChE Journal*, 2, (3), 393-403.
- Marceta Kaninski, M. P., Maksic, A. D., Stojic, D. L. & Miljanic, S. S., 2004, Ionic activators in the electrolytic production of hydrogen--cost reduction-analysis of the cathode, *Journal of Power Sources*, 131, (1-2), 107-111.
- Marshall, A., Borresen, B., Hagen, G., Tsyppkin, M. & Tunold, R., 2007, Hydrogen production by advanced proton exchange membrane (PEM) water electrolyzers - Reduced energy consumption by improved electrocatalysis, *Energy*, 32, (4), 431-436.
- Mathew, S. 2006. *Wind Energy: Fundamentals, Resource Analysis and Economics*, Springer.
- Matsushima, H., Fukunaka, Y. & Kuribayashi, K., 2006, Water electrolysis under microgravity. Part II. Description of gas bubble evolution phenomena, *Electrochimica Acta*, 51, (20), 4190-4198.
- Matsushima, H., Kiuchi, D., Fukunaka, Y. & Kuribayashi, K., 2009, Single bubble growth during water electrolysis under microgravity, *Electrochemistry Communications*, 11, (8), 1721-1723.
- Matsushima, H., Nishida, T., Konishi, Y., Fukunaka, Y., Ito, Y. & Kuribayashi, K., 2003, Water electrolysis under microgravity - Part 1. Experimental technique, *Electrochimica Acta*, 48, (28), 4119-4125.

- Mauer, A. E., Kirk, D. W. & Thorpe, S. J., 2007, The role of iron in the prevention of nickel electrode deactivation in alkaline electrolysis, *Electrochimica Acta*, 52, (11), 3505-3509.
- Miles, M. H., Huang, Y. H. & Srinivasan, S., 1978, Oxygen-Electrode Reaction in Alkaline-Solutions on Oxide Electrodes Prepared by Thermal-Decomposition Method, *Journal of the Electrochemical Society*, 125, (12), 1931-1934.
- Miles, M. H., Kissel, G., Lu, P. W. T. & Srinivasan, S., 1976, Effect of Temperature on Electrode Kinetic Parameters for Hydrogen and Oxygen Evolution Reactions on Nickel Electrodes in Alkaline Solutions, *Journal of the Electrochemical Society*, 123, (3), 332-336.
- Momirlan, M. & Veziroglu, T. N., 2002, Current status of hydrogen energy, *Renewable & Sustainable Energy Reviews*, 6, (1-2), 141-179.
- Moriarty, P. & Honnery, D., 2012, What is the global potential for renewable energy?, *Renewable and Sustainable Energy Reviews*, 16, (1), 244-252.
- Mueller-Langer, F., Tzimas, E., Kaltschmitt, M. & Peteves, S., 2007, Techno-economic assessment of hydrogen production processes for the hydrogen economy for the short and medium term, *International Journal of Hydrogen Energy*, 32, (16), 3797-3810.
- Navarro-Flores, E., Chong, Z. W. & Omanovic, S., 2005, Characterization of Ni, NiMo, NiW and NiFe electroactive coatings as electrocatalysts for hydrogen evolution in an acidic medium, *Journal of Molecular Catalysis a-Chemical*, 226, (2), 179-197.
- Newman, J. S. 1991. *Electrochemical Systems*, New Jersey, Prentice Hall.
- Oi, T. & Sakaki, Y., 2004, Optimum hydrogen generation capacity and current density of the PEM-type water electrolyzer operated only during the off-peak period of electricity demand, *Journal of Power Sources*, 129, (2), 229-237.
- Oldham, K. B. & Myland, J. C. 1993. *Fundamentals of Electrochemical Science*, San Diego, Academic Press.
- Orazem, M. E. & Tribollet, B. 2008. *Electrochemical Impedance Spectroscopy*, Hoboken, Wiley-Interscience.
- Pickett, D. J. 1979. *Electrochemical Reactor design*, Amsterdam Elsevier.
- Pletcher, D. & Walsh, F. C. 1990. *Industrial Electrochemistry*, London, Blackie Academic & Professional.
- Potvin, E. & Brossard, L., 1992, Electrocatalytic activity of Ni-Fe anodes for alkaline water electrolysis, *Materials Chemistry and Physics*, 31, (4), 311-318.

- Raj, I. A., 1993, Nickel-Based, Binary-Composite Electrocatalysts for the Cathodes in the Energy-Efficient Industrial-Production of Hydrogen from Alkaline-Water Electrolytic Cells, *Journal of Materials Science*, 28, (16), 4375-4382.
- Ramachandran, R. & Menon, R. K., 1998, An overview of industrial uses of hydrogen, *International Journal of Hydrogen Energy*, 23, (7), 593-598.
- Rami, A. & Lasia, A., 1992, Kinetics of hydrogen evolution on Ni-Al alloy electrodes *Journal of Applied Electrochemistry*, 22, (4), 376-382.
- Resch, G., Held, A., Faber, T., Panzer, C., Toro, F. & Haas, R., 2008, Potentials and prospects for renewable energies at global scale, *Energy Policy*, 36, (11), 4048-4056.
- Richards, M. & Shenoy, A., 2007, H<sub>2</sub>-MHR pre-conceptual design summary for hydrogen production, *Nuclear Engineering and Technology*, 39, (1), 1-8.
- Rieger, P. H. 1987. *Electrochemistry*, New Jersey, Prentice-Hall.
- Rosa, V. M., Santos, M. B. F. & Dasilva, E. P., 1995, New Materials for Water Electrolysis Diaphragms, *International Journal of Hydrogen Energy*, 20, (9), 697-700.
- Rosen, M. A. & Scott, D. S., 1998, Comparative efficiency assessments for a range of hydrogen production processes, *International Journal of Hydrogen Energy*, 23, (8), 653-659.
- Rossmesl, J., Logadottir, A. & Norskov, J. K., 2005, Electrolysis of water on (oxidized) metal surfaces, *Chemical Physics*, 319, (1-3), 178-184.
- Sato, S., Lin, S. Y., Suzuki, Y. & Hatano, H., 2003, Hydrogen production from heavy oil in the presence of calcium hydroxide, *Fuel*, 82, (5), 561-567.
- Sheela, G., Pushpavanam, M. & Pushpavanam, S., 2002, Zinc-nickel alloy electrodeposits for water electrolysis, *International Journal of Hydrogen Energy*, 27, (6), 627-633.
- Shervedani, R. K. & Madram, A. R., 2007, Kinetics of hydrogen evolution reaction on nanocrystalline electrodeposited Ni<sub>62</sub>Fe<sub>35</sub>C<sub>3</sub> cathode in alkaline solution by electrochemical impedance spectroscopy, *Electrochimica Acta*, 53, 426-433.
- Singh, R. N., Mishra, D., Anindita, Sinha, A. S. K. & Singh, A., 2007, Novel electrocatalysts for generating oxygen from alkaline water electrolysis, *Electrochemistry Communications*, 9, (6), 1369-1373.
- Soares, D. M., Teschke, O. & Torriani, I., 1992, Hydride Effect on the Kinetics of the Hydrogen Evolution Reaction on Nickel Cathodes in Alkaline Media, *Journal of the Electrochemical Society*, 139, (1), 98-105.

- Solmaz, R., Doner, A., Sahin, I., Yuce, A. O., Kardas, G., Yazici, B. & Erbil, M., 2009, The stability of NiCoZn electrocatalyst for hydrogen evolution activity in alkaline solution during long-term electrolysis, *International Journal of Hydrogen Energy*, 34, (19), 7910-7918.
- Song, S., Zhang, H., Liu, B., Zhao, P., Zhang, Y. & Yi, B., 2007, An Improved Catalyst-Coated Membrane Structure for PEM Water Electrolyzer, *Electrochemical and Solid-State Letters*, 10, (8), B122-B125.
- Spacil, H. S. & Tedmon, C. S., 1969, Electrochemical Dissociation of Water Vapor in Solid Oxide Electrolyte Cells .I. Thermodynamics and Cell Characteristics, *Journal of the Electrochemical Society*, 116, (12), 1618-&.
- Spreng, D., 2005, Distribution of energy consumption and the 2000 W/capita target, *Energy Policy*, 33, (15), 1905-1911.
- Steinfeld, A., 2002, Solar hydrogen production via a two-step water-splitting thermochemical cycle based on Zn/ZnO redox reactions, *International Journal of Hydrogen Energy*, 27, (6), 611-619.
- Stojic, D. L., Grozdic, T. D., Marceta Kaninski, M. P., Maksic, A. D. & Simic, N. D., 2006, Intermetallics as advanced cathode materials in hydrogen production via electrolysis, *International Journal of Hydrogen Energy*, 31, (7), 841-846.
- Stojic, D. L., Grozdic, T. D., Marceta Kaninski, M. P. & Stanic, V., 2007, Electrocatalytic effects of Mo-Pt intermetallics singly and with ionic activators. Hydrogen production via electrolysis, *International Journal of Hydrogen Energy*, 32, (13), 2314-2319.
- Stojic, D. L., Marceta, M. P., Sovilj, S. P. & Miljanic, S. S., 2003, Hydrogen generation from water electrolysis--possibilities of energy saving, *Journal of Power Sources*, 118, (1-2), 315-319.
- Suban, M., Tusek, J. & Uran, M., 2001, Use of hydrogen in welding engineering in former times and today, *Journal of Materials Processing Technology*, 119, (1-3), 193-198.
- T.Forsyth & Baring-Gould, I. 2007. Distributed wind market applications. Colorado: Nathional Renewable Energy laboratory.
- Tadmor, R., 2004, Line energy and the relation between advancing, receding, and young contact angles, *Langmuir*, 20, (18), 7659-7664.
- Tarasatti, S., 1999, Water electrolysis: who first?, *Journal of Electroanalytical Chemistry*, 476, 90-91.
- Thorncroft, G. E. & Klausner, J. F., 2001, Bubble forces and detachment models, *Multiphase Science and Technology*, 13, (3-4), 35-76.
- Trasatti, S., 1971, Work function, electronegativity and electrochemical behaviour of metals: 2. Potentials of zero charge and electrochemical

- work functions, *Journal of Electroanalytical Chemistry*, 33, (2), 351-&.
- Trommer, D., Noembrini, F., Fasciana, A., Rodriguez, D., Morales, A., Romero, M. & Steinfeld, A., 2005, Hydrogen production by steam-gasification of petroleum coke using concentrated solar power - I. Thermodynamic and kinetic analyses, *International Journal of Hydrogen Energy*, 30, (6), 605-618.
- Turner, J. A., 1999, A Realizable Renewable Energy Future, *Science*, 285, (5428), 687.
- Turner, J. A., 2004, Sustainable hydrogen production, *Science*, 305, (5686), 972-974.
- Van Der Geld, C. W. M., 2004, Prediction of dynamic contact angle histories of a bubble growing at a wall, *International Journal of Heat and Fluid Flow*, 25, (1), 74-80.
- Van Helden, W. G. J., Van Der Geld, C. W. M. & Boot, P. G. M., 1995, Forces on bubbles growing and detaching in flow along a vertical wall, *International Journal of Heat and Mass Transfer*, 38, (11), 2075-2088.
- Varkaraki, E., Lymberopoulos, N. & Zachariou, A., 2003, Hydrogen based emergency back-up system for telecommunication applications, *Journal of Power Sources*, 118, (1-2), 14-22.
- Viswanath, R. P., 2004, A patent for generation of electrolytic hydrogen by a cost effective and cheaper route, *International Journal of Hydrogen Energy*, 29, (11), 1191-1194.
- Vogt, H., 1989, The problem of the departure diameter of bubbles at gas evolving electrodes, *Electrochimica Acta*, 34, (10), 1429-1432.
- Vogt, H., Aras, O. & Balzer, R. J., 2004, The limits of the analogy between boiling and gas evolution at electrodes, *International Journal of Heat and Mass Transfer*, 47, (4), 787-795.
- Vogt, H. & Balzer, R. J., 2005, The bubble coverage of gas-evolving electrodes in stagnant electrolytes, *Electrochimica Acta*, 50, (10), 2073-2079.
- Wei, Z. D., Ji, M. B., Chen, S. G., Liu, Y., Sun, C. X., Yin, G. Z., Shen, P. K. & Chan, S. H., 2007, Water electrolysis on carbon electrodes enhanced by surfactant, *Electrochimica Acta*, 52, (9), 3323-3329.
- Weissenborn, P. K. & Pugh, R. J., 1995, Surface-Tension and Bubble Coalescence Phenomena of Aqueous-Solutions of Electrolytes, *Langmuir*, 11, (5), 1422-1426.
- Wendt, H., Hofmann, H. & Plzak, V., 1989, Materials Research and Development of Electrocatalysts for Alkaline Water Electrolysis, *Materials Chemistry and Physics*, 22, (1-2), 27-49.

- 
- Wendt, H. & Kreysa, G. 1999. *Electrochemical Engineering*, Berlin, Springer-Verlag Berlin Heidelberg.
- Yeoh, G. H., Cheung, S. C. P., Tu, J. Y. & Ho, M. K. M., 2008, Fundamental consideration of wall heat partition of vertical subcooled boiling flows, *International Journal of Heat and Mass Transfer*, 51, (15-16), 3840-3853.
- Young, D. C., Mill, G. A. & Wall, R., 2007, Feasibility of renewable energy storage using hydrogen in remote communities in Bhutan, *International Journal of Hydrogen Energy*, 32, (8), 997-1009.
- Zeng, K. & Zhang, D., 2010, Recent progress in alkaline water electrolysis for hydrogen production and applications, *Progress in Energy and Combustion Science*, 36, (3), 307-326.
- Zeng, L. Z., Klausner, J. F. & Mei, R., 1993, A unified model for the prediction of bubble detachment diameters in boiling systems-- I. Pool boiling, *International Journal of Heat and Mass Transfer*, 36, (9), 2261-2270.

## Publications

- Zeng, K. & Zhang, D. 2010a. A kinetic study of hydrogen evolution on Ni-based electrodes in alkaline water electrolysis. *Proceedings of the 40th Australasian Chemical Engineering Conference, Chemeca 2010*. Adelaide, South Australia.
- Zeng, K. & Zhang, D., 2010b, Recent progress in alkaline water electrolysis for hydrogen production and applications, *Progress in Energy and Combustion Science*, 36 (3), 307-326.
- Zeng, K. & Zhang, D., 2012a, Evaluating the Behaviour of Electrolytic Gas Bubbles and Their Effect on the Cell Voltage in Alkaline Water Electrolysis, *Industrial and Engineering Chemistry Research*, Submitted.
- Zeng, K. & Zhang, D., 2012b, Evaluating the effect of surface modifications on Ni based electrodes for alkaline water electrolysis, *Fuel*, Submitted.
- Zhang, D. & Zeng, K. 2012. The role of renewable energy driven water electrolysis in distributed energy. *International Conference of Applied Energy*. Suzhou.